REPORT DOCUMENTATION PAGE

Form Approved OMB NO. 0704-0188

1. REPORT DATE (DD-MM-YYYY)	2. REPORT TYPE	3. DATES COVERED (From - To)
29-07-2015	Book Chapter	-

4. TITLE AND SUBTITLE
Chapter 3: Basic Electronic Structures and Charge Carrier Generation in Organic Optoelectronic Materials

5a. CONTRACT NUMBER
W911NF-11-1-0158

5b. GRANT NUMBER

5c. PROGRAM ELEMENT NUMBER
206022

6. AUTHORS
Sam-Shajing Sun

5d. PROJECT NUMBER

5e. TASK NUMBER

5f. WORK UNIT NUMBER

7. PERFORMING ORGANIZATION NAMES AND ADDRESSES
Norfolk State University
700 Park Avenue
McDemmond Center for Applied Research, Suite 601
Norfolk, VA 23504 -8060

8. PERFORMING ORGANIZATION REPORT NUMBER

9. SPONSORING/MONITORING AGENCY NAME(S) AND ADDRESS (ES)
U.S. Army Research Office
P.O. Box 12211
Research Triangle Park, NC 27709-2211

10. SPONSOR/MONITOR'S ACRONYM(S)
ARO

11. SPONSOR/MONITOR'S REPORT NUMBER(S)
58948-CH-REP.14

12. DISTRIBUTION AVAILIBILITY STATEMENT
Approved for public release; distribution is unlimited.

13. SUPPLEMENTARY NOTES
The views, opinions and/or findings contained in this report are those of the author(s) and should not contrued as an official Department of the Army position, policy or decision, unless so designated by other documentation.

14. ABSTRACT
This chapter briefly introduces some fundamental concepts and principles in a mainly qualitative way (for students with diverse backgrounds at the college senior level) related to electronic structures, energy and charge carrier transfers of electronic and optoelectronic materials, with emphasis on organic and polymeric ?-conjugated materials. Specifically, the basic concepts and principles of quantum theory, electrons, orbitals, bands, ground and excited states, excitons and charge carriers, charge carrier generation mechanisms, charge and exciton/energy transfers, are briefly discussed. Both exciton and band models are presented to illustrate electronic transitions

15. SUBJECT TERMS
Organic electronic, optical, optoelectronic materials, basic electronic structures, charge carrier generation and transports

16. SECURITY CLASSIFICATION OF:			17. LIMITATION OF ABSTRACT	15. NUMBER OF PAGES	19a. NAME OF RESPONSIBLE PERSON
a. REPORT	b. ABSTRACT	c. THIS PAGE			Sam-Shajing Sun
UU	UU	UU	UU		19b. TELEPHONE NUMBER 757-823-2993

Report Title

Chapter 3: Basic Electronic Structures and Charge Carrier Generation in Organic Optoelectronic Materials

ABSTRACT

This chapter briefly introduces some fundamental concepts and principles in a mainly qualitative way (for students with diverse backgrounds at the college senior level) related to electronic structures, energy and charge carrier transfers of electronic and optoelectronic materials, with emphasis on organic and polymeric ?-conjugated materials. Specifically, the basic concepts and principles of quantum theory, electrons, orbitals, bands, ground and excited states, excitons and charge carriers, charge carrier generation mechanisms, charge and exciton/energy transfers, are briefly discussed. Both exciton and band models are presented to illustrate electronic transitions, carrier generations, and carrier transport processes.

Chapter 3

Basic Electronic Structures and Charge Carrier Generation in Organic Optoelectronic Materials

Sam-Shajing Sun

Table of Contents

Abstract This chapter briefly introduces some fundamental concepts and principles in a mainly qualitative way (for students with diverse backgrounds at the college senior level) related to electronic structures, energy and charge carrier transfers of electronic and optoelectronic materials, with emphasis on organic and polymeric π-conjugated materials. Specifically, the basic concepts and principles of quantum theory, electrons, orbitals, bands, ground and excited states, excitons and charge carriers, charge carrier generation mechanisms, charge and exciton/energy transfers, are briefly discussed. Both exciton and band models are presented to illustrate electronic transitions, carrier generations, and carrier transport processes.

3.1 Introduction

Traditional or classic inorganic electronic and optoelectronic materials and devices have changed the way people live and think in the twentieth century. The development of classic and quantum mechanical theories, particularly the discovery and development of classic inorganic semiconductors and subsequent electronic/optoelectronic devices such as radios, telephones, televisions, integrated circuits and computers, has given birth to the human society of an “information age” and a “global village,” where the information is processed and transferred at the level and speed of electrons and photons. Nonetheless, the demand and motivation for faster speed, larger capacity, smaller size, lighter weight, flexible shape, and lower cost devices have driven people to pay attention to the rapidly developing organic- and polymer-based electronic and optoelectronic materials, particularly since the discovery of conducting polymers in the 1970s [1–3]. The 2000 Nobel prizes in chemistry (awarded to Alan G. MacDiarmid, Alan J. Heeger, and Hideki Shirakawa) manifested the progress and the potential of this field. There are similarities as well as differences between inorganic and organic semiconductors, and certain fundamental mechanisms of organic/polymeric optoelectronic processes are still under investigation and discussion. This chapter intends to introduce non expert readers to a brief account of the principles and concepts of both inorganic and organic semiconductors, and some basic concepts and principles on electronic structures and charge carrier generation mechanisms of mainly organic/polymeric semiconductors.

3.2 Electron States, Orbitals, and Bands

3.2.1 Electron States and Behaviour in Materials

The electronic and optoelectronic properties of a material are directly correlated to the electronic structure (or electron configurations) of the material, and how the material is perturbed (or excited) by external forces such as electromagnetic radiation, heat, pressure (or mechanical force), and steady-state electric or magnetic fields. One fundamental question is where and how the electrons are located in the material and how they behave and respond to external perturbations. For instance, if many free or mobile electrons in a material are simultaneously moving coherently toward one direction driven by an external applied electric field, this would form an electric current. In this case, the average or summed velocity of all electrons (also called drift velocity of electrons) would be nonzero [4].

Materials are typically made out of molecules—the basic building block of a material. Each molecule, in turn, is made up of atoms. There are over 110 different kinds of atoms also called elements discovered so far, and they are positioned in the periodic table according to their electronic structure [5]. An atom is composed of a nucleus (containing neutrons and positively charged protons) and negatively charged electrons surrounding the nucleus. Note that certain materials such as diamond, silicon, and metals are made up of a single type of atom. For a neutral atom, the number of protons in the nucleus is equal to the number of surrounding electrons, hence the materials appear neutral. A cation is a positively charged ion after a neutral atom loses electrons. Anions are negatively charged ions resulting after neutral atoms gain electrons.

According to modern quantum theory, an electron can be treated as both a particle and a wave, called wave–particle duality. And it can also be described by a space- and time-dependent wave function $\psi(x, y, z, t)$ or $\psi(\mathbf{r}, t)$ (also called eigenfunction) from the Schrödinger equations (or Schrödinger postulates) [5, 6]

$$\hat{H}\psi(\mathbf{r},t) = i\hbar\frac{\partial\psi(\mathbf{r},t)}{\partial t} \qquad (3.1)$$

Where $\hat{H}$ is a Hamiltonian operator in the form of

$$\hat{H} = -\frac{\hbar^2}{2m}\nabla^2 + E_{\mathrm{p}}(x, y, z, t) = -\frac{\hbar^2}{2m}\nabla^2 + E_{\mathrm{p}}(r, t) \qquad (3.2)$$

Where

E_{p} is the time- and space-dependent potential energy of the electron

m is the physical, rest, or free mass of the electron ($m = 9.1 \times 10^{-31}$ kg, as compared to the effective or dynamic mass m^* of the electron that can be either smaller or bigger than m depending on the electron interaction with the materials)

$\hbar$ ($\hbar = h/2\pi$) is the reduced Planck constant (also known as Dirac's constant, pronounced h-bar)

h is the Planck's constant

t is the time

Particle spatial position may be in Cartesian (x, y, z) or spherical ($\boldsymbol{r}$) = (r, θ, ϕ) coordinates. ∇^2 is the Laplacian operator or del-squared operator in the forms of

$$\nabla^2 = \frac{\partial^2}{\partial x^2} + \frac{\partial^2}{\partial y^2} + \frac{\partial^2}{\partial z^2} = \frac{1}{r^2}\left[\frac{\partial}{\partial r}\left(r^2\frac{\partial}{\partial r}\right) + \frac{1}{\sin\theta}\frac{\partial}{\partial\theta}\left(\sin\theta\frac{\partial}{\partial\theta}\right) + \frac{1}{\sin^2\theta}\frac{\partial^2}{\partial\phi^2}\right] \qquad (3.3)$$

For most problems concerning electronic structures of the materials, the stationary or time-independent state wave function $\psi(\boldsymbol{r})$ would be sufficient ($\psi(\boldsymbol{r}, t) = \psi(\boldsymbol{r})\exp(-iEt/\hbar)$), and the Schrödinger equation can therefore be simplified as

$$\hat{H}\psi(\boldsymbol{r}) = E\psi(\boldsymbol{r}) \qquad (3.4)$$

where E is the electron total energy (also called eigenvalue of ψ) expressed as

$$E(\boldsymbol{r}) = E_{\mathrm{p}}(\boldsymbol{r}) + E_{\mathrm{k}}(\boldsymbol{r}) \qquad (3.5)$$

where $E_{\mathrm{k}}(\boldsymbol{r})$ is the kinetic energy of the electron. The Hamiltonian operator now becomes

$$\hat{H} = -\frac{\hbar^2}{2m}\nabla^2 + E_{\mathrm{p}}(\boldsymbol{r}) \qquad (3.6)$$

In physics, the Schrödinger equation (proposed by the Austrian physicist Erwin Schrödinger in 1926) is of central importance in nonrelativistic quantum mechanics, playing a role for microscopic particles analogous to Newton's second law in classical mechanics for macroscopic particles. Microscopic particles include elementary particles, such as electrons, as well as systems of particles, such as atomic nuclei. Macroscopic particles vary in mass from small dust particles to heavy planets in the solar system. Though the Schrödinger equation cannot be derived, it can be shown to be consistent with experiments. The most valid test of a model is whether it faithfully describes the real world. The wave nature of the electron has been clearly shown in experiments like electron diffraction experiments [5–7].

For a free electron in space without any boundary conditions, by solving the Schrödinger equation (Equation 3.1), for instance, a time-dependent wave function of the electron in one dimension (x) can be in a form of

$$\psi(x,t) = A\mathrm{e}^{i(kx-\omega t)} \tag{3.7}$$

Where

A is a constant

$\boldsymbol{k}$ is called the electron wave vector that has the same direction as the electron momentum $\boldsymbol{p}$

The magnitude $|k|$ (called wave number) is related to the electron de Broglie wavelength λ by

$$|k| = \frac{2\pi}{\lambda} \tag{3.8}$$

Wave vector $\boldsymbol{k}$ in fact reflects traveling direction and momentum of an electron wave.

Also from the solutions of the Schrödinger equations, the total energy E of a free electron in space would be the same as its kinetic energy (since the potential energy is zero) and can be expressed as

$$E = \frac{\hbar^2}{2m}k^2 = \frac{p^2}{2m} \tag{3.9}$$

With

$$\boldsymbol{p} = m\boldsymbol{v} = \hbar\boldsymbol{k} \tag{3.10}$$

Where $\boldsymbol{v}$ is the electron velocity.

Equation 3.9 indicates that for a free electron in space without any boundary conditions, its energy is continuous as shown in Figure 3.1a.

Unlike in classic mechanics where the exact position and momentum of a moving object at a specific time can be determined simultaneously and precisely, in quantum mechanics, the exact position and momentum (or speed) of an electron cannot be determined simultaneously and precisely, and this is called Heisenberg uncertainty principle that can be mathematically expressed as [5]

$$\Delta\boldsymbol{r}\,\Delta\boldsymbol{p} \geq \hbar/2 \tag{3.11}$$

Where

$\Delta\boldsymbol{r}$ is the uncertainty of the position

$\Delta\boldsymbol{p}$ is the uncertainty of the momentum of the electron

Equation 3.11 implies that the product of the two uncertainties of an electron is at least $\hbar/2$.

Most importantly, the probability of finding an electron (or the electron probability density ρ) anywhere in the space can be expressed by [5]

$$\rho = \psi\psi^*(\mathrm{d}x\ \mathrm{d}y\ \mathrm{d}z) \tag{3.12}$$

Where ψ^* represents the complex conjugate of ψ (if ψ contains imaginary part). Since the electron probability density in the whole space is unity, the normalization condition requires

$$\int_{-\infty}^{\infty}\int_{-\infty}^{\infty}\int_{-\infty}^{\infty}\psi\psi^{*}\,\mathrm{d}x\,\mathrm{d}y\,\mathrm{d}z=1 \qquad (3.13)$$

Electron wave functions are typically obtained by solving the Schrödinger equations with certain conditions such as specific boundary conditions and the general normalization condition mentioned above. Additionally, for electrons moving around the nuclei, the much heavier nuclei are treated (or approximated) as static when deriving the electron wave functions. This is called Born–Oppenheimer or adiabatic approximation [5–7].

For an electron confined in an one-dimension potential well of size L with infinitely high potential barrier walls ($U = \infty$ as shown in Figure 3.2a and c), like a particle completely confined in a box (a "particle-in-a-box" case) or a bound electron in an atom as shown in Figure 3.3a, the electron wave function would become zero outside the potential well, i.e., $\psi(x) = 0$ for $x \le 0$ or $x \ge L$. By solving the time-independent Schrödinger equation, the electron wave function in one dimension box will be in the form of

$$\psi_n(x) = A_n \sin\left(\frac{n\pi}{L}x\right) \qquad (3.14)$$

Where n is a non-zero integer. The wave functions with n = 1, 2, and 3 are schematically shown in Figure 3.2a, and the corresponding electron probability densities are shown in Figure 3.2c. The total energy E of such a completely confined electron is in the general form

$$E_n = \frac{\hbar^2\pi^2}{2mL^2}n^2 \qquad (3.15)$$

Where the energy difference between two adjacent electron orbital energy levels (also called energy gap or E_g) can be in the general form

$$E_g = E_{n+1} - E_n = \frac{\hbar^2\pi^2}{2mL^2}(2n+1) \qquad (3.16)$$

Equation 3.15 reveals that for an electron completely confined in a box, only certain discrete energy levels (or orbitals) are allowed as shown in Figures 3.1b, 3.2a, and 3.3a. Since electrons in such an atom can only absorb or emit energies (or photons) among these discrete energy levels, therefore, only certain characteristic photon absorption and emission spectrum lines are allowed and shown in atomic spectra. This is the fundamental principle behind the atomic spectroscopy.

Equation 3.16 indicates that the energy gap (E_g) between two adjacent energy levels (*e.g.*, between n+1 and n levels) is inversely proportional to the square size of the box (or the electron delocalization square area of box with size L). This has become one of the most well-known features of the "particle-in-a-box" principle, *i.e.*, the larger the box size, the smaller the energy gaps of the particle in the box. This principle can be graphically illustrated in Figure 3.4, where the electron orbital levels are plotted versus the number of repeat units of a conjugated organic or polymeric molecular system. As Figure 3.4 illustrates, when the repeat units are small such as in small molecules or oligomers, energy gaps between each electron orbitals are relatively large. As the number of repeat units (corresponding to conjugation length or electron delocalization) increases, the energy gap between each adjacent energy levels, such as the energy gap E_g between the lowest unoccupied molecular orbital (LUMO) and the highest occupied molecular orbital (HOMO) decreases. Such E_g is essential for all

electronic and optical properties of the materials. The extreme case of a very big box or a large electron delocalization can be represented by delocalized electron bands such as occupied valence band (VB) and un-occupied conduction band (CB) in typical crystal semiconductors as shown in Figure 3.4. Such E_g versus conjugation size trends have already been experimentally demonstrated in organic thiophene oligomers (as illustrated in Figures 10.6 and 10.7 in chapter ten of this book).

For an electron confined in a one-dimension potential well of size L but with finite height potential barrier walls ($U = U_0$, shown in Figure 3.2b and d), similar to a bound electron in a two-atom system as shown in Figure 3.3b, the solutions to the Schrödinger equation give wave functions with exponentially decaying penetration into the classically forbidden region outside the potential well [6, 7]. The penetration of a potential barrier by an electron wave is called "tunnelling." Tunnelling is a quantum mechanical effect and has important applications such as tunnel diodes and tunnel electron microscope. Confining a particle to a smaller space requires larger confinement energy. Since the wave function penetration effectively "enlarges the box," the finite well energy levels are lower than those for the infinite well (Figure 3.2b and d).

For an electron in a two-atom molecule as shown in Figure 3.3b, while the lower energy electron orbitals near the nuclei may still be separated (or confined) by an interatomic electronic potential barrier, the higher atomic electron orbitals, particularly those orbitals with energy levels higher than the inter-nuclei potential barrier, may overlap and couple to each other depending on their spatial orientation and form new interatomic orbitals called molecular orbitals (MOs) (to be discussed in more detail later in this chapter), so that an electron from either atom can stay in the interatomic molecular orbital and move among the two atoms. This electron is said to be delocalized among the two atoms.

For an electron in a periodically structured atomic or molecular lattice (such as in a closely packed atomic or molecular crystal) with periodic or alternating potential wells and barriers as shown in Figure 3.3c, the potential $E_p(\boldsymbol{r})$ can be represented as

$$E_p(\boldsymbol{r}) = E_p(\boldsymbol{r} + \boldsymbol{R}) \tag{3.17}$$

Where $\boldsymbol{R}$ represents a spatial repeat unit. The solutions of the Schrödinger equation for the electron wave function ψ in such periodic potential is called a Bloch function, a Bloch wave, or a Bloch state in the form of [6, 7]

$$\psi_{\boldsymbol{k}}(r) = u_{\boldsymbol{k}}(r)\mathrm{e}^{ikr} \tag{3.18}$$

Where

e^{ikr} is a typical plane wave envelope function

$u_k(r)$ is a periodic function that has the same periodicity as the potential in a form

$$u_{\boldsymbol{k}}(\boldsymbol{r}) = u_{\boldsymbol{k}}(\boldsymbol{r} + \boldsymbol{R}) \tag{3.19}$$

The concept of the Bloch function was developed by Felix Bloch in 1928 to describe the conduction of electrons in crystalline solids. Equation 3.18 (also called Bloch equation or Bloch's theorem) implies that for an electron in a periodic electronic potential lattice, the electron wave function is also in a periodic form. More generally, a Bloch wave description applies to any wave-like phenomenon in a periodic medium. For example, a periodic dielectric in electromagnetism leads to photonic crystals (i.e., materials which exhibit band gaps for photons), and a periodic acoustic medium leads to phononic crystals (i.e., materials which exhibit band gaps for phonons—quantized modes of lattice vibration).

From mathematical solutions of the Schrödinger equation (Equation 3.4) and the Bloch equation (Equation 3.18), a set of discrete energy states $E_n(\boldsymbol{k})$ can be obtained, where n is an integer (n = 1, 2, 3, …) [6,7]. A plot of $E_n(\boldsymbol{k})$ versus $\boldsymbol{k}$ is schematically shown in Figure 3.5. As Figure 3.5 shows, at each n value, the electron energy (bold curves) can vary continuously along the electron wave vector $\boldsymbol{k}$ (also called $\boldsymbol{k}$-space) within a confined energy zone or band (between the two dashed lines) called "Brillouin zones" or "bands." The maximum vertical energy dispersion within each allowed electron bands (E_w in Figure 3.5) is called bandwidth (BW), and the minimum forbidden energy region between the allowed bands (E_g in Figure 3.5) is called band gap, energy gap, or stop band. It is a region where the electron is forbidden from occupying or propagating.

According to Fermi-Dirac statistics (equation 3.20 and Figure 3.6), in the absence of any energetic perturbations (*i.e.*, at absolute zero temperature and without any external radiations), all electrons shall be located at the lowest possible energy orbitals or bands. Thus, the highest electron completely occupied molecular orbital (*i.e.*, the highest orbital that is filled with two electrons with opposite spin) is called highest occupied molecular orbital (HOMO), and the lowest electron unoccupied molecular orbital (*i.e.*, the lowest orbital that is empty) is called lowest unoccupied molecular orbital (LUMO). Additionally, a single occupied molecular orbital (i.e., the orbital that has only one electron) is called SOMO. Additionally, from Bloch's theorem, HOMOs can overlap and couple to each other in a closely packed periodic structure to form HOMO bands, or stable valence bands (VB) if the bandwidths E_w are substantial (*i.e.*, above 0.1 eV) [8,9], and LUMOs (or SOMOs) can overlap and couple to each other in a closely packed periodic structure to form LUMO (or SOMO) bands, or stable conduction bands (CB) if the bandwidths E_w are substantial (*i.e.*, above 0.1 eV). Note that 1) the SOMO band is half filled resulting in a metallic or semi-metallic band (Figure 3.7), and 2) the effective orbital coupling and band formation require substantial matching and *overlapping* of coupling orbital energy levels, orbital spacing (or distances), orbital orientations and geometries, *etc*. For traditional crystalline insulators and semiconductors, the band gap generally refers to the energy difference (E_g) between the top of the valence band and the bottom of the conduction band (CB) as shown in Figure 3.5.

The ionization potential (IP) of a material is the energy necessary to bring the electrons from the uppermost occupied states, *i.e.*, HOMO, or the valence band maximum (VBM), to just outside the surface (or the vacuum energy level, E_{VAC}) with zero kinetic energy (Figure 3.5). The electron affinity (EA) is defined as the energy difference between the LUMO or conduction band minimum (CBM) and the E_{VAC}.

Electrons belong to a class of fundamental particles called fermions with half-integer spins. The probability $f(E)$ of a fermion at energy state E can be described by the Fermi-Dirac statistics or distribution function

$$f(E) = \frac{1}{e^{(E-E_{\mathrm{F}})/kT}+1} \qquad (3.20)$$

Where E_{F} is the Fermi energy level of fermions, k is Boltzmann constant, and T is absolute temperature. A plot of $f(E)$ versus E/E_{F} is schematically shown in Figure 3.6 for two different temperatures at 100K and 1000K. Clearly higher temperature would excite more electrons at higher energy states.

Based on equation 3.20, the Fermi energy level, E_{F}, of a material can be defined as 1) the HOMO level or valence band maximum (VBM) at absolute zero temperature (*i.e.*, $T=0$, $f(E)=0$ for $E>E_F$, and $f(E)=1$ for $E<E_F$), or 2) a hypothetical energy level with 50% probability of finding an electron occupying a state (an average valence electron state or level) at a thermodynamic equilibrium at any non-zero temperature state (when $T\neq 0$, $f(E)=0.5$ for $E=E_F$), or 3) the total chemical or electrochemical potential for electrons which is a thermodynamic quantity (work) required to add one electron to the body. In classic semiconductors with certain excitations or doping, the E_{F} level is typically located between the VB and CB depending on actual charge carrier densities and energy perturbations [4]. The work function is defined as the energy difference between the E_{F}, and the E_{VAC}. Figure 3.7(a) exhibits a general scheme of occupied (filled) and unoccupied (non-filled) electron

states or bands versus the density of states (DOS) for several classic materials including insulators, p-type semiconductors (p-SC), intrinsic semiconductors (i-SC), n-type semiconductors (n-SC), semi-metals, and metals at zero absolute temperature and without any energetic radiations. Figure 3.7(b) exhibits a general scheme of occupied (filled) and unoccupied (non-filled) electron states or bands versus the density of states (DOS) for same materials at non-zero absolute temperature or with certain energetic radiations. The Fermi level E_F of these materials is also indicated. At non-zero temperature and/or with certain energetic radiations, some electrons in occupied states can be excited to unoccupied states, and that would shift the E_F level up.

In most chemical reactions, and in most electronic and optoelectronic processes, it is predominantly the valence electron transfers between the HOMO, the LUMO, the SOMO, the VB, and the CB. These orbitals and bands are therefore also called frontier orbitals/bands, and the information such as energy levels, shapes, orientations, and spatial distances of the frontier orbitals/bands is very crucial for the electronic and optoelectronic properties of the materials.

Because bands are solutions of the Bloch equation, in order for the materials to form or exhibit electronic bands, it is crucial that the materials possess a periodic potential structure to satisfy the Bloch's theorem requirements. In most typical amorphous molecular or polymeric solids where the closely packed periodic potential structures are absent or very poor, it is not surprising that the bands are difficult to form or ever exist. However, in certain polycrystalline materials where both amorphous and crystalline domains coexist, bands may exist in the crystalline domains. Therefore, the band size (BS) may be defined as the average size of the actual periodic domain or path (or an effective conjugation size corresponding to the size a particle box) where Bloch function is applicable, and where electron transport is of coherent or tunnelling type. In a classic single crystal semiconductor, since the Bloch function can be applicable to the whole crystal (except the boundary or edge regions of the crystal), the band size is therefore roughly the same as the single crystal size. On the contrary, in the amorphous domains where the bands are poor or does not exist, charge transport follows incoherent or hopping mechanisms as will be discussed in detail in Chapter 4 of this book. The mean free path (MFP, l), or mean free distance (MFD) is defined in semiconductor physics as an average non-scattering (ballistic) electron transport length between two consecutive scattering centres as expressed by

$$l = v\tau \tag{3.21}$$

Where

v is the electron velocity

τ is the average electron transport relaxation time, also called mean free time (MFT), defined as the average time an electron travels between the two scattering centers [6,7]

3.2.2 Atomic Orbitals of Carbon Materials

By solving the Schrödinger equations for electrons surrounding a nucleus, similar to the case of an electron in a potential well, with either infinite or finite walls, it can be found that the electrons are located only in certain energetically and spatially discrete electron orbitals surrounding the nucleus, and the orbitals are subject to the confinement of the nuclear electronic potential wells (Figures 3.1 through 3.3). Each electron orbital is differentiated by its energy level, shape, and orientation as defined by the wave functions mentioned earlier. Such electron orbitals in atoms are called atomic orbitals (AOs). Also from the wave function solutions, each electron in an atom can be represented by a set of four unique quantum numbers [5,10]. These are the principal (or main shell) quantum number n (n = 1, 2, 3, …) representing the main energy level or main shell of an electron; the orbital (also known as the azimuthal, angular, or subshell) quantum number l (l = 0 for s-type orbital, l = 1 for p-type orbital, l = 2 for d-type orbital, …, $n-1$, etc.) representing the subshells or types of an electron orbital; the magnetic quantum number m_l (m_l = 0, ±1, …, ±l) representing the orientations (or angular momentum)

of an orbital along a specified axis; and the spin quantum number m_s (m_s = 1/2 or –1/2) representing the spin orientation or spin angular momentum of an electron. Table 3.1 summarizes these quantum states and numbers of an electron in an atom.

From particle physics and statistical mechanics, since electrons have half integer spin quantum numbers, they belong to a family of elementary particles called fermions. The energy/state distribution of fermions in traditional semiconductors can be described by the Fermi–Dirac statistics (see equation 3.20). Fermions are in contrast to another major family of elementary particles called bosons that have integer spin quantum numbers, such as photons. The energy/state distribution of bosons can be described by Bose–Einstein statistics.

The spatial shapes of the *s*-, *p*-atomic and sp^n (n = 1, 2, 3) hybrid atomic orbitals are schematically illustrated in Figure 3.8. In the figure, two different colors (dark and light) of the orbital lobes reflect the positive or negative phases of the electron wave function. The electron orbital shape roughly reflects the electron probability density as represented in Equation 3.12. As Figure 3.8 shows, the *s* orbital has a spherical symmetric shape with the same phase in all directions, while the *p* (including sp^n) orbital has a dumbbell shape with two lobes of different phases and sizes.

According to Pauli Exclusion Principle, no two identical fermions may occupy the same quantum state simultaneously. For electrons in a single atom, the principle states that no two electrons can have the same four quantum numbers, i.e., every electron must be unique. Therefore, each electron orbital in an atom can only accommodate a maximum of two electrons with opposite spins. Also from Aufbau principle and Hund's rule, at ground state, the electrons will first occupy lowest energy state, and will first fill different orbitals with same single spin electron each before filling the same orbital with two electrons of opposite spins. Thus, the maximum number of electrons in each main shell is $2n^2$. While there are unlimited number of AOs surrounding a nucleus, there are, however, limited number of electrons in an atom. For instance, in a neutral and stable isotope of carbon atom ^{12}C, there are six protons and six electrons, and the quantum numbers (or identity) of the six electrons in ground state can be represented by (n, l, m_l, m_s) as 1,0,0,1/2; 1,0,0,–1/2; 2,0,0,1/2; 2,0,0,–1/2; 2,1,0,1/2; 2,1,1 (or –1), 1/2; or can be simplified as $1s^2 2s^2 2p^2$. The silicon electron configuration can be represented as $1s^2 2s^2 2p^6 3s^2 3p^2$.

As stated earlier, in typical chemical reactions, including most electron transfer processes encountered in electronic and optoelectronic materials and devices, it is typically the valence or outer shell electrons (*e.g.*, the $2s^2 2p^2$ electrons in carbon), or the electrons at the frontier orbitals such as HOMOs and LUMOs, that are engaged in electron transfer and chemical bonding processes. The outer shell electrons are also called valence shell electrons or simply valence electrons, as these electrons are involved in forming valence chemical bonds during most chemical reactions [10]. For instance, each of the four valence electrons of the carbon (2,0,0,1/2; 2,0,0,–1/2; 2,1,0,1/2; 2,1,1 [or –1],1/2) couple with the one 1,0,0,1/2 electron of four hydrogen atoms forming a methane molecule, CH_4, where the four valence chemical bonds (also called σ bonds, or σ molecular orbitals) are formed connecting the carbon and four hydrogen atoms. While each σ bonding orbital contains two electrons, one from the carbon, and one from the hydrogen, yet the σ antibonding orbital is empty. Since the four valence electrons ($2s^2 2p^2$) in carbon are different, while experimentally the four valence bonds in CH_4 appear to be the same, in order to account for this, Linus Pauling proposed a hybridized orbital theory. In chemistry, hybridisation or hybridization is the concept of mixing atomic orbitals to form new hybrid orbitals suitable for the qualitative description of atomic bonding properties. In this methane case, for instance, hybridization theory postulated that during the CH_4 bonding formation process, the carbon 2*s* orbital hybridizes with three 2*p* orbitals forming a four equivalent (same energy and shaped) sp^3 hybridized atomic orbitals (HAOs, see Figure 3.9a), where each HAO contains one electron, and that the four sp^3 hybridized orbitals are in a tetrahedral geometry with an angle of about 109.5° between any two orbital lobes (Figure 3.9d). Mathematically, the four hybridized sp^3 orbitals can be derived by different linear combinations of the one *s* and three *p* orbitals (See Chapter 33 of this book for more detailed studies on this). Alternatively, the one carbon 2*s* orbital can hybridize with two 2*p* orbitals to form three equivalent sp^2 HAOs (Figure 3.9b) in a triangular plane geometry with an angle of 120° between any

two orbital lobes (Figure 3.9e). Finally, the carbon 2*s* orbital can also hybridize with one carbon 2*p* orbital to form two equivalent *sp* hybridized orbitals (Figure 3.9c) in a linear (180°) shape (Figure3.9f).

3.2.3 Molecular Orbitals of Carbon Materials

When two atoms are spatially very close to each other, and that substantial overlap (or coupling) of two AOs occurs, there is a possibility of two same electrons to coexist at the same location and at the same time, and this is prohibited from Pauli exclusion principle. Therefore, the two overlapped atomic orbitals split and form two new different energy (and shaped) orbitals called molecular orbitals (MOs). From mathematics, the linear combinations of any two atomic orbital wave functions can generate a pair of molecular orbital wave functions of different shapes and energy levels, one with energy level below the original atomic orbital level called bonding molecular orbital, and another with energy level above the original atomic orbital energy level called antibonding molecular orbital as shown in Figure 3.10 [5,10]. As shown in Figure 3.10a, when the two *s* atomic orbitals overlap in phase, a σ bonding molecular orbital is formed. When the two s atomic orbitals overlap or couple out of phase, a higher energy $\sigma*$ antibonding type orbital is formed. The amount of energy decrease in σ bonding molecular orbital is the same as the amount of energy raise in $\sigma*$ antibonding molecular orbital as shown in Figure 3.10b.

Likewise, as shown in Figure 3.11a, when the two *p* atomic orbitals overlap and couple in phase, a π bonding molecular orbital is formed. When the two *p* atomic orbitals overlap and couple out of phase, a higher energy $\pi*$ antibonding type orbital is formed. The amount of energy decrease in π bonding molecular orbital is the same as the amount of energy raise in $\pi*$ antibonding molecular orbital as shown in Figure 3.11b. Since the atomic valence electrons typically occupy only bonding molecular orbitals, the total energy of the molecular state would decrease in comparison to atomic state, the molecular states are therefore typically more stable than their atomic states.

Similarly, as shown in Figure 3.12a, when the lobes of two sp^n (n = 1, 2, 3) HAOs (or two *p* orbitals in horizontal orientation) overlap and couple in phase along the atomic centre axis, a lower energy level σ bonding molecular orbital is formed. When such overlap is out of phase, a higher energy $\sigma*$ type antibonding orbital is formed. The amount of energy decrease in σ bonding molecular orbital is the same as the amount of energy raise in $\sigma*$ antibonding molecular orbital as shown in Figure 3.12b.

Thus, the potential problem of two same electrons coexisting at the same spatial location is resolved. The molecular chemical structures of most carbon-based organic compounds are in fact formed from carbon sp^3 HAOs coupling to each other forming relatively stable σ single bonds, as the energy required to excite an electron from σ to $\sigma*$ level is much higher than typical thermal heating or UV–Vis level energies [10].

In some cases, certain valence electrons from atomic orbitals are not participating in molecular orbital formation or remain intact during molecular formation, such AOs in molecules are called nonbonding orbitals, and the electrons in it are called nonbonding electrons. In Figure 3.13, for instance, during the formation of ethanal molecule, the centre carbon atom uses one of its three sp^2 HAOs to couple with the one 1*s* AO of the left hydrogen atom forming a $\sigma1$ molecular orbital (or $\sigma1$ single chemical bond). The centre carbon atom uses its second sp^2 HAO to couple with one of the four sp^3 HAOs of the right side carbon forming the $\sigma2$ single bond. The remaining three sp^3 HAOs of the right side carbon each would couple with the 1*s* AO of three hydrogen and form three σ bonds. The centre carbon atom uses its third sp^2 HAO to couple with one of the sp^2 HAOs of top oxygen forming the $\sigma3$ bond. The remaining p_z orbitals in both centre carbon and top oxygen overlap and couple in direction normal to the triangular plane forming a π bond. Such two chemical bonds together (one σ and one π bond between the two atoms) is called a double bond and is typically represented by double lines as shown [10]. The two electron pairs remained in the two sp^2 HAOs of the top oxygen are called nonbonding or loan pair electrons, and their orbitals are also called nonbonding orbitals $n1$ and $n2$. During the formation of acetylene molecule as shown in Figure 3.13b, the two carbon atoms are in *sp* hybridization, each carbon uses one of its

two *sp* HAOs couple with the 1s electron of a hydrogen atom forming $\sigma 1'$ and $\sigma 2'$ bonds. The remaining *sp* orbitals from each carbon then couple to each other forming the C–C $\sigma 3'$ bond. Since each carbon now still has two *p* orbitals, and that the two *p* orbitals are orthogonal to each other in a plane normal to the C–C $\sigma 3'$ bond (e.g., assuming that the C–C $\sigma 3'$ bond is in *X*-axis or direction, the two *p* orbitals are called p_y and p_z orbitals). The coupling and overlaps of the p_y and p_z orbitals in the Y and Z directions formed two π bounds ($\pi 1'$ and $\pi 2'$) orthogonal to each other. Thus, a triple (alkyne) bound is formed, and ethyne (acetylene) molecule has a linear shape [10].

3.2.4 Electronic Structures and States of Representative Organic Materials

To illustrate the electronic structures of carbon-based materials, diamond and graphene are used here as examples. In the case of diamond as shown in Figure 3.14a, each carbon atom couples with four other carbon atoms via four sp^3 HAOs and forms four σ single chemical bonds in a tetrahedral three-dimensional (3-D) network. Due to the relatively large energy gap between the σ and σ^* orbitals of the C–C bonds (*i.e.*, energy gap of about 5.5 eV in diamond [7], much bigger than the typical energy perturbation at ambient condition such as room temperature and daylight of 0.02–3 eV), no electrons are expected to be excited and there are practically no free electrons at σ^* conduction band and no free holes at σ valence band. This explains why diamond is an insulator in pure form and at ambient conditions. This is in contrast to silicon (or Germanium) crystals where the energy gap between the conduction band and the valence band is much smaller on the order of 1–2 eV, *i.e.*, within daylight and ambient perturbation range, some electrons are excited from the valence band into the conduction band, so that semiconductors are formed. In the case of graphene (single layer graphite sheet, see Figure 3.14b), each carbon only couples with three other carbons to form σ bonds using three sp^2 HAOs, and thus a big carbon sheet or plane is formed. The remaining p_z orbitals on each carbon and normal to the carbon plane can overlap and couple with each other forming a two dimensional (2-D) π electron band (bands). If there are no any distortions or defects, the electronic band size may be regarded as the size of the entire graphene sheet. Due to the fact that each p_z orbital contains only one electron, and up to two electrons can be in one p_z orbital, so the π electron band is in fact theoretically half-filled like a metallic or semi-metallic band (as depicted in Figure 3.6). However, distortions, defects, and boundaries/edges of the carbon plane may break up such half-filled metallic band and yield energy gaps between conduction and valence band. In graphite, the interaction between graphene planes is rather weak, of the van der Waals type, and the overlap of wave functions on different planes is essentially non-existent. This explains why graphene or graphite is mainly conducting along the 2-D direction. Carbon nanotubes (CNTs) and fullerenes (C_{60} and derivatives) can be regarded to a certain degree as graphene sheets bent toward the shapes of tubes and spheres. In the case of fullerenes and CNTs, however, some carbon pentagons are necessary to mix with carbon hexagons in order to form a smooth sphere or tube surface. Since CNTs and fullerenes have half-filled π electron band in both curved and relatively flat geometries, metallic, semimetallic (expected in relatively flat domains), and gaped semiconducting domains (expected in curved domains) are expected and indeed are the cases (see Chapter 8 of this book).

In ethene (ethylene) molecule as shown in Figure 3.15a, each of the two carbons uses three sp^2 HAOs to couple with two hydrogens and one other carbon forming three σ bonds. The two remaining p_z orbitals on the two carbon atoms normal to the ethylene plane overlap and couple to each other forming a π bond as shown in Figure 3.15b, and the π bonding orbital is schematically shown in Figure 3.15c. For conjugated polymer polyacetylene (PA) shown in Figure 3.15d, like in ethylene, each carbon on PA backbone uses three sp^2 HAOs forming three σ bonds with one hydrogen and two other carbons in a triangular manner as shown in Figure 3.15e. If all C–H atoms are in the same plane without any backbone distortion or twist, all p_z orbitals normal to such plane could then well overlap and couple to each other forming a long one-dimensional (1-D) and half-filled π electron band similar to graphene as depicted in Figure 3.15e and f. If so, then the PA should be metallic along the backbone direction. In reality, however, due to the well-known Peierls distortion mechanism in all 1-D metals [6,7], every

adjacent p_z orbitals are paired on PA backbone forming a single-double bond alternating conjugated polymer backbone shown in Figure 3.15g and h, where the π bonding orbitals (HOMOs) couple to each other forming a HOMO band (or valence band), and the π antibonding orbitals (LUMOs) overlap and couple forming a LUMO band (or conduction band). The difference of the single and double bond length is called the bond length alternation (BLA). The BLA is expected to become zero in a perfect or undistorted spatial conjugation situation such as in benzene or graphene 2-D sheet where the bandwidth is largest and band gap is smallest. The BLA would become largest in distorted PA chain where the bandwidth is smallest, band gap is largest, and single and double bonds on the conjugated chain are well defined. The actual BLA would be between the two mentioned extreme cases depending on the extent of orbital overlaps and coupling, and those depending critically on factors such as PA backbone length (related to average polymer molecular weight, MW), backbone shape or geometry (*e.g.*, trans- versus cis-, flat or straight versus twisted or bent), backbone packing pattern or morphologies, *etc*. For instance, Figure 3.15j depicts two PA chains in a straight and geometry matched close packing pattern. If all PA chains are packed as in Figure 3.15j, then the BLA and band gap would be small, and band size and bandwidth would be large.

In general, the more ordered and less distorted packing of PA backbones, the more well-defined solid-state structural periodicity and better coupling between electronic orbitals of adjacent carbon sites, the weaker lattice thermal vibrations or less electron–lattice (electron–phonon) vibronic coupling (*i.e.*, at lower temperatures), the larger the bandwidth, and smaller the band gap (BG), the material's electronic properties are leaning more toward the "band regime", where the photo carrier generation may be the "primary mechanism" type and the carrier transport is dominated by coherent or band mechanism. On the contrary, the less ordered packing of PA backbones, the less defined solid-state structural periodicity and therefore the poorer electronic couplings between electronic orbitals of adjacent carbon sites, the more intense lattice thermal vibrations or stronger electron–phonon vibronic couplings (i.e., at higher temperatures), the smaller the bandwidth, the larger the band gap, the materials electronic properties are leaning more toward the "exciton regime", where the photo carrier generation would be the "secondary mechanism" type, and the carrier transport is dominated by incoherent (or hopping) mechanism [9]. Therefore, even for materials having the same molecular or chemical structures, different morphologies in solid state (*i.e.*, well-ordered crystalline versus disordered amorphous) or even temperatures may render the materials in either the band-like transport regime or exciton-like hopping transport regimes. For instance, the conductivity (σ, in unit of $\Omega^{-1}\text{cm}^{-1}$ or S cm^{-1}) of doped polyacetylenes (PA) can vary from about 0.01 $\Omega^{-1}\text{cm}^{-1}$ (*i.e.*, a semiconductor with AsF_5 doping and without stretching) all the way to about 100,000 $\Omega^{-1}\text{cm}^{-1}$ (*i.e.*, a metal or conductor with iodine doping and stretching). Figure 3.35 depicts a conductivity chart of some key materials [1–3]. The conductivity (σ) of a material is defined as

$$\sigma = qN\mu \qquad (3.22)$$

Where

q is the basic electronic charge unit of the mobile charge carriers

N is the number density of mobile charge carriers (in units of number of carriers per unit volume (*e.g.*, cm^{-3})

μ is the charge carrier mobility (in units of $\text{cm}^2\ \text{Vs}^{-1}$)

Carrier transport and modelling in organics are being reviewed in Chapter 4 as well as in Ref. [9].

While doping and defects/impurities in materials mainly affect the densities (N) of mobile charge carriers (to be elaborated in Section 3.3), the couplings and overlap of frontier orbitals (HOMOs or LUMOs) would affect the bandwidth and band gap, and that would critically affect the carrier transport mechanisms (either coherent or incoherent) and carrier mobility (μ). The dramatic conductivity differences of stretched and un-stretched PA films demonstrate the effects of molecular packing versus charge mobility. As a matter of fact, the estimated

best charge mobility (μ) of doped polyacetylene is in the range of 100–200 $cm^2 Vs^{-1}$, and this is in contrast to the measured charge mobility of 15,000 cm^2 Vs in graphite, and the measured charge mobility of 80,000–100,000 cm^2 Vs in single wall carbon nano tubes or CNTs [9].

While polyacetylene may be regarded as a conjugated 1-D metal subject to Peierls distortion (though ordered and close solid-state molecular packing may minimize the distortion), a graphite sheet or graphene can be regarded as a conjugated 2-D metal, though it is also subject to distortions and boundaries of the carbon plane. In the case of CNTs, due to a cylindrical 3-D shape, certain distortions of a plane in graphene 2-D sheet are in fact being restrained, and this may account for a better charge mobility of CNTs.

It was suggested at least 0.1 eV bandwidth is necessary for a band to be stable [8], *i.e.*, those materials with bandwidth less than 0.1 eV should be treated as in charge carrier hopping transport regime. While most organic semiconductors have bandwidths less than 0.1 eV, certain organic crystals have been observed to have bandwidth up to 0.2 eV [8]. These are in contrary to classic inorganic crystalline semiconductors that typically exhibit bandwidths of several electron volts [6,7]. While band regime could exist in certain carefully grown and processed organic crystals at low temperatures, the hopping regime is believed to be predominant in most organic or polymeric conjugated semiconductors, particularly solution processed polymers. It is also reasonable to expect both band domains and hopping domains coexist in a particular organic or polymeric semiconductor thin film due to coexistence of both crystalline and amorphous domains.

In addition to electronic orbitals and bands, the electron spin configurations or states are further represented by spin terms as listed in Table 3.2. Specifically, if there is a single unpaired electron, the spin quantum number (m_s) is one half, the sum (S) of spin quantum numbers is one half, the multiplicity ($2S + 1$) is 2, and the spin term is called a Doublet. If all electrons are paired, the spin quantum numbers are positive and negative one halves in equal quantities, so the sum (S) of spin quantum numbers is zero, the multiplicity ($2S + 1$) is 1, and the spin term is called a Singlet. If two unpaired electrons have the same spins (located in two different orbitals), the spin quantum numbers are two one-halves, so the sum (S) of spin quantum numbers is one, the multiplicity ($2S + 1$) is 3, and the spin term is called a Triplet.

Certain molecular self-assembly or aggregates also form special electronic states. H and J-aggregates are such examples. Specifically, J-aggregates (Figure 3.16a) are formed with the monomeric molecules arranged in one dimension such that the transition moment of the monomers is parallel and the angle between the transition moment and the line joining the molecular centres is zero (ideal case). The strong coupling of several self-assembled monomers results in a coherent excitation at lower energy or redshifted wavelengths relative to the monomer. In addition, the spectrum gets narrower and the vibrational coupling to the molecular modes will be largely absent. H-aggregates (Figure 3.16b) are again a 1-D arrangement of strongly coupled monomers, but the transition moments of the monomers are perpendicular (ideal case) to the line of centres. In contrast to the side-by-side arrangement of molecules in J-aggregates, the arrangement in H-aggregates is face-to-face. The dipolar coupling between monomers in H-aggregates leads to a higher energy gap or blue shift of the absorption band.

Experimentally, the absorptions (and emissions) for the H-aggregates would be blue shifted compared to non-aggregates, and the absorptions (and emissions) of the J-aggregates would be redshifted compared to non-aggregates. Typically, solid state or higher concentrations in solution at lower temperatures would favour aggregates formation, while dilute solutions in higher temperatures would favour non-aggregates (single molecular) state. Therefore, the typical aggregates component peaks should vary with these conditions.

In some cases the oblique orientation in molecular aggregates can also be observed. In this case the dipole-allowed transitions occur to both low and high energy states resulting in splitting of the radiation and absorption bands (see Figure 33.4 of this book). This situation was observed in Rhodamine 6G molecular aggregates and studied both theoretically and experimentally (see chapter 33 for more details).

Finally, excimers and exciplexes are examples of excited state aggregates [14]. An excimer (originally short for excited dimer) is a short-lived dimer composed of two identical molecules, at least one of which is in an electronic excited state. Excimers are often diatomic and are formed between two atoms or molecules that would not bond if both were in the ground state. The lifetime of an excimer is very short, on the order of nanoseconds. An exciplex is

similar except it is composed of two different molecules. Excimers or exciplexes are only formed when one of the dimer components is in the excited state. When the excimer/exciplex returns to the ground state, its components dissociate and often repel each other. The wavelength of an excimer/exciplex's emission is longer (smaller energy) than that of the excited monomer's emission. An excimer can thus be measured by fluorescent emissions.

3.3 Electronic Transitions and Carrier Generations

3.3.1 Electron Transfers and Electronic Transitions

3.3.1.1 Electron Transfers

In any electronic transitions involving an electron transfer process, e.g., an electron is transferred from an initial orbital to a final orbital (corresponding to a whole system electronic transition from an initial state to a final state) as occurres in many chemical and optoelectronic processes, the transition can be represented by an initial state function ψ_i and a final state function ψ_f. Assuming the transition is driven by a perturbation V, according to perturbation theory, the transition probability P_{if} can be expressed by [8]

$$P_{if} = \frac{1}{\hbar^2}\left|\langle \psi_i \,|\, V \,|\, \psi_f \rangle\right|^2 \left[\frac{\sin(\omega_{fi} t/2)}{\omega_{fi}/2}\right]^2 \qquad (3.23)$$

Where

t is the transition time

ω_{fi} is an angular frequency related to the transition energy $\hbar\omega_{fi}$ between the states i and f

$\langle \psi_i|V|\psi_f \rangle = V_{if}$ is called the electronic coupling matrix element of the electronic transition

If the final state has a continuum or distribution of states (*e.g.*, different vibrational levels) represented by a density of state $\rho(E_f)$, the transition probability per unit time, or the transition rate constant (often shortened as transition rate or electron transfer rate) k_{if} can then be expressed by the Fermi's Golden Rule as

$$k_{if} = \frac{2\pi}{\hbar}|V_{if}|^2\ \rho(E_f) \qquad (3.24)$$

The expression for the rate obtained within the Frank–Condon approximation factorizes into an electronic and a nuclear vibrational contribution as [8]

$$k_{if} = \frac{2\pi}{\hbar}|V_{if}|^2\ (\text{FCWD}) \qquad (3.25)$$

Where FCWD is the Frank–Condon-weighted density of states. When all vibrational modes are classical or at high temperatures regime (i.e., $\hbar\omega_i << kT$), the FCWD can be in the Arrhenius form of

$$\text{FCWD} = \frac{1}{\sqrt{4\pi\lambda kT}}\exp\left[-\frac{\Delta G^{\#}}{kT}\right] = \frac{1}{\sqrt{4\pi\lambda kT}}\exp\left[-\frac{(\Delta G^0+\lambda)^2}{4\lambda kT}\right] \qquad (3.26)$$

Where

λ is the total lattice/nuclei and surrounding media reorganization energy cost of the transition

$\Delta G^{\#} = (\Delta G^0 + \lambda)^2/4\lambda$ is the transition activation energy

ΔG^0 is the standard Gibbs free energy change from the initial to final states

This leads to the semi classical Marcus electron transfer equation

$$k_{if} = \frac{2\pi}{\hbar} |V_{if}|^2 \frac{1}{\sqrt{4\pi\lambda kT}} \exp\left[-\frac{(\Delta G^0 + \lambda)^2}{4\lambda kT} \right] \qquad (3.27)$$

When certain lattice vibrational modes of the final state (countering the electron transfer) are much stronger compared to electron thermal energy (i.e., $\hbar\omega_i >> kT$), the transition rate constant can then be better represented by Bixon and Jortner modified Marcus equation as

$$k_{if} = \frac{2\pi}{\hbar} |V_{if}|^2 \frac{1}{\sqrt{4\pi\lambda_s kT}} \sum_{n=0}^{\infty} \left\{ e^{-S_i} \frac{S_i^n}{n!} \exp\left[-\frac{(\Delta G^0 + \lambda_s + n\hbar\omega_i)^2}{4\lambda_s kT} \right] \right\} \qquad (3.28)$$

Where the reorganization energy is divided into classic (or solvent) contribution (λ_s) and a strong lattice vibrational mode contribution ($\lambda_i = n\hbar\omega_i$). The Huang–Rhys factor $S_i = \lambda_i/\hbar\omega_i$ is a measure of the electron–phonon interactions.

In fact, any additional driving or counter-driving forces affecting the electron transfer can also be taken into account. These forces may include electromagnetic radiation, thermal or mechanical forces driving the electron transfer (*e.g.*, "hot" initial state vibrational modes), electrical forces, magnetic forces, *etc*. Assuming ΔF to represent the sum of all those additional forces (driving force with negative signs and counter-driving forces with positive signs), the electron transfer rate constant in semi classic form could then be represented by

$$k_{if} = \frac{2\pi}{\hbar} |V_{if}|^2 \frac{1}{\sqrt{4\pi\lambda kT}} \exp\left[-\frac{(\Delta G^0 + \lambda + \Delta F)^2}{4\lambda kT} \right] \qquad (3.29)$$

By definition, in any electron transfer reaction or process, the electron donor (D) is the entity that donates (contributes) the electron during such process, and likewise, the electron acceptor (A) is the entity that accepts (captures) the electron during such process. The profiles of a donor/acceptor (D/A) pair (such as the relative frontier orbital levels) could be different in different electron transfer processes (e.g., excited state or ground state electron transfers), and a donor may become an acceptor in different electron transfer processes. In analogy, in an energy (or exciton) transfer process, the energy donor (D) is the entity that donates (contributes) the exciton, and likewise, the energy acceptor (A) is the entity that accepts (captures) the exciton. The profiles of an energy transfer D/A pair (including the relative frontier orbital levels) may be different in different energy transfer processes, and a donor may be an acceptor in different energy transfer processes.

Figure 3.17a exhibits a typical or classic scheme of Gibbs free energy potential profile and evolution versus the nuclear or lattice coordinates where an electron is transferred from an electron donor (D) to an electron acceptor (A) as represented by a reaction $D/A \rightarrow D^+/A^-$, and the reaction is accompanied by a system (including both donor and acceptor) standard Gibbs free energy reduction of ΔG^0 (driving force with a negative sign) and a reorganization energy cost of λ (counter-driving force with positive value) [11]. Q_r represents the nuclear/lattice geometry or coordinate of the initial or reactant state, $Q^\#$ represents the nuclear/lattice geometry or coordinate of transfer activation state, and Q_p represents the nuclear/lattice geometry or coordinate of the final or product state. $\Delta G^\#$ is the activation energy. Figure 3.17b shows a correlation between the electron transfer rate constant *k* versus the reaction standard Gibbs free energy change based on equation 3.26 of Marcus theory. As the figure shows, when $-\Delta G^0 = \lambda$ (or $\Delta G^0 + \lambda = 0$), *k* reaches its maximum and $\Delta G^\# = 0$. On the left side of the maximum

k value where k increases with $-\Delta G^0$, this is called normal region, where the electron transfer becomes faster with increasing driving force $-\Delta G^0$. However, on the right side of the maximum k value where electron transfer becomes slower with increasing driving force $-\Delta G^0$, this is called Marcus "inverted region", and this was somewhat unexpected in the early days [11]. In essence, Marcus theory predicts that electronic transition or electron transfer becomes fastest when all the driving and counter-driving forces are balanced.

In spatial domain, as shown in Figure 3.18, the electron transfer rate constant k correlates to the transfer distance r between the donor (D) and the acceptor (A) depending on the actual paths or mechanisms of the transfer process. For instance, in a coherent (super-exchange, tunnelling, or band-like) type electron transfer, where the electronic coupling between the donor and acceptor is strong and the electron scattering is weak, the transfer rate constant is correlated to the transfer distance by

$$k = k_0 \mathrm{e}^{-\beta r} \tag{3.30}$$

Where the coefficient β varies in a range of 0.2–1.4 depending on the systems under consideration [12]. In an incoherent (or hopping) style electron transfer, where the electronic coupling between the donor and acceptor is relatively weak and the electron scattering is strong, the transfer rate is correlated to the transfer distance by

$$k = \frac{k_0}{r} \tag{3.31}$$

In the hopping case, the electron transfer rate may be approximated by Marcus electron transfer model [8,9], or approximated by Abbrium–Miller model (see Chapter 4).

The correlation of materials conductivity versus temperature are critically related to the two major types of charge transport mechanisms as schematically shown in Figure 3.19, where in the coherent or band-like charge transport case at relatively low temperature, increasing temperature would result in lower conductivity due to increasing thermal or lattice vibration would interrupt the electronic orbital coupling or band structure for the coherent electron transport. In the case of incoherent or hopping charge transport case, increasing temperature would result in higher conductivity due to thermal or lattice vibration would facilitates the charge hopping.

Electron transfer rate is essential to many chemical, physical, and biological processes, particularly electronic and optoelectronic properties of many molecular materials systems.

3.3.1.2 Electronic Transitions

Using a simple diatomic molecular system as an example, the potential energy surfaces of ground (S_0) and first excited (S_1) states versus the diatomic nuclear distance can be schematically represented as top-distorted parabola (also called the Morse potential) curves as shown in Figure 3.20 [5]. The horizontal lines (labelled as ν_n, ν'_n, ν''_n, where $n = 0, 1, 2, ...$) within each potential wells represent different vibrational energy levels. From quantum mechanics and by treating the diatomic molecular system as a harmonic oscillator (particularly near the bottom of the potential well), the vibrational energy levels E_ν can be represented by

$$E_\nu = \left(\nu + \frac{1}{2}\right) h\nu_o \tag{3.32}$$

where

ν is the vibrational quantum numbers ($\nu = 0, 1, 2, \ldots$)

ν_o is the fundamental frequency of the vibration between the two nuclei

Figure 3.20 illustrates that the potential energy minimum of ground (S_0) and first excited (S_1) states can be at different nuclear coordinates (*e.g.*, different inter-nuclear distance in a simple diatomic system). Both the typical intra-molecular vibrational modes (represented by v_n and v'_n), and an inter-molecular vibrational mode (represented by v'_0, due to excited state molecular aggregates) are shown. According to the Frank–Condon principle [5], an electronic transition typically proceed in a vertical transition manner (i.e., transitions $v_0 \rightarrow v'_1$ or $v'_0 \rightarrow v_1$ as shown in Figure 3.20), so that the nuclear coordinates essentially remain static during the initial ultra-fast electronic transition or electron transfer. If we apply Equation 3.29 to the case of a photo driven electron transfer (or transition), for instance, the photon driving force would be $\Delta F = -h\nu$. Assuming all nuclear vibrational modes are classical ($\hbar\omega_i << kT$), the rate (or intensity) of the transition would therefore be proportional to the energy factor exp $[-(\Delta G_0 + \lambda - h\nu)^2/4\lambda kT]$, which would yield a Gaussian bell-shaped photo absorption peak, where the peak maximum corresponds to $h\nu = \Delta G^0 + \lambda$, and the low energy edge of the absorption peak could be used to estimate the potential energy gap ΔE of the system under certain approximations.

Once the molecule is at v'_1 level in S_1 state, it typically relaxes to the lower and more stable v'_0 level and geometry in S_1 state, called exciton vibronic relaxation, also called Kasha's rule. Relaxation/decay from excited S_1 state to ground S_0 state is also vertical, *i.e.*, it may proceed between different vibrational levels if ground and excited states have different potential minimum (*e.g.*, from v'_0 level in S_1 state to v_1 level in S_0 state shown in Figure 3.20). Excited state relaxation can be either radiative, *i.e.*, via emitting photons, or non-radiative decay, *i.e.*, via lattice thermal relaxation.

The excitation or absorption processes can be characterized by various absorption spectroscopic techniques (such as UV–Vis) in different electromagnetic energy ranges corresponding to the absorption energy, and the decay processes can also be studied by various emission spectroscopic techniques (such as fluorescence if the decay is radiative in UV–Vis region).

Figure 3.21 schematically depicts idealized absorption and emission mirror peak bands with component peaks representing either vibrational or aggregates modes. To determine if a component peak comes from vibrations or aggregations, spectroscopic concentration or temperature-dependent experiments can be performed, as aggregate peaks are more intense in the solid state or higher concentrations in solution and at lower temperatures.

Stokes shift refers to the energy difference (or the redshift) of the emission spectrum peak versus the absorption spectrum peak (see Figure 3.21) [5]. In addition to vibrational relaxations that contribute to the Stokes shift, in solid states, several other factors can also contribute to the Stokes shift, for example, any lattice structural reorganizations (or electronic polarization changes) after electronic transitions, aggregates (J- or H-type), or any excimers/exciplexes formations. Note if the potential energy surfaces of the ground and first excited states are the same or similar in shape, then the Stokes shift (which is in fact the sum of reorganization energies of both absorption and emission between S_0 and S_1 states) becomes about twice the magnitude of the reorganization energies in either $v_0 \rightarrow v'_1$ or $v'_0 \rightarrow v_1$ transitions (Figure 3.20).

In addition to the basic two-level electronic transitions described above, other major types of transitions are also encountered often. Those include transitions at higher excited state levels (also called super-excitations), intersystem crossing transitions, collisional quenchings, internal conversions, etc. All those transitions can be summarized in a Jablonski's diagram as shown in Figure 3.22 [5]. In this figure, S_0 represents the system ground state, S_1 represents the first excited state, S_2 represents the second excited state, and T_1 represents the first triplet state. 1a and 2a represent absorptions to S_1 and S_2 states; 1b and 2b represent vibrational and structural relaxations within S_1 and S_2 states; 1c and 2c represent singlet excited state emissions or fluorescence of S_1 and S_2 states; 1d represents an intersystem crossing from S_1 to T_1 state, i.e., a singlet exciton becomes a triplet exciton via an electron spin flip; 2d and 3d represent transitions from S_2 to S_1 states via either collision (2d) or internal conversion/structural relaxation (3d); and 1e represents radiative relaxation from the triplet exciton state T_1 to the singlet ground state S_0. Since this T_1–S_0 transition requires a spin flip coupled with an exciton relaxation, the process is somewhat hindered as compared to a singlet decay, therefore, such radiative decay (also called phosphorescence emission) is a much slower process compared to the singlet fluorescence emission in 1c and 2c. Alternatively, the S_1 exciton can relax to ground S_0 state via

non-radiative mechanisms, such as thermal or structural relaxations. In these processes, heat instead of light would be released.

Light absorption or intensity attenuation on propagating through a material or an optical media can be described by Beer-Lambert law (or Beer's law). In a solution media, Beer's law can be expressed as

$$T = \frac{I}{I_o} = 10^{-A} \qquad (3.33)$$

And

$$A = \alpha l = \varepsilon c l \qquad (3.34)$$

Where T is the light transmittance through a solution media with materials concentration c and a light propagation length of l, I_o is the light intensity when entering the media, I is the light intensity when exiting the media, A is the light absorbance, α is the light absorption coefficient ($\alpha=\varepsilon c$), and ε is the light absorption extinction coefficient (or molar absorptivity). Both transmittance T and absorbance A are unit less and can be measured directly from a UV-Vis spectrophotometer. If the solution concentration c is in unit of M (Molarity = Moles/Litter), length l is in unit of centimetre (cm), the absorption coefficient α would then have a unit of cm^{-1}, and the absorption extinction coefficient ε unit would be $M^{-1}cm^{-1}$.

In general, the electronic transitions of valence electrons in molecules such as organic compounds can be measured by UV/Vis spectroscopy provided that the excitation energy gap E_g is in the UV or visible range of the electromagnetic radiation range for these compound. For instance, electrons residing in the HOMO of a sigma bond can be excited to the LUMO of that bond. This process is denoted as $\sigma \rightarrow \sigma^*$ transition. Likewise, promotion of an electron from a π bonding orbital to an antibonding π^* orbital is denoted as $\pi \rightarrow \pi^*$ transition. Auxochromes (a group of atoms such as –OH, $–NH_2$, and aldehyde groups attached to an organic chromophore that modifies the ability of that chromophore to absorb light) with loan pair electrons denoted as n have their own transitions, as do aromatic π bond transitions. The following molecular electronic transitions are quite common:

- $\sigma \rightarrow \sigma^*$
- $\pi \rightarrow \pi^*$
- $n \rightarrow \sigma^*$
- $n \rightarrow \pi^*$

In addition to these assignments, electronic transitions also have the so-called bands associated with them. The following bands have been reported in literature: the R-band from the German *radikalartig* or radical-like, the K-band from the German *Konjugierte* or conjugated, the B-band from benzoic, and the E-band from ethylenic (system devised by A. Burawoy in 1930). For example the absorption spectrum for ethane shows $\sigma \rightarrow \sigma^*$ transition at 135 nm and that of water shows $n \rightarrow \pi^*$ transition at 167 nm with an absorption extinction coefficient of 7000. Benzene has three aromatic $\pi \rightarrow \pi^*$ transitions; two E-bands at 180 and 200 nm and one B-band at 255 nm with absorption extinction coefficients of 60,000, 8,000, and 215, respectively. These absorptions are not narrow bands but are generally broad because the electronic transitions are superimposed on the other molecular energy states. Additionally, many colored dye molecules or chromophores (such as porphyrin dyes with their core chemical/electronic structures similar to that of Chlorophylls which are the green colored pigment in natural plants) typically exhibit two major electronic absorption bands, one lower energy absorption band between

500-800 nm called Q-band, and one higher energy band between 200-500 nm called B-band, S-band, or Soret band. For instance, in the UV-Vis absorption spectra of Chlorophyll-a and Chlorophyll-b as shown in Figure 3.23a, the Q band peaks appear between 600-700 nm and the B, S, or Soret band peaks appear between 400-500 nm. The optical excitation energy gap E_g for Chlorophylls are estimated from its Q band lower energy onset of about 700 nm (1.8 eV). Solar irradiation spectrum is shown in Figure 3.23b, where the top curve exhibit air mass zero (AM0) solar spectrum at top of the atmosphere, and the lower curve exhibits air mass 1.5g (AM 1.5g) solar spectrum at sea level. As Figure 3.23 illustrates, Chlorophylls exhibit intense green color due to their absorption of other colors in visible spectrum except the green sunlight photons.

The electronic transitions of molecules in solution can also depend strongly on the type of solvent with additional bathochromic shifts (a change of spectral band position in the absorption, reflectance, transmittance, or emission spectrum of a molecule to a longer wavelength or lower frequency, also called red shift or hypochromic shifts (a change of spectral band position in the absorption, reflectance, transmittance, or emission spectrum of a molecule to a shorter wavelength or higher frequency, also called blue shift). As briefly mentioned earlier, molecular aggregates in both solution and solid states would also cause bathochromic or hypochromic shifts depending on the nature and type of the aggregates.

3.3.2 Carrier Generation Mechanisms

3.3.2.1 Excitons Versus Charge Carriers

When an energy matched photon hits a semiconductor, an exciton is usually first formed as shown in Figure 3.24. An exciton is a bound state of an electron and an imaginary particle called hole (a vacant site of an electron with one positive charge), and thus is also called a correlated electron–hole pair. Correlated means free electron spins are not detectable via the electron spin resonance (ESR) or electron paramagnetic resonance (EPR) even if the excited single electron is at the LUMO orbital, and one remaining single electron is at HOMO orbital after the excitation. Exciton is a quasi-particle. A quasiparticle refers to a particle-like entity arising in certain systems of interacting particles. It can be thought of as a single particle moving through the system, surrounded by a cloud of other particles that are being pushed out of the way or dragged along by its motion, so that the entire entity moves along somewhat like a free particle. Excitons are integer spin particles thus obeying Bose statistics in the low-density limit. An exciton can diffuse in the material from one site to another called exciton diffusion or more frequently called energy transfer process (to be described in detail later). Excitons can be treated in two limiting cases that depend on the properties of the material in question.

In a classic or traditional inorganic semiconductor as shown in Figure 3.24a, the dielectric constant is generally large, and as a result, charge screening effectively reduces the Coulomb interaction between electrons and holes of the photo generated excitons. The end result is a relatively large Wannier–Mott (or Wannier) type exciton (with typical size over 10 nm) much larger than the typical lattice nuclear spacing. As a result, the effect of the lattice potential can be incorporated into the effective mass of the electron and hole, and because of the lower effective masses and the screened Coulomb interaction, the exciton binding energy (E_B), *i.e.*, the minimum energy required to dissociate an exciton into a free (or uncorrelated) electron and a free hole is relatively small (typically much less than 0.01 eV in Wannier type exciton), therefore, thermal energy of an electron ($E_T = kT$ = 0.025 eV at room temperature, or thermal phonon energy $\hbar\omega$) would be sufficient to dissociate the Wannier type excitons (Figure 3.25).

The Bohr radius (r) or average size of an exciton in a semiconductor can be expressed by [6,15].

$$r = r_0 \varepsilon \left(\frac{m}{m^*} \right) \qquad (3.35)$$

where

r_0 is the Bohr radius of hydrogen or atomic unit of length (about 0.053 nm)

ε is the dielectric constant of the materials

m and m^* are the rest (or free) and dynamic (or effective) mass of the electron, respectively

The concept of effective mass m^* is used because an electron would appear either heavier or lighter in a solid-state material depending on the interactions between the electron and the phonon, and it can be expressed by [6,7]

$$m^* = \frac{F}{\left(\frac{\mathrm{d}v}{\mathrm{d}t}\right)} = \frac{\hbar^2}{\left(\frac{\mathrm{d}^2 E}{\mathrm{d}k^2}\right)} \qquad (3.36)$$

Where

F is the net driving force

v is the velocity

E is the energy

k is the wave number of the electron

Equation 3.36 shows that the effective mass is inversely proportional to the curvature of the electron energy bands (E–k curve).

In general, the effective mass of the electron would become bigger with smaller charge delocalization or larger energy gap of the materials. For instance, the charge delocalization is typically smaller in organic semiconductors as compared to inorganic semiconductors, therefore, the electron effective mass is much bigger in organic semiconductors than in inorganic semiconductors. Additionally as mentioned above, the dielectric constants (ε) of organic semiconductors are generally smaller than inorganic semiconductors, and this results in poorer charge screening in organics. Both factors contribute to the average smaller exciton size of organic semiconductors as reflected in Equation 3.35. Finally, the Columbic potential E_c is inversely proportional to both the exciton size and the dielectric constant of the material as represented by

$$E_c = -\frac{e^2}{4\pi\varepsilon\varepsilon_0 r} \qquad (3.37)$$

A plot of E_c versus the exciton radius or size r is shown schematically in Figure 3.25, where the typical inorganic Wannier type exciton are larger than 10 nm and their Columbic potential or exciton binding energy (E_B) are generally less than the room temperature thermal energy (kT = 0.025 eV). On the other hand, the typical organic Frenkel type excitons generally have a size of less than 2 nm and their Columbic potential or exciton binding energy (E_B) are typically over the room temperature thermal energy (kT = 0.025 eV).

Thus, in typical inorganic semiconductors and at room temperature, the photo generated free electrons would be delocalized and traveling in the conduction band (CB), and the photo generated free holes would be delocalized and traveling in the valence band (VB). Both free electrons and holes (also called mobile charged carriers, or simply carriers) can be regarded as generated directly from photo excitations in inorganic semiconductors. Free, uncorrelated, or mobile electrons and holes imply the electrons and holes can each move independently as individ-

ual particles and each can be detected by ESR. This is why free charge carrier photo generation in classic inorganic semiconductors is called primary photo carrier generation mechanism, and is also termed VB–CB transitions or simply band-to-band transitions [6,7].

In most organic and polymeric semiconductors as shown in Figure 3.24b, the dielectric constant is generally much smaller than in inorganics, as a result, the Coulomb interaction between electron and hole of an exciton becomes very strong, therefore, a much smaller sized (mostly <2 nm) Frenkel-type exciton (also called exciton–polaron due to significant polarization and lattice distortion) is formed upon photo excitation [13–15]. The exciton orbital levels are within the LUMO/HOMO gap as shown in Figure 3.24b [13]. The exciton–polaron binding energy is relatively large (E_B is in the range of 0.1–1.5 eV [2,3,13–15]), *i.e.*, thermal energy of electron at room temperature kT, or lattice thermal vibration/phonon energies ($\hbar\omega$) would not be sufficient to dissociate a Frenkel-type exciton, therefore, additional or secondary forces are needed in order to dissociate a Frenkel-type exciton into free electrons and holes [15]. This is why photo carriers in organics are generated mostly via a secondary photo carrier generation mechanism, also called photo doping mechanism referring a photo-induced charge separation [15].

In organics, free electron charge carriers are also termed electron–polarons or negative polarons; and free holes are also termed hole–polarons or positive polarons. Polarons are defined due to an electron or a hole in organics typically induces a relatively large local polarization (also called induced or transient dipoles) and lattice distortion. The carrier together with the induced polarization is considered as one entity, which is called a polaron. Polaron is originally defined as a quasiparticle composed of a charge plus its accompanying polarization field. The resulting lattice polarization acts as a potential well that hinders the movements of the charge, thus decreasing its mobility. For instance, a slow moving electron in a dielectric crystal interacting with lattice ions through long-range forces will permanently be surrounded by a region of lattice polarization and deformation caused by the moving electron. Moving through the crystal, the electron carries the lattice distortion with it, thus one may speak of a cloud of phonons accompanying the electron. The polaron LUMO/HOMO levels are located between the pristine molecular LUMO/HOMO levels (see Figure 3.35) [13,14].

Finally, orbitals higher than LUMOs can also participate in the exciton formation (also called super-excitation), and this would lead to the formation of different types of excitons in the same material as demonstrated in some ultrafast two-photon absorption experiments.

Figure 3.26 schematically exhibits ground state S_0, photo excited exciton state S_1, and exciton dissociated (or charge separated) state S_1' of a general molecular system in (a) frontier orbital representation and (b) free energy representation (Note the free energy can be represented by a single lattice coordinate, while the potential energy has multi-coordinates for a polyatomic molecular system. Also, the free energy change could approximate the potential energy change when the entropy change is small or negligible). Here, the main difference between S_1 and S_1' states is that, in S_1 or exciton state, the electron at LUMO is strongly correlated with the hole at HOMO, such that this exciton diffuses as one single quasiparticle. The S_1 state may also be an excimer or an exciplex as described earlier. While in S_1' or charge separated state, the electron at LUMO is regarded as uncorrelated to the hole at HOMO, so that electrons and holes can each diffuse separately as two independent or free charge carriers. Please note that in Figure 3.26a, the two schematic HOMO/LUMO pairs may not necessarily be immediately adjacent to each other, i.e., a certain spatial distance or several atomic/lattice sites may exist between the two charges.

Figure 3.26b schematically exhibits system free energy surfaces for the three states. In the figure, the energy gap, E_g (also called optical excitation energy gap) between S_0 and S_1 states can be experimentally estimated from the absorption band edge of typical UV–Vis spectrum. λ_1 is the reorganization energy of the $S_0 \rightarrow S_1$ transition and λ_2 is the reorganization energy during the $S_1 \rightarrow S_1'$ transition. Since the $S_1 \rightarrow S_1'$ transition is mainly exciton dissociation, the free energy gap between S_1 and S_1' states is mainly the exciton columbic binding energy E_c. Therefore, the electronic energy gap between S_0 and S_1' states is

$$E_g^{'} = E_g + E_c \qquad (3.38)$$

Based on semi-classical Marcus model, the magnitude of optimal driving force for the $S_1 \rightarrow S_1'$ transition appears to be

$$E_B = \lambda_2 + E_c \qquad (3.39)$$

Where E_B approximates the total exciton binding energy. As mentioned earlier, for most organic or polymeric noncrystalline semiconductors, room temperature thermal energy would not be sufficient to overcome E_B, additional force (or energy) is therefore needed in order to dissociate a Frenkel-type exciton into free charge carriers, the so-called secondary photo carrier generation mechanism [15]. The extra force or energy can be from externally applied electric fields, high temperature thermal energy, and in most cases from the frontier orbital level offsets between an electron donor and an electron acceptor (such as LUMO offset δE) as shown in Figure 3.27a [15]. As Figure 3.27a shows, the frontier orbital energy offset (δE—the energy difference between D-LUMO and A-LUMO) is in fact a key driving force to overcome E_B in order to incur the excited state electron transfer from the donor to the acceptor, as the D-LUMO $\rightarrow$ A-LUMO transition (exciton dissociation) is typically much faster than the D-LUMO $\rightarrow$ D-HOMO transition (exciton decay) [16]. This is somewhat analogous to a p/n junction as shown in Figure 3.27b where the electric field at the p/n junction facilitates the electron and hole separation, where electrons are pushed from the p-type semiconductor into the n-type semiconductor, and holes are pushed from n-type semiconductor into the p-type semiconductor [6,7]. However, while free charge carriers (electrons and holes) are generated in either p- or n-type traditional semiconductors, mainly neutral exciton or electron-hole polaron pair are generated in organic donor or acceptor phases. Therefore, a donor/acceptor interface appears essential for photo charge carrier generation in typical organic optoelectronic such as photovoltaic devices [15, 16].

3.3.2.2 Photo Doping (Photo-electric Processes)

The photo-induced charge separation due to the presence of a donor (D)/acceptor (A1) pair (a weak D/A pair with weak coupling WC) is also called photo doping (or photo-electric) process as schematically illustrated in Figures 3.27a, 3.28a, 3.29, and 3.33a. Specifically, in the photo doping process, the A1-LUMO is close and slightly lower than the D-LUMO, the free energy difference (ΔE_1) for the D-LUMO $\rightarrow$ A1-LUMO electron transfer could be optimum (*e.g.*, $\Delta E_1 = \lambda_1$ as exhibited in Figures 3.28a and 3.29), so that such transition can be much faster than the donor exciton decay (*i.e.*, electron transfer from D-LUMO to D-HOMO) [16]. Note if the D-HOMO/A-LUMO coupling is stronger than D-HOMO/D-LUMO (such as in the thermal or chemical doping cases shown in Figures 3.28b-c, 3.30, 3.31, 3.32, and 3.33c), then photo (or thermal) driven electron transfer from D-HOMO to A-LUMO may proceed directly to form an inter-molecular uncorrelated or weakly correlated charge pair. This is a strong donor/acceptor pair with weak coupling (WC) case as exhibited in Figure 3.33c and is the predominant charge carrier generation mechanism in chemical or thermal doping processes.

3.3.2.3 Chemical/Thermal Doping (Chemo-electric/Thermo-electric Processes)

In the donor (D)/acceptor (A2) incurred chemical doping (chemo-electric) or ground state charge transfer process (strong D/A pair with weak electronic coupling) as schematically shown in Figures 3.28b and 3.30, the LUMO of the acceptor (A2) is a little lower and weakly coupled to the HOMO of the donor (D), so the electron can transfer directly from the D-HOMO to the A2-LUMO even without any external energetic perturbation or driving forces [16,17]. For instance, in case the LUMO of A2 is lower than the HOMO of D, the free energy driving force ΔE_2 due to D-HOMO/A2-LUMO orbital offset could become optimum (*e.g.*, $\Delta E_2 = \lambda_2$ as shown in

Figure 3.30) to drive a ground state electron transfer at even absolute zero temperature [16]. At non-zero temperature, even if the LUMO of acceptor is the same or slightly higher than the HOMO of D, electron transfer would still proceed due to thermal doping (thermos-electric) process as schematically shown in Figures 3.28c, 3.31, and 3.32 [6,16,17]. Though the transfer rate due to thermal doping may be very low due to weak driving forces, however, once such transfer occurs, and if the donor is a minority dopant dispersed in the majority acceptor phase as shown in Figures 3.32 and 3.34b, the left over hole is trapped at the donor dopant site, and the free or mobile electron (negative polaron) can diffuse away in the acceptor LUMO band forming a n-type semiconductor (or a conductor, depending on the carrier density and mobility). The donor dopant, or any donor type impurity or defect site, can also be called the hole trap. Figure 3.32 further illustrate that, once the electron transferred from the D-HOMO to the A-LUMO as a result of heat or ΔT, it can move away from the donor dopant site in the acceptor LUMO band due to both mobile electron density or chemical potential gradient or a temperature gradient ΔT. Such electron transport or migration in the material would result a spatial voltage ΔV as shown in Figure 3.32c. The thermoelectric Seebeck coefficient (S), the thermal power factor (TPF), and a figure of merit (ZT) of thermal electric materials are defined as

$$S = \Delta V / \Delta T \tag{3.40}$$

$$TPF = S^2\sigma \tag{3.41}$$

$$ZT = S^2\sigma\, T/\kappa \tag{3.42}$$

Where σ is the electrical conductivity, and κ is the thermal conductivity (see Chapter 32 of this book 2nd edition for more details). Clearly, in order to increase the Seebeck coefficient and other thermoelectric properties, it is crucial to 1) increase thermal doping generated charge carrier density which contribute to both ΔV and σ, and 2) improve electron transport or the acceptor LUMO bandwidth E_w that also contribute to both ΔV and σ. Thermal doping generated electron density is proportional to the thermal incurred electron transfer rate which in turn are related to the driving forces such as ΔT and the counter driving forces such as ΔE_3 and λ_3 (Figure 3.31).

If the acceptor is the minority dopant dispersed in the majority donor phase, then the free and mobile hole (positive polaron) thus diffuses in the donor HOMO band, and the electron at acceptor LUMO is trapped forming an p-type semiconductor as shown in Figure 3.34c (or a conductor depending on the density and mobility of the carriers). The acceptor dopant, or any acceptor type impurity or structure defect, can therefore be called an electron trap. Certainly, the separated electrons and holes can still recombine as well. If the pair of recombining electron and hole is from the same original orbital or pair, it is called geminate pair and the recombination is called geminate recombination. If the pair of recombining electron and hole is not from the original pair, it is called non-geminate pair and the recombination is called non-geminate recombination [13].

Chemical doping can also be described in a classic way in certain systems [6, 7]. For instance, when each atom (or nuclear site) has four valence electrons in its HOMOs in the majority phase, and the minority dopant has five valence electrons (donor type) in its HOMOs, four valence electrons from the dopant would couple with four valence electrons from the nearby four majority nuclei filling four new HOMO bonding orbitals. The fifth or the left over valence electron from the dopant can then be easily excited (via thermal or photo means) into the LUMO band of the majority phase forming an n-type semiconductor leaving a hole trapped at the dopant site. Alternatively, when each atom (or nuclear site) has four valence electrons in its HOMOs in the majority phase, and the minority dopant has three valence electrons (acceptor type) in its HOMOs, three valence electrons from the dopant would couple with four valence electrons from the nearby four majority nuclei filling four new HOMO bonding orbitals. The one new HOMO orbital that has only one electron (containing one vacant site for an electron) can be easily filled by an electron from the HOMO band of the majority phase forming a p-type semiconductor and leaving an electron trapped at the dopant site.

However, as Figure 3.33b illustrates, if a weak donor/acceptor pair is strongly coupled like in a conjugated

system, the original D-HOMO and A-HOMO shall overlap and generate a lower energy bonding and a higher energy anti-bonding molecular orbitals, while the original D-LUMO and A-LUMO would overlap and generate a lower energy bonding and a higher energy anti-bonding molecular orbital. The optical excitation energy gap changes from E_g' to the new E_g. Likewise, as illustrated in Figure 3.33d, if a strong donor/acceptor pair is strongly coupled via conjugated bonds, the D-HOMO and A-LUMO can overlap and generate a new bonding and anti-bonding molecular orbitals, with both electrons from the D-HOMO transferring to and staying at the newly generated bonding orbital forming a new frontier orbitals of the D-A pair or complex, sometimes called exciplex. Figure 3.33e exhibits potential energy profiles of a weakly coupled D/A pair, where U_i represents the potential energy of D/A at initial state or before electron transfer, U_f represents the potential energy of D^+/A^- at final state or after the electron transfer, $2V_{if}$ represents the electronic coupling matrix element of such electron transfer, and E_a' represents the activation energy of such electron transfer. Likewise, Figure 3.33f exhibits potential energy profiles of a strongly coupled D-A pair, where U_i' represents the potential energy of D-A at initial or ground state, U_f' represents the potential energy of D-A* at the final state. In weak coupling (WC) (Figures 3.33a, c and e) where the electronic coupling matrix element ($2V_{if}$) is relatively small and there is a non-zero energy barrier exists between the electron transfer initial and final states, electron can be localized at D (before electron transfer) or A (after the electron transfer). Though a non-zero activation energy has to be overcome for electron transfer in weak coupling, however, the energy barrier or charge localization between the initial and final states also stabilizes the charge separated states and hinders the charge recombination. On the other hand, in strong coupling (SC) situation (Figures 3.33b, d and f) where the $2V_{if}$ can be very large and the energy barrier can become zero, so the electron can move or delocalize between D and A in D-A complex, there is also no energy barrier to stabilize the charge separated states, or there is essentially no charge separation or charge carrier generation upon D-A formation. However, D-A strong coupling has been extensively used as a chemical approach to engineering tailored frontier orbitals of organic conjugated materials.

In general, as shown in Figure 3.34, n-type doping refers to a minority donor type dopant trapping a hole (or positive polaron) from the majority phase via donating an electron (or create a negative polaron) into the LUMO band of the majority phase, and p-type doping generally refers to a minority acceptor type dopant trapping an electron from the majority phase leaving a mobile hole (or positive polaron) at the HOMO band of the majority phase.

3.3.2.4 Electrode Doping (Electro-electric Processes)

Finally, p-type electrode doping (electro-electric) process refers to the case where the mobile holes are injected from an electrode into the HOMO band of the material, and n-type electrode doping refers to the case where the mobile electrons are injected from an electrode into the LUMO band of the material as schematically shown in Figure 3.28d. In order to incur electrode doping, the electrode work function or Fermi level (E_F) needs to match the electrical potential to match the frontier orbital of the material to be doped. The Fermi level of an electrode can be tuned by adjusting the electrical potential of the electrode from a reference electrode.

3.3.2.5 Summary of Charge Carrier Generations

In summary, compared to classic or traditional inorganic semiconductors, the frontier orbital schemes of intrinsic organic or polymeric semiconductor can be shown in Figure 3.34a, *i.e.*, instead of uncorrelated free electrons and holes upon photo excitation, an exciton (also called an exciton–polaron, or a correlated electron–hole pair) is typically generated in most organic or polymeric semiconductors. Though the exciton can diffuse via

energy transfer in the material before decay (either radiative or nonradiative), exciton itself does not contribute to the charge carrier density or conductivity of the materials. However, like in traditional extrinsic semiconductors, an n-type organic semiconductor (or conductor) could be generated upon a donor type of chemical (or thermal) doping as depicted in Figures 3.28b-c, 3.30-32, 3.33c, and 3.34b. Likewise, a p-type organic semiconductor (or conductor) may be formed upon an acceptor type of chemical (or thermal) doping as depicted in Figures 3.28b-c, 3.30-32, and 3.34c. Finally, a donor and an acceptor can form a two-phase (binary phase, or bipolar type) material as shown in Figure 3.34d. In this case, the charge carriers generated at the D/A interface (via either photo doping or chemical/thermal doping mechanisms) can diffuse away from the interface in two separate phases due to chemical potential gradient [15]. This is somewhat similar to a traditional p/n junction semiconductor device. The main difference here is that the charge carriers are only generated at the D/A interface but not in D or A phase. This is a key mechanism of organic photovoltaics, *i.e.,* photo doping in a donor/acceptor binary heterojunction system [15,16].

In addition to the free holes (positive polarons, the orbital levels are schematically shown in Figure 3.35a) and free electrons (negative polarons, Figure 3.35b), a number of other key charge (or energy) carriers in conjugated organic and polymeric materials include mobile positive bipolarons (Figure 3.35c), mobile negative bipolarons (Figure 3.35d), neutral solitons (Figure 3.35e), positive solitons (Figure 3.35f), negative solitons (Figure 3.35g), and energy carrier exciton–polarons (Figure 3.35h) [13,14]. Except the exciton–polaron (Figure 3.35h) that is an energy carrier but not a charge carrier, all other charged or neutral entities (Figure 3.35a through g) can be driven by an applied electric field and therefore called electric charge carriers, or simply carriers.

Specifically, while two polarons of opposite charge can couple and spin–correlate to each other forming an exciton–polaron (Figure 3.35h, and may subsequently decay to ground state by emitting a photon, a key mechanism in organic light emitting materials/devices), two polarons of the same charge can also couple and spin–correlate to each other forming a relatively stable bipolaron entity (a quasiparticle) that can diffuse as a charge carrier containing either two positive (Figure 3.35c) or two negative (Figure 3.35d) unit charges. When two polarons are close together, they can lower their energy by sharing the same distortions, which leads to an effective attraction between the two polarons. The correlated two unit charges typically share one orbital in a bipolaron, or remain in two separate orbitals forming a meta-stable polaron-pair. In either case, they are strongly coupled and correlated in a lower energy state. While a bipolaron is not responsive in the typical ESR single electron detection regime, a polaron-pair would exhibit a singlet-triplet splitting. Both bipolarons and polaron-pairs have integer spins and thus share some of the properties of bosons. Similar to a polaron, the frontier orbital levels of a bipolaron (and a polaron-pair) are also within the HOMO/LUMO gap of pristine material, but closer to the centre than that of a polaron. Precise definition of a soliton is not straight forward and it involves substantial mathematics, however, a neutral soliton (Figure 3.35e) formation in polyacetylenes may be simplified as due to, for instance, a degenerate ground state structural distortion, or conjugation paring symmetry rearrangement in the polyacetylene backbone, so that one p_z electron of a backbone carbon atom somehow does not participate in the backbone conjugated π bands formation, thus generating one mobile soliton carrier (Figure 3.35e-g). The positive soliton (Figure 3.35f) can be regarded as a neutral soliton (Figure 3.35e) that losses its electron, and the negative soliton (Figure 3.35g) can be regarded as a neutral soliton (Figure 3.35e) that gained an electron with opposite spin.

Overall electrical conductivities (σ) of conjugated organic and polymeric materials are due to both density (N) and mobility (μ, Equation 3.22) of the mobile charge carriers as a result of the impurities, defects, and doping of the material.

Figure 3.36 shows electrical conductivity (σ) of some representative materials at room temperature (except poly-sulfur-nitride, which is a superconductor at 0.3 K). The resistivity (ρ, in unit of Ω cm) is the inverse of the conductivity ($\rho = 1/\sigma$). Depending on the magnitudes of carrier density (N) and carrier mobility (μ), from Figure 3.36, it can be seen that either insulator ($\sigma < 10^{-7}\ \Omega^{-1}\text{cm}^{-1}$), semiconductor ($10^{-7}\ \Omega^{-1}\text{cm}^{-1} \le \sigma \le 10^{2}\ \Omega^{-1}\text{cm}^{-1}$), or conductor ($\sigma > 10^{2}\ \Omega^{-1}\text{cm}^{-1}$) may be obtained from organic or polymeric conjugated materials.

The degradation of organic and polymeric electronic materials in air can be attributed partly to the electron transfers between the organic materials and oxygen and subsequent chemical reactions. For instance, it could be photo doping process of electrons transferring from HOMO/LUMO of the materials to LUMO of oxygen where light is involved, or chemical/thermal doping processes from HOMO of the materials to LUMO of the oxygen where light is not involved. In case of photo doping degradation mechanism, keep materials in dark or isolate materials from oxygen or both can help stabilizing the materials. In case of chemical/thermal doping degradation mechanism, keep materials isolated (encapsulated) from air or oxygen is essential. Materials can also be made more stable by engineering its frontier orbitals in reference to oxygen LUMO to prevent or minimize the photo or thermal/chemical doping probabilities.

3.3.2.6 Charge Transfer Versus Energy Transfer

In addition to the electron or charge transfers (CT), energy transfer (or exciton transfer ET) is also very common and critical in organic optoelectronic materials and devices. Energy transfer is essentially exciton transport or diffusion from one site to another. Figure 3.37 illustrates the general relative frontier orbital levels in the cases of (a) electron or charge transfer (CT) and (b) energy transfer (ET). As the figure exhibits, when two sets of frontier orbitals are positioned in profile (a), electrons can be transferred from D-HOMO to A-LUMO in photo doping or chemical doping situations. Alternatively, if photo excitation occurs at acceptor site (i.e., A-HOMO $\rightarrow$ A-LUMO excitation), then the electron transfer from D-HOMO to the hole site at A-HOMO can also proceed (corresponding to the hole transfer from A-HOMO to D-HOMO) [16].

Among a number of energy (or exciton) transfer mechanisms, Förster and Dexter energy transfers are two well-known types of transfer mechanisms [16]. Förster energy transfer, also called Förster resonance energy transfer, describes an energy transfer mechanism between two fluorescent molecules as shown in Figure 3.38a. A fluorescent donor molecule is excited at its specific fluorescence excitation wavelength. By a long-range dipole–dipole coupling mechanism, this excited state is then non-radiative transferred to a second molecule, the acceptor. The donor returns to the electronic ground state. When both molecules are fluorescent, the term fluorescence resonance energy transfer (FRET) is also used, although the energy is not actually transferred by fluorescence.

The FRET efficiency is determined by three parameters:

1. Distance between the donor and the acceptor
2. Spectral overlap of the donor emission spectrum and the acceptor absorption spectrum
3. Relative orientation of the donor emission dipole moment and the acceptor absorption dipole moment

Due to the fact that the donor exciton relaxation energy is typically smaller than the absorbed photon energy (e.g., due to Stokes shift), the Förster energy transfer would result in gradual energy reduction or spectra red-shift along the exciton diffusion or propagation direction. The most efficient Förster energy transfer occurs when the acceptor energy gap matches the donor emitted photon energy well, *i.e.*, transfer coupling may be poor if the acceptor gap is too far away compared to the donor exciton energy. Also, the Förster energy transfer can occur between two remote sites of above 10 nm and is sensitive to molecular dipole orientation, *i.e.*, those molecular dipoles aligned in parallel would have most effective energy transfer.

In contrast, in a Dexter energy transfer process as shown in Figure 3.38b, the electron near D-LUMO first transfers to the A-LUMO, and the hole near the D-HOMO at the same time transfers to A-HOMO, the electron at A-LUMO then relaxes with the hole at A-HOMO to form a new exciton, so it may be regarded as two separate charge transfer processes occurring simultaneously. Because of this, Dexter energy transfer can only

proceed at close or adjacent sites (typically <1 nm), and it can proceed with both singlet and triplet exciton transfer, while Förster energy transfer can only proceed with singlet exciton transfer. Also, in the Dexter energy transfer, the A-HOMO and A-LUMO both are desirably located within the energy gap of the D-HOMO and D-LUMO (Figure 3.38b), while the relative positions of HOMO and LUMO are not critical in Förster energy transfer, as long as the energy gap of the acceptor matches the donor exciton emission. Even if the gap of the acceptor does not match the donor exciton emission well, Dexter energy transfer may occur as long as the energy offsets between the donor and acceptor are optimal for charge transfer.

When a donor and an acceptor entity are close to each other, predicting whether electron or energy transfer may occur will depend on the system free energy schemes as shown in Figure 3.39. For instance, if the free energy minimum of (D^+/A^-) is lower than both (D*/A) and (D/A*) as shown in Figure 3.39a, electron transfer from D* to A would occur and (D^+/A^-) would be the energetically stable or measurable product. If the free energy minimum of (D^+/A^-) is lower than (D*/A) but higher than the (D/A*) as shown in Figure 3.39b, then energy transfer of (D*/A) to (D/A*) would dominate, or (D/A*) would be the energetically stable or measurable product [8]. When there exist narrow energy gapped defect states (or a site) whose frontier orbital states are in the middle of the majority phase energy gap similar to an exciton–polaron, then an exciton can be trapped via energy transfer to this defect site. The defect site can therefore be called an exciton trap.

Charge transfer (CT) and/or energy transfer (ET) in a D/A pair can be experimentally determined via photoluminescence (PL) measurements if donor and acceptor exhibit PL emissions. For instance, as schematically illustrated in Figure 3.40, assuming a hypothetic pristine donor (exciton/energy or charge donor) exhibits a normalized PL emission peak at 500 nm (2.48 eV), and a hypothetic pristine acceptor (exciton/energy or charge acceptor) exhibits a normalized PL emission peak at 600 nm (2.07 eV), and both have the same quantity. In the case where photo induced charge transfer (CT) occurs between the pair, the PL emissions of both should be quenched by a same quanta corresponding to the number of transferred charges (designated as ΔPL_{CT} that can be measured/estimated directly from the PL emission peak changes), for instance, by a hypothetical ΔPL_{CT} = 50% PL peak decrease of D+A (CT) curve in Figure 3.40. In the case where photo induced energy or exciton transfer proceeds from the donor to the acceptor, then the donor PL should be decreased by the same quanta (designated as ΔPL_{ET}) while the acceptor PL should be increased by the same amount, for instance, by a hypothetical ΔPL_{ET} = 30% in D+A (ET) as shown in Figure 3.40.

Suppose both CT and ET may occur simultaneously in a D+A blend, *i.e.*, in a hypothetic case of D+A (CT+ET). Using ΔPL_D as the total PL emission peak change of D, ΔPL_A as the total PL emission peak change of A, ΔPL_{DD} represents the donor PL emission peak change due to the D concentration change, ΔPL_{DA} represents the donor PL emission peak change due to the A concentration change, ΔPL_{AD} represents the acceptor PL emission peak change due to the D concentration change, ΔPL_{AA} represents the acceptor PL emission peak change due to the A concentration change, and assuming other factors such as aggregation induced PL quenching can be neglected in very dilute solution, the following relationships or approximations may apply

$$\Delta PL_D = \Delta PL_{CT} + \Delta PL_{ET} + \Delta PL_{DD} + \Delta PL_{DA} \qquad (3.43)$$

$$\Delta PL_A = \Delta PL_{CT} - \Delta PL_{ET} + \Delta PL_{AA} + \Delta PL_{AD} \qquad (3.44)$$

Combining equations 3.43 and 3.44, one obtains

$$\Delta PL_{CT} = (\Delta PL_D + \Delta PL_A - \Delta PL_{DD} - \Delta PL_{DA} - \Delta PL_{AA} - \Delta PL_{AD})/2 \qquad (3.45)$$

For all measured ΔPL values, positive values correspond to PL emission quench or drop, and negative values indicate PL emission increase or rise. ΔPL_{ET} value is assumed positive (PL emission drop) in equation 3.43, so

a negative sign is added in front of ΔPL_{ET} in equation 3.44 to designate acceptor PL emission peak increase due to the energy transfer. Equation 3.45 provides an estimate of charge transfer (CT) contribution if both CT and ET occurs in a D/A pair and both exhibit PL. Note in many D/A pair PL quenching studies where the D concentration is fixed, ΔPL_{DD} and ΔPL_{AD} should become zero or neglected. If acceptor emission does not contribute to donor peak emission (other than CT and ET), than ΔPL_{DA} can be neglected. If donor emission does not contribute to acceptor peak emission (other than CT and ET), than ΔPL_{AD} can also be neglected.

Due to the lifetime of the exciton, *i.e.*, where one excited electron at LUMO decays back to its HOMO within the typical exciton lifetime of nano to pico second timescales, there exists an average distance of the exciton diffusion, called the average exciton diffusion length (AEDL). The AEDL is highly sensitive to the molecular chemical structures, molecular packing pattern, or morphology of the materials in solid states as briefly reflected in both Förster and Dexter type of energy transfers discussed above. For instance, the AEDL can be in the range from 5 nm in amorphous polyphenylenevinylenes (PPV) thin film to above 100 nm in some organic molecular single crystals [2,3,13–15]. AEDL is very critical for organic D/A type light harvesting such as organic solar cell applications [15].

3.4 Analytical Techniques

3.4.1 Determination of Frontier Orbital Levels

The frontier orbital levels (HOMOs and LUMOs) can be determined or estimated using a number of spectroscopic techniques, including x-ray photoemission spectroscopy (XPS), ultraviolet photoemission spectroscopy (UPS), and inverse photoemission spectroscopy (IPES) (see Chapter 20). The UPS and IPES measurements probe directly the occupied and unoccupied electronic structure in the molecular interface region. Alternatively, the molecular frontier orbital levels can also be estimated from electrochemical analysis such as cyclic voltammetry (CV, probing HOMO and/or LUMO electrons directly) in combination with UV–Vis optical absorption spectra (estimating the E_g), and this appears to be a convenient and cost effective way of estimating frontier orbital levels in a typical research lab. As illustrated in Figure 3.41, the Fermi level of a standard or reference electrode (mostly silver or standard calomel electrode SCE) is located between the LUMO and HOMO levels of most organic conjugated materials. In order for a working electrode (typically a platinum wire whose Fermi level can be adjusted in reference to the reference electrode via an electric potential) to take an electron from the HOMO of the molecule, a positive or oxidation potential (in reference to the standard or reference electrode) needs to be applied to the working electrode to gradually lower the potential or the Fermi level of the working electrode (*e.g.*, potential scan from 0→2 volt as shown in Figure 3.42) until it passes the HOMO level of the sample to be measured where an electron transfers from the HOMO of the sample onto the electrode, generating an upward oxidation-oxidative current peak P_{oo} where the onset position can be designated as E_{oo}. As a result of the P_{oo} peak, a cation of the sample is formed nearby the working electrode (*e.g.*, $S - e^- \rightarrow S^+$). If such cation formation (also called p-type electrode doping) does not degrade or decompose the sample, as the working electrode potential or Fermi level goes back from positive oxidation position to the original zero potential position (corresponding to the Fermi level of the standard or reference electrode as shown in Figure 3.41), the earlier gained electron on working electrode can return back to the sample HOMO as the working electrode potential or Fermi level passes the materials HOMO level, generating a downward or oxidation-reductive current peak P_{or} where the onset position can be designated as E_{or} (see Figure 3.42), so the sample become neutral again (*e.g.*, $S^+ + e^- \rightarrow S$). This sample CV at positive oxidation potential scan range or p-type electrode doping is thus called reversible. Ferrocene is an excellent reference materials used in CV because it is inexpensive, chemically very stable, and electrochemically reversible in the p-type electrode doping or CV positive oxidation potential scan up to 2 volts, though the Ferrocene LUMO cannot be measured in the range of 0 to -2 volts. Figure 3.42 exhibits a measured CV data curve of 0.003M Ferrocene dissolved in 0.1M Tetrabutylammonium hexafluorophosphate (TBA-HFP) in solvent dichloromethane

(DM) using an Ag/AgCl reference electrode at ambient or room temperature. The potential scan sequence is 0→-2→2→0 volt. As a matter of fact, the oxidation scans of many materials are irreversible, so the oxidation-reductive peaks (P_{or}) may not be available in many materials. When the working electrode is applied a negative or reductive potential (in reference to the standard or reference electrode) and its Fermi level gradually increases until it passes the LUMO level of the sample, an electron can transfer from the working electrode onto the LUMO orbital of the sample forming an anion (*e.g.*, $S + e^- \rightarrow S^-$). This corresponds to a reduction-reductive current peak P_{rr} (see CV curve of F4-TCNQ in Figure 3.43), where the onset position can be designated as E_{rr}. If such anion formation (also called n-type electrode doping) does not degrade or decompose the sample, as the working electrode potential goes back from the negative reduction position to the original zero potential position (corresponding to the Fermi level of the standard or reference electrode as shown in Figure 3.41), the earlier gained electron on the sample LUMO can transfer back to the working electrode as the working electrode potential or Fermi level passes the sample LUMO level, generating an upward or reduction-oxidative current peak P_{ro}, where the onset position can be designated as E_{ro} (see Figure 3.43), so the sample become neutral again (*e.g.*, $S^- - e^- \rightarrow S$). In this case, the CV scans of the sample at negative reduction potential or n-type electrode doping is thus called reversible. Figure 3.43 exhibits a measured CV data curve of 0.001M 2,3,5,6-Tetrafluoro-7,7,8,8-tetracyanoquinodimethane (F4-TCNQ) dissolved in 0.1M Tetrabutylammonium hexafluorophosphate (TBA-HFP) in solvent dichloromethane (DM) using an Ag/AgCl reference electrode at ambient temperature. The potential scan sequence is 0→-2→2→0 volt. Figure 3.43 reveals that the CV scans of F4-TCNQ is reversible in both oxidation and reduction range between -2 to +2 volts.

As Figure 3.41 illustrates, the frontier electron orbital (such as LUMO or HOMO) levels of the samples can be estimated if the Fermi level of the standard or the reference electrode is known and nearby the sample frontier orbitals. However, since the electrode Fermi level would change due to different environmental and measurement conditions including solvent, electrolyte, concentration, temperature, *etc*., a reference standard compound (such as Ferrocene whose HOMO level is set at -4.8 eV and assumed to be stable) is typically used to calibrate the reference electrode. Once the oxidative or reductive peaks of both the sample and the Ferrocene are measured, the sample LUMO and HOMO levels can then be calculated using equation

$$\text{Electron Orbital Level (eV)} = X - E_{xy}\,(\text{Sample}) - 4.8 \qquad (3.46)$$

Where

X is one of the CV measured Ferrocene HOMO parameters (*e.g.*, E_{oo} or E_{or} in Figure 3.42).

E_{xy} (Sample) is one of the measured sample electron orbital parameters corresponding to the same parameter of the Ferrocene HOMO. For example, if the sample upward oxidation peaks (E_{oo} or E_{ro}) are used, then Ferrocene upward oxidation peak (E_{oo} value) must be used in the calculation. If the sample downward reduction peaks (E_{rr} or E_{or}) are used, then Ferrocene downward peak (or E_{or}) must be used. Note E_{oo} or E_{or} are positive values, while E_{rr} or E_{ro} are negative values.

In many cyclic voltammetry (CV) measurements that involve non-reversible oxidation or reduction scans, only one onset of an oxidation (or a reduction) peak of the sample may be measured, *i.e.*, only one frontier orbital (either the HOMO or the LUMO) but not both are measured. The other frontier orbital can then be estimated from the UV–Vis absorption low energy edge E_g that approximates the HOMO–LUMO gap.

3.4.2 Other Techniques

There are a variety of experimental techniques that have been used to study or analyse the electronic and optical properties of organic and polymeric materials, including, but not limited to, basic techniques such as voltage–current measurements with or without lights, absorption, and emission spectroscopy in both ground and excited states and in either CW or pulsed modes, ESR spectroscopy with or without lights and at different temperatures, x-ray and small angle neutron scattering techniques, thin film characterization tools, various electron microscopies, *etc*. The readers are referred to relevant chapters of this and other textbooks for more details.

3.5 Summary

The electronic, optoelectronic, and photonic properties of a material are correlated directly and critically to the electronic structures and electron behaviours in the material, and electronic structures are also affected by the packing or morphologies of the materials in solid states. In general, all materials are composed of molecules and atoms, and there are over 110 different kinds of atoms called elements that have been discovered so far (as listed in the chemical Periodic Table). Each atom is composed of a nucleus (containing neutrons and positively charged protons) and negatively charged electrons (a class of particles called fermions with half integer spins) located in electron orbitals surrounding the nuclei. Electron orbitals have different shapes, orientations, and discrete energy levels, and electrons can transfer from one orbital to another under certain conditions. The number of electrons is the same as the number of protons in a neutral atom, and the number of protons determines the kind of element. When atoms combine to form molecules, certain atomic orbitals are overlapping or coupling to form molecular orbitals or chemical bonds. Two atomic orbitals strongly couple (both spatially and energetically) to form two new electronic orbitals such as two molecular orbitals, one with lower energy called bonding molecular orbital and one with higher energy called antibonding molecular orbital, thus new frontier orbitals (HOMOs and LUMOs) are formed. Like many elementary particles, the electron exhibits a character of both particle and wave called particle–wave duality. In typical atomic or molecular materials containing both electrons and nuclei, the behaviour of each electron can be described and represented by a wave function with four unique quantum numbers obtained from solutions of the Schrödinger equation. When solving the electron wave functions, Born–Oppenheimer or adiabatic approximation assumes the relatively heavy nuclei remain static during the ultra-fast electron movements. While the electron wave function represents the electron orbital, the square of the wave function at any spatial point represents the probability density of the electron at that point. Unlike classic large objects where the exact position and momentum of the objects can be determined simultaneously and precisely from principles of classic mechanics, the exact position and momentum of an electron cannot be determined simultaneously and precisely (Heisenberg uncertainty principle). Since each electron in an atom or a spatial point must be unique (Pauli Exclusion Principle), each electron orbital can therefore accommodate a maximum of two electrons with opposite spins. A correlated electron pair typically refers to a pair of two electrons in two separate orbitals but strongly interacting or correlating to each other and acting like one quasiparticle, these mainly include exciton–polarons, polaron-pairs or bi-polarons, exciplexes, *etc*. Electron can transfer from one orbital to another either intra-atomic or interatomic, provided such transfer is spatially and energetically allowable and favourable. The Franck–Condon principle dictates that during the initial ultra-fast electronic transition, the nuclei coordinates essentially remain static. The rate constant of the electronic transition or electron transfer can be described by Fermi's Golden Rule or by the Marcus theory. One key feature of Marcus equation is that, in addition to a spatial electronic orbital coupling matrix element, the rate of the electron transfer is also dependent on a Gaussian exponential energy matching term, and the rate would become fastest when all driving and counter-driving forces are balanced to zero. Electrons can transfer from higher to lower energy orbitals without the need of an external driving force, or transfer to same or higher lying orbitals with external or additional driving forces. These additional or external forces may include, but may not limited to, thermal forces, electrical forces, magnetic forces, energetic radiations, *etc*. Electron transport in a material (*i.e*., from one site to a distant remote site)

via incoherent interorbital electron transfers is called hopping transport. In a material with periodic and closely packed atomic structure or electronic potential, the Bloch theorem dictates that HOMOs would couple to each other forming a valence band (VB), and LUMOs would couple to each other forming a conduction band. Electron transport in a band is coherent and much more smooth and faster than hopping. The bandwidth, band gap, and band size all depend on the interatomic and intermolecular electron orbital overlaps and couplings and therefore, the atomic/molecular packing assembly or morphology of the materials. Most electronic, optoelectronic, and photonic processes in materials are mainly due to the valence electron transfers between the frontier orbitals, *i.e.*, HOMOs, LUMOs, and SOMOs, or frontier bands such as CB and VB. The electronic conductivity of a material is dependent on both the charge carrier density and mobility. Primary carrier generations (*i.e.*, via VB–CB transitions like in classic inorganic semiconductors) in organic semiconductors are rare, and this is mainly due to the exciton binding energies of most organic amorphous type semiconductors are much larger than room temperature thermal energy, so that charge carriers in most organic and polymeric materials (including positive or negative polarons; positive or negative bipolarons; and positive, negative, or neutral solitons) are typically generated by a secondary carrier generation process, *i.e.*, via either chemical, thermal, electrode, or photo doping processes where an electron donor/acceptor pair or the materials frontier orbitals and electrode fermi levels are weakly coupled. The principle of carrier generation via doping is that an orbital energy offset (δE of either D-LUMO/A-LUMO or D-HOMO/A-HOMO) between a weakly coupled donor/acceptor binary pair constitutes a key driving (or counter-driving) force for the interatomic electron transfer, and that charge separation and transport are further facilitated by chemical potential gradient, thermal or lattice vibration gradient, materials energetic disorders, *etc*.

Exercise Questions

1. Why and an electron be treated as both a particle and a wave? What is the evidence to support this duality?
2. What are the main differences of an electron orbital versus the orbitals of the planets surrounding the Sun?
3. What is ***k***-space? Why is electron energy plotted in ***k***-space instead of the regular 3-D space?
4. What key assumptions or materials criteria are used to derive the electronic band model?
5. What are frontier orbitals and their relationships with electron bands?
6. What are the key differences of a graphene sheet versus a linear conjugated polymer in terms of electronic structures and properties?
7. Why is charge transport or mobility sensitive to the molecular packing or materials morphology?
8. How does thermal energy affect electron transfer processes?
9. How does Fermi's Golden Rule and the Marcus electron transfer model relate to each other? Are the two models applicable for intra-atomic interorbital electron transfers?
10. Why do many excitons favorably incur charge dissociation instead of the exciton decay at a donor/acceptor interface?
11. What are the common driving and counter-driving forces for electron transfers?
12. What are the relationships of Stokes shift versus the reorganization energies? In what conditions can Stokes shift be used to estimate the reorganization energies?
13. Why do triplet excitons have longer lifetimes compared to singlet excitons?
14. What are the key differences of excitons in typical organic semiconductors compared to excitons in typical inorganic semiconductors?
15. Why do most inorganic semiconductors fit a primary photo carrier generation model, while most organic semiconductors fit a secondary photo carrier generation model?
16. Using the CV data in Figures 3.42 and 3.43, calculate the two electron orbital levels of F4-TCNQ based on E_{oo} and E_{ro} values. Assuming the two measured F4-TCNQ electron orbitals are LUMO-2 and LUMO-1 (from left to right), calculate the HOMO level of F4-TCNQ if its E_g is 3 eV.

List of abbreviations

A	acceptor
AEDL	average exciton diffusion length
AO	atomic orbital
BG	band gap
BLA	bond length alternation
BS	band size
BW	bandwidth
CB	conduction band
CBM	conduction band minimum
CT	charge transfer
CV	cyclic voltammetry
D	donor
EA	electron affinity
E_B	exciton binding energy
E_F	Fermi energy
E_g	energy gap
EPR	electron paramagnetic resonance
ESR	electron spin resonance
ET	energy transfer
FCWD	Frank–Condon-weighted density of states
FRET	Förster resonance energy transfer
HAO	hybrid atomic orbitals
HOMO	highest occupied molecular orbital
IP	ionization potential
IPES	inverse photoemission spectroscopy
LUMO	lowest unoccupied molecular orbital
MFD	mean free distance
MFP	mean free path
MFT	mean free time
MO	molecular orbital
MW	molecular weight
PA	polyacetylene
PPV	polyphenylenevinylene
SC	strong coupling
SOMO	singly occupied molecular orbital
UPS	ultraviolet photoemission spectroscopy
VB	valence band
VBM	valence band maximum
WC	weak coupling
XPS	x-ray photoemission spectroscopy

Acknowledgment

The author wishes to acknowledge and thank a number of funding agencies (particularly NASA, DoD, and NSF) for partial support of the author's research/educational activities related to the subject of this chapter. The author particularly wishes to thank Professor Larry Dalton (Chemistry), Professor Henry A. Rowe (Chemistry), Professor Igor V. Bondarev (Physics), Dr. Demetrio Filho (Physics), and Dr. Vladmir Gavrilenko (Materials Science) for manuscript review, and Dr. Natasha Kirova for suggestions/comments on bipolaron/polaron-pairs.

References

1. Chiang, C.K., Druy, M.A., Gau, S.C., Heeger, A.J., Louis, E.J., MacDiarmid, A.G., Park, Y.W., and Shirakawa, H., Synthesis of highly conducting films of derivatives of polyacetylene, (CH)x, *J. Am. Chem. Soc.*, 100, 1013–1015, 1978.
2. Skotheim, T.A. and Reynolds, J.R., eds., *Handbook of Conducting Polymers*, 3rd edition, CRC Press: Boca Raton, Florida, 2007.
3. Nalwa, H.S., ed., *Handbook of Organic Electronics and Photonics*, American Scientific Publishers: Los Angeles, California, 2008.
4. Kwok, H.L., *Electronic Materials*, PWS: Boston, Massachusetts, 1997.

5. Laidler, K.J., Meiser, J.H., and Sanctuary, B.C., *Physical Chemistry*, 4th edition, Houghton Mifflin: Boston, Massachusetts, 2003.
6. Pierret, R.F., *Advanced Semiconductor Fundamentals*, 2nd edition, Prentice Hall/Pearson Education: Upper Saddle River, New Jersey, 2003.
7. Sze, S.M. and Ng, K.K., *Physics of Semiconductor Devices*, 3rd edition, Wiley Interscience: New York, 2006.
8. Brédas, J-L., Beljonne, D., Coropceanu, V., and Cornil, J., Charge-transfer and energy-transfer processes in π-conjugated oligomers and polymers: A molecular picture, *Chem. Rev.*, 104, 4971–5003, 2004.
9. Coropceanu, V., Cornil, J., Filho, D., Olivier, Y., Silbey, R., and Brédas, J-L., Charge transport in organic semiconductors, *Chem. Rev.*, 107, 926–952, 2007.
10. Ege, S., *Organic Chemistry*, 5th edition, Houghton Mifflin: Boston, Massachusetts, 2004.
11. Jortner, J. and Bixon, M., eds., *Electron Transfer—From Isolated Molecules to Biomolecules, Part 1, Advances in Chemical Physics*, Vol. 106, John Wiley and Sons, Inc: New York, 1999.
12. Pourtois, G., Beljonne, D., Cornil, J., Ratner, M., and Brédas, J-L., Photoinduced electron transfer processes along molecular wires based on phenylenevinylene oligomers: A quantum-chemical insight, *J. Am. Chem. Soc.*, 124, 4436–4447, 2002.
13. Arkhipov, V. and Bässler, H., Exciton dissociation in conjugated polymers, in *Handbook of Luminescence, Display Materials, and Devices*, Vol. 1, eds. Nalwa, H. and Rohwer, L., American Scientific Publishers: Los Angeles, California, 2003, Chapter 5, pp. 279–342.
14. Barford, W., *Electronic and Optical Properties of Conjugated Polymers*, Clarendon Press: Oxford, United Kingdom, 2005.
15. Sun, S. and Sariciftci, N., eds., *Organic Photovoltaics: Mechanisms, Materials and Devices*, CRC Press/Taylor & Francis: Boca Raton, Florida, 2005.
16. Sun, S., Organic and polymeric solar cells, in *Handbook of Organic Electronics and Photonics*, ed., Nalwa, S.H., American Scientific Publishers: Los Angeles, California, 2008, Vol. 3, Chapter 7, pp. 313–350.
17. Walzer, K., Maennig, B., Pfeiffer, M., and Leo, K., Highly efficient organic devices based on electrically doped transport layers, *Chem. Rev.*, 107, 1233–1271, 2007.

Figures and Captions

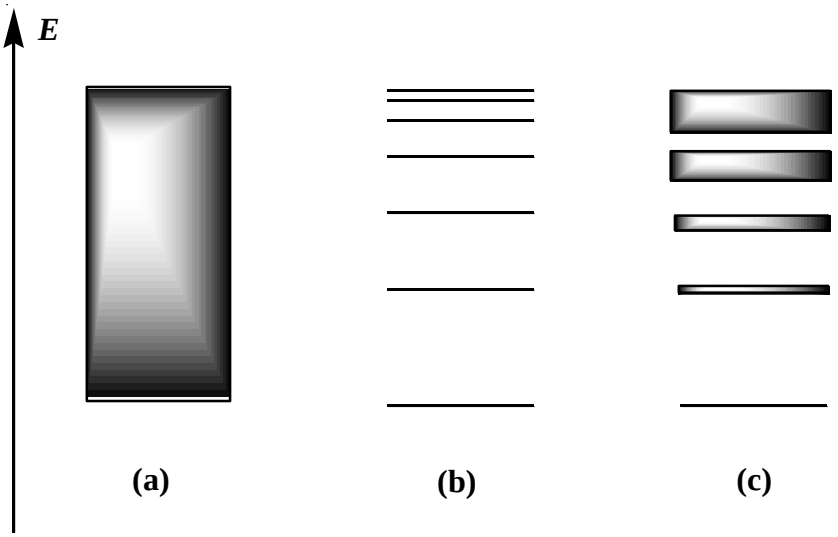

FIGURE 3.1 Schematic representation of electron energy levels/states for (a) electron in free space; (b) electron in a confined box; (c) electron in a periodic (such as crystalline) lattice.

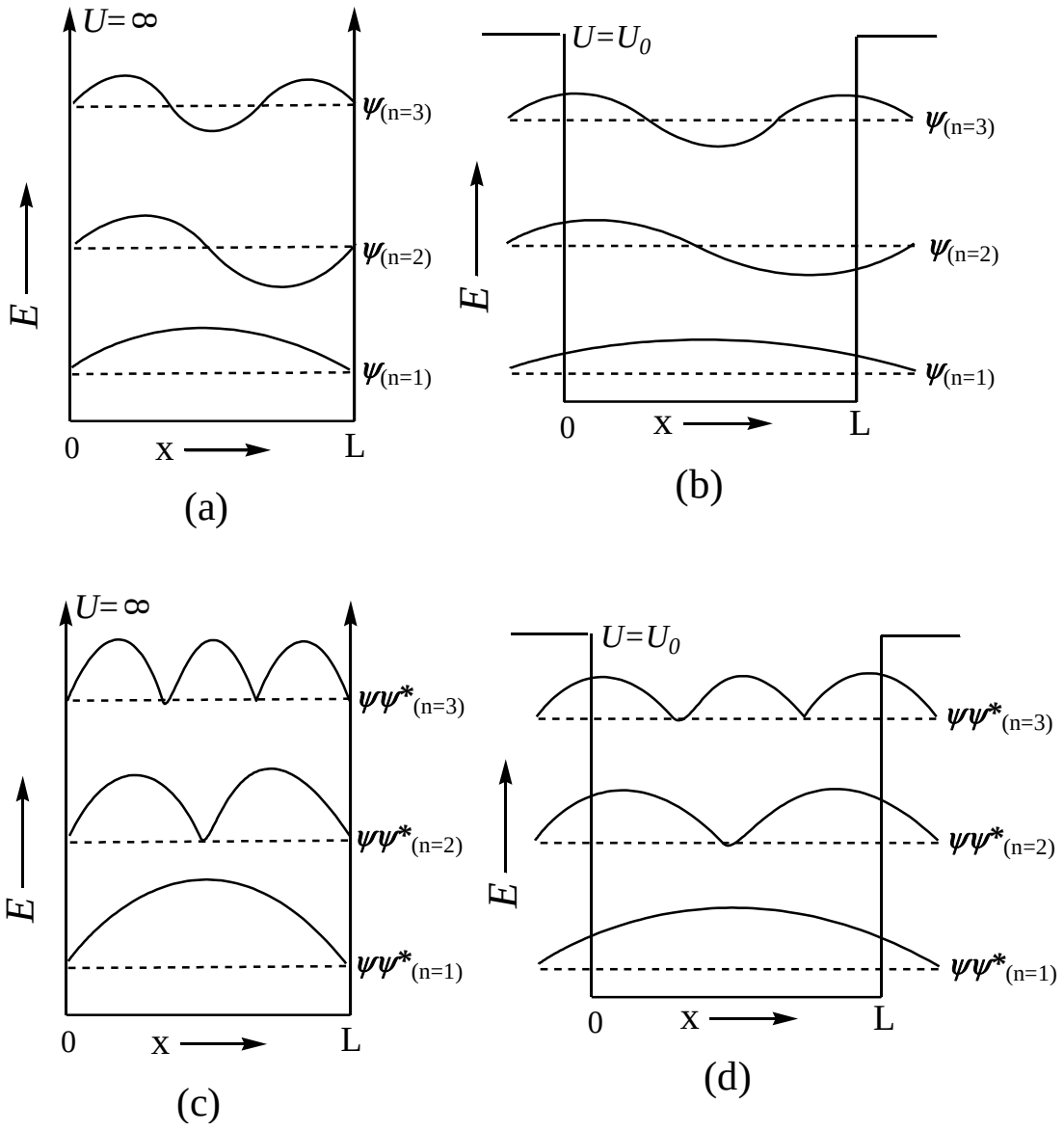

FIGURE 3.2 Scheme of electron wave functions confined in a one-dimensional (1-D) size *L* potential well with (a) infinite height potential walls; (b) finite height potential walls. Scheme of electron probability densities confined in a 1-D size *L* potential well with (c) infinite height potential walls; (d) finite height potential walls.

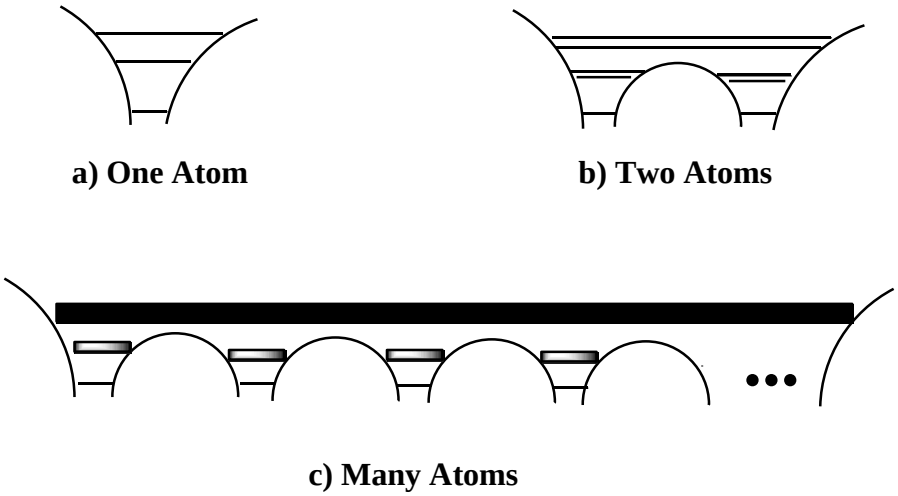

FIGURE 3.3 Schematic representation of atomic electronic potential surfaces and electron orbital levels in (a) one atom; (b) two atoms; (c) many atoms (such as crystalline) periodic structure.

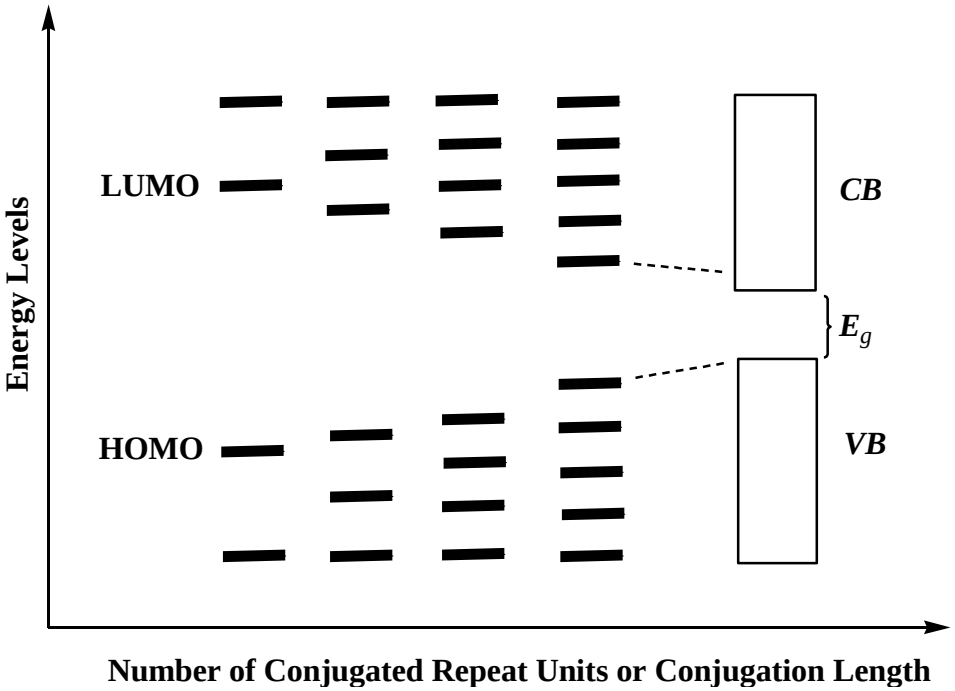

FIGURE 3.4 Schematic representation of the evolution of excitation energy gap (E_g) versus the number of repeat units in a conjugated organic system illustrating the "Particle-In-A-Box" principle. The scheme also exhibits an evolution from molecular electron orbitals to bands.

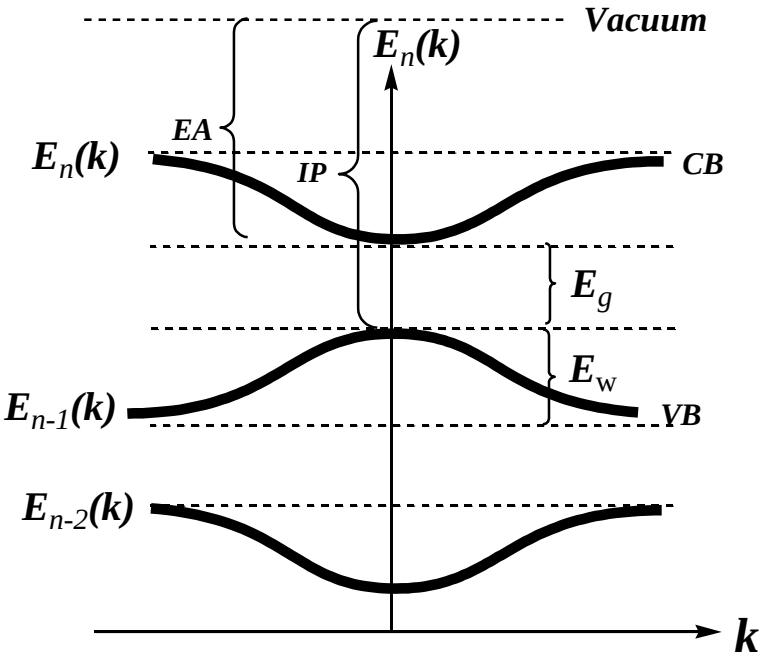

FIGURE 3.5 Schematic representations of electron energy $E_n(\boldsymbol{k})$ versus electron wave vector $\boldsymbol{k}$ in a periodic crystalline lattice where Bloch function is applicable. *CB*, conduction band; *VB*, valence band; *EA*, electron affinity; *IP*, ionization potential; E_g, band gap; E_w, bandwidth.

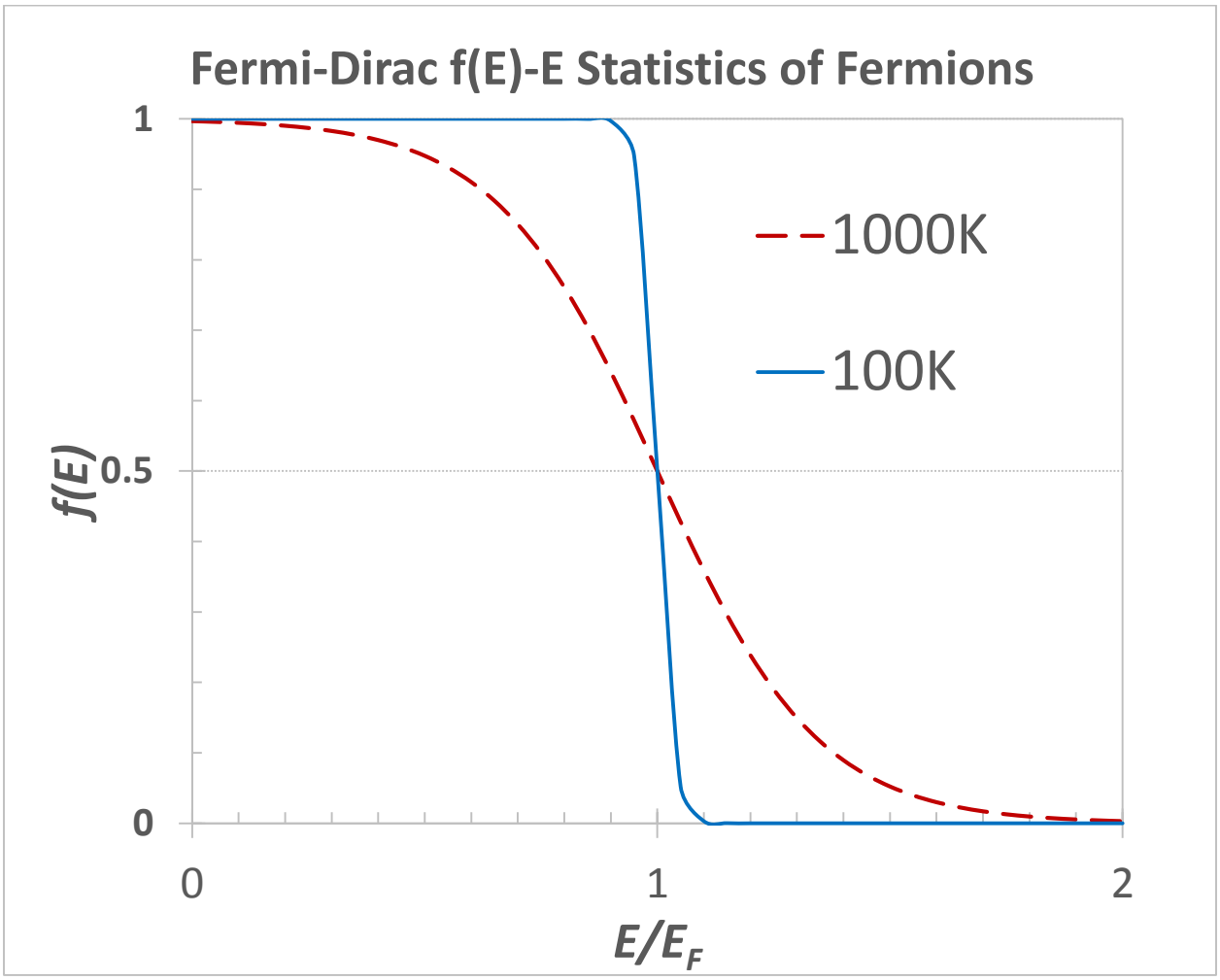

FIGURE 3.6 Fermi-Dirac statistics or distribution function curves for fermion particles such as electrons. *f(E)* represents the probability of an electron at energy state *E*. E_F is the Fermi energy. Solid curve represents the distribution at 100 Kelvin degree, while the dashed curve represents the distribution at 1000 Kelvin degree.

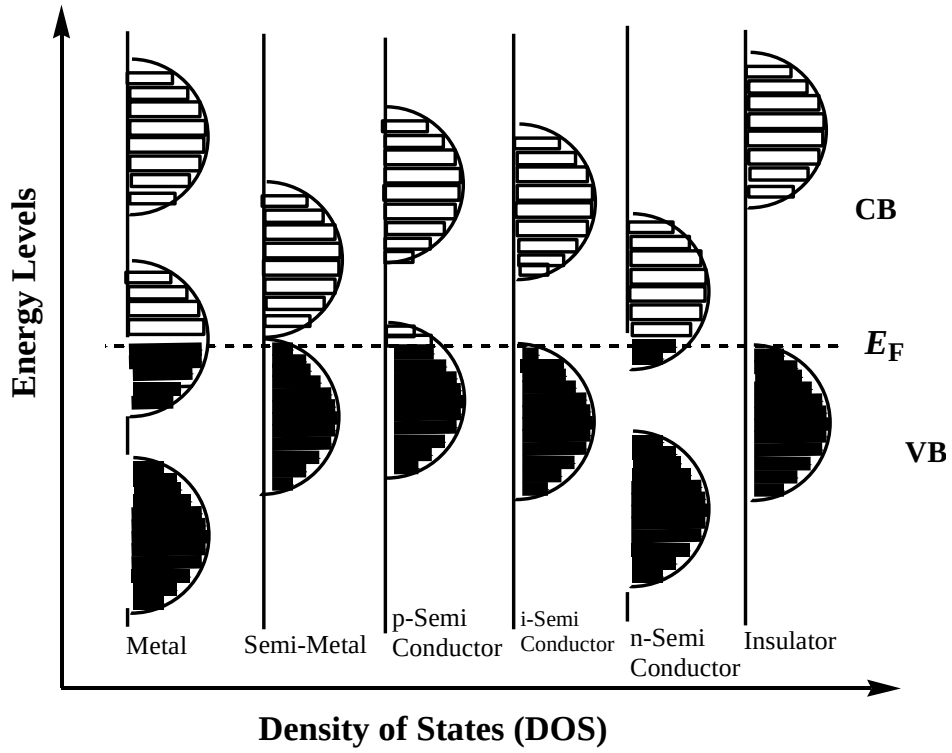

(a)

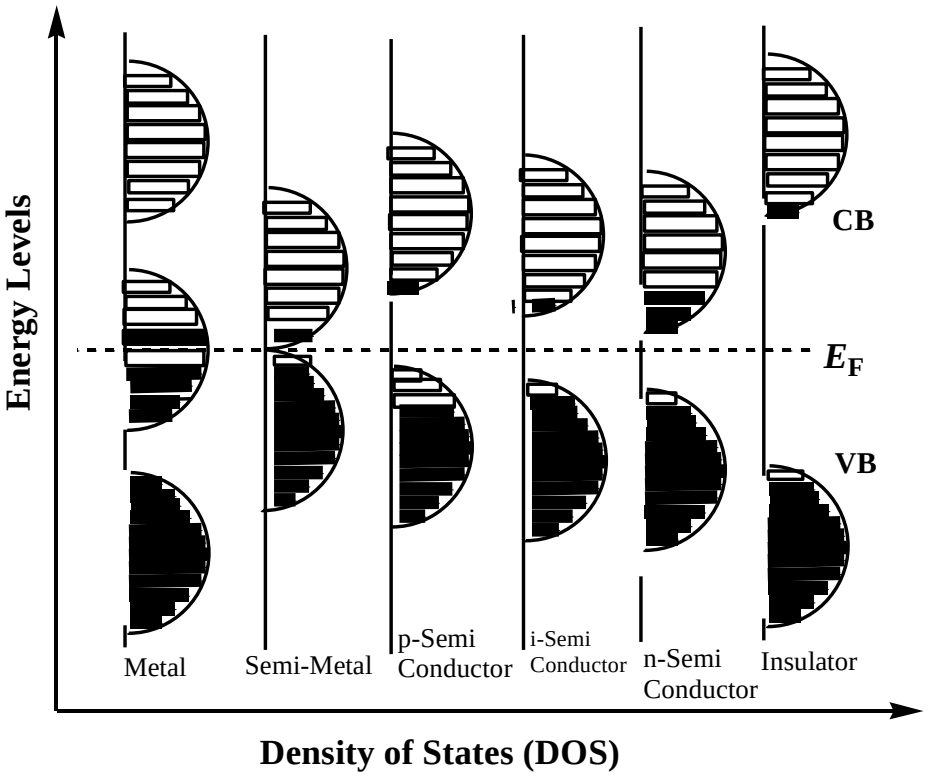

(b)

FIGURE 3.7 Schematic representations of electron bands and Density of States (DOS) of several classic materials including metals, semi-metals,

semiconductors (p-type, n-type and intrinsic type) and insulators in (a) ground state or at absolute zero temperature; and (b) excited or non-zero temperature states. E_F presents fermi energy level.

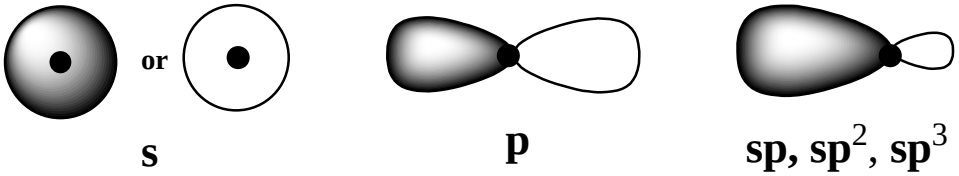

FIGURE 3.8 Shapes of some representative atomic electron orbitals. The dark dot in the middle represents the nucleus. The two colors of the orbital lobes represent the positive and negative phases of the electron wave functions. The orbital shapes roughly represent the electron probability density in space.

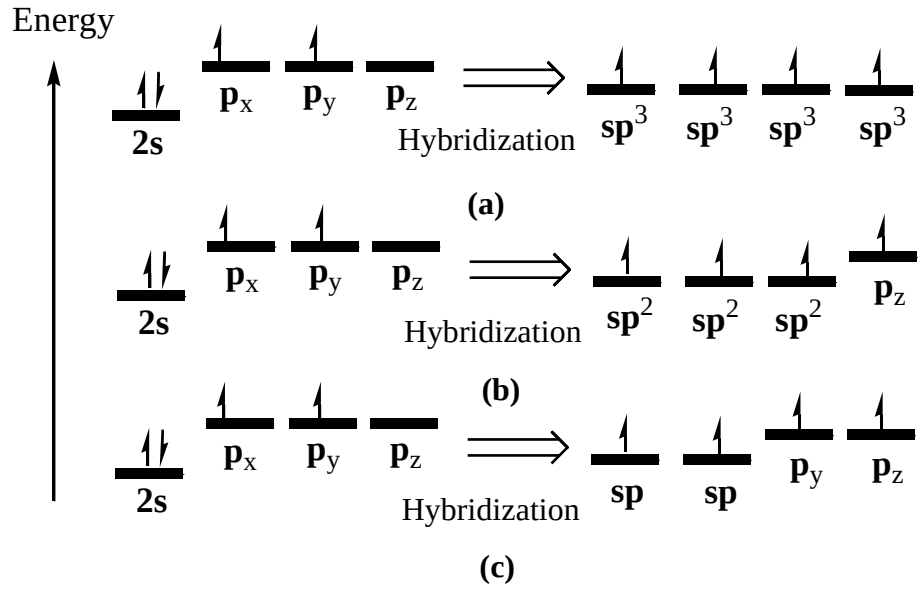

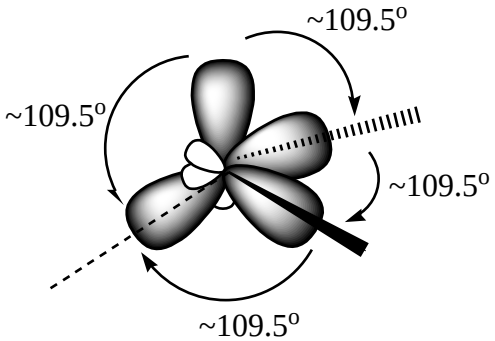

Four *sp*^{3} hybridized orbitals of a carbon atom in 3-D. Tetrahedral shape with all bond angles around 109.5°.

(d)

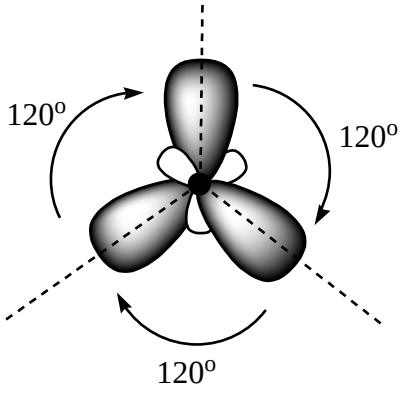

Three *sp*^{2} hybridized orbitals of a carbon atom in a plane. Triangular shape with all bond angles around 120°.

(e)

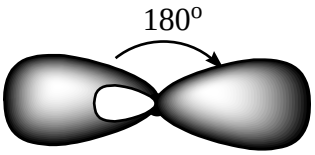

Two *sp* hybridized orbitals of a carbon atom in linear shape with bond angle around 180°.

(f)

FIGURE 3.9 Scheme of AO hybridizations in (a) sp^3 hybridization; (b) sp^2 hybridization; (c) *sp* hybridization; (d) shape of sp^2 hybridized orbitals; (e) shape of sp^3 hybridized orbitals, and (f) shape of *sp* hybridized orbital.

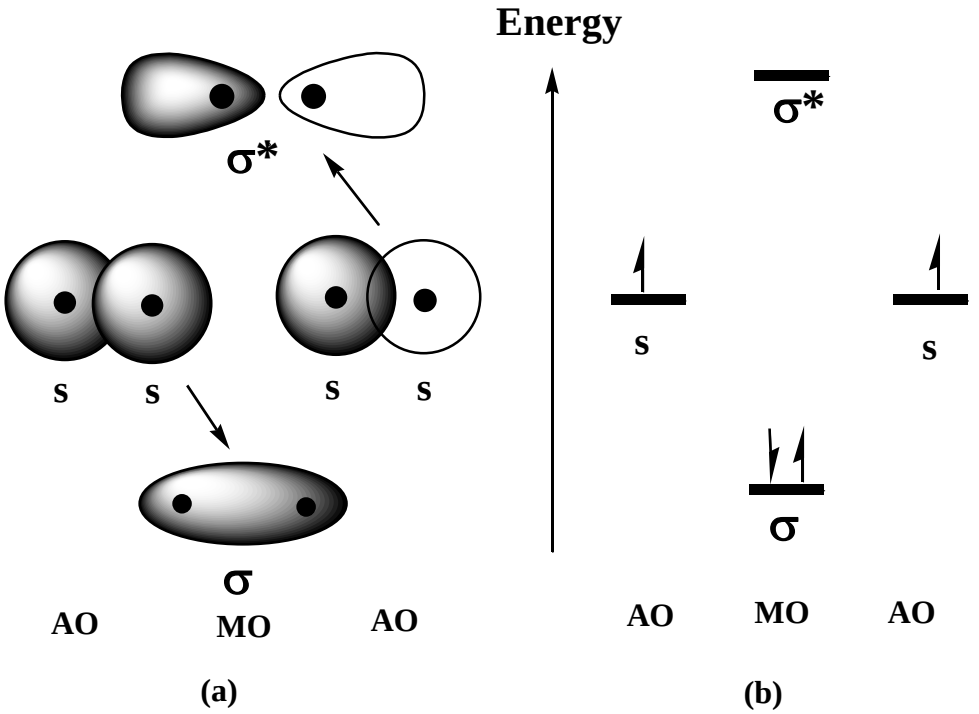

FIGURE 3.10 Scheme of a pair of σ-type MOs formed from the overlap of two *s* atomic orbitals in (a) orbital shape representation; (b) orbital energy level representation.

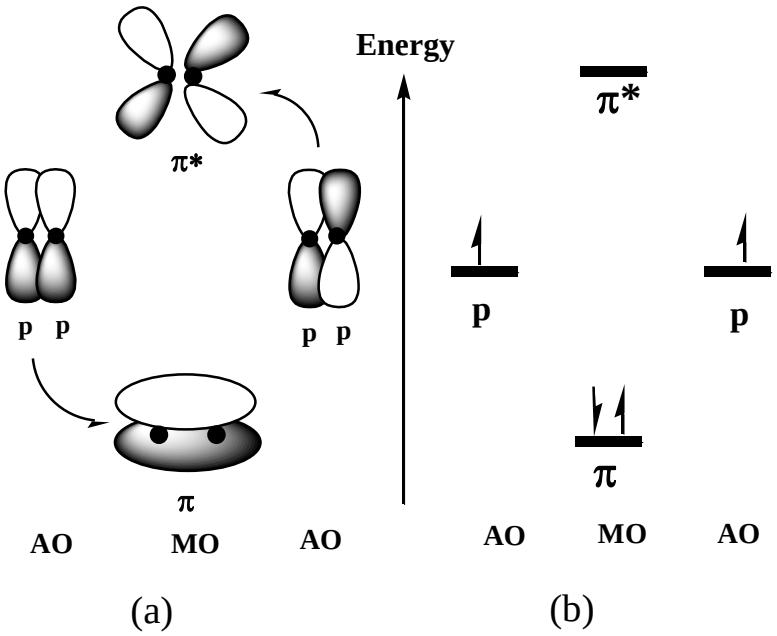

FIGURE 3.11 Scheme of a pair of π-type molecular orbitals formed from the overlap of two vertically aligned parallel p atomic orbitals in (a) orbital shape representation; (b) orbital energy level representation.

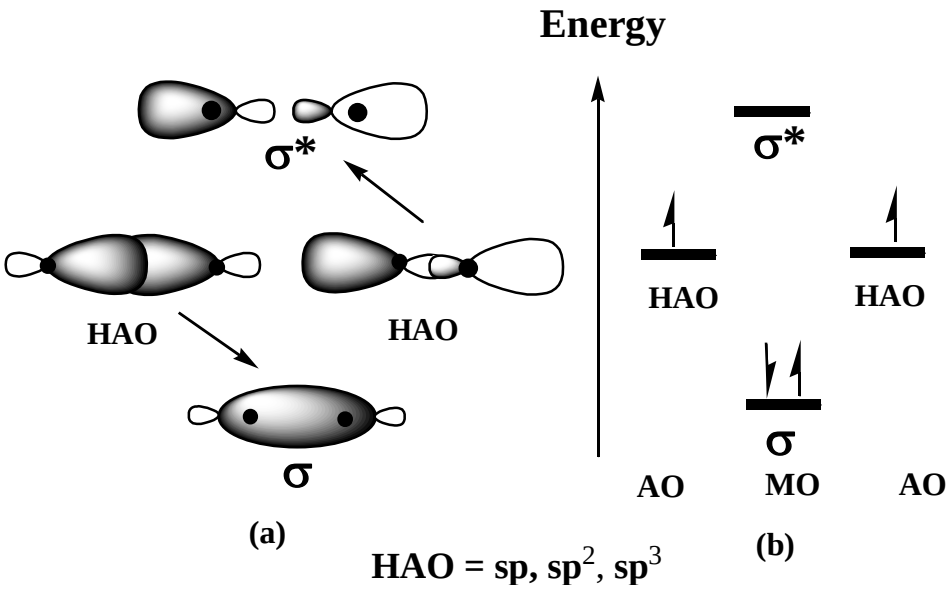

FIGURE 3.12 Scheme of a pair of σ-type molecular orbitals formed from the overlap of two horizontally aligned sp^n HAOs in (a) orbital shape representation; (b) orbital energy level representation.

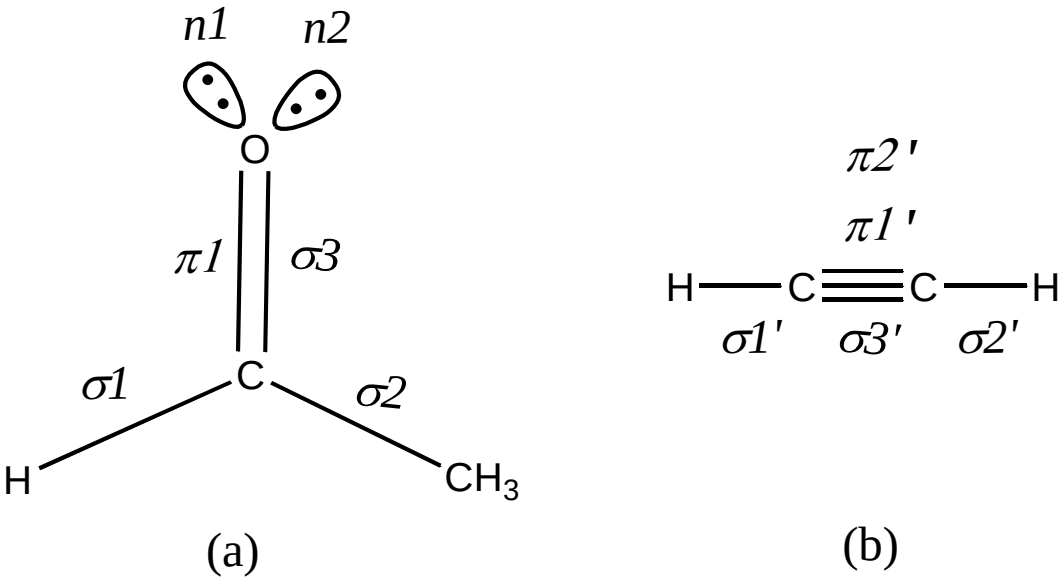

FIGURE 3.13 Schematic chemical structures of (a) ethanal (ethyl aldehyde); (b) ethyne (acetylene).

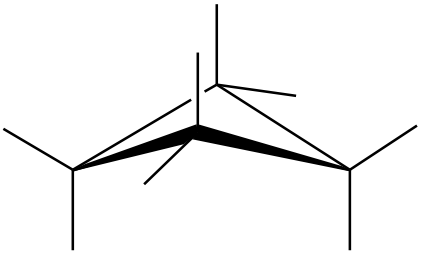

C-sp^3 + C-sp^3 --> C-C σ bonds in tetrahedral 3-D network

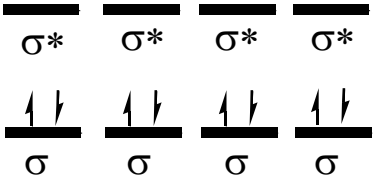

(a) Diamond

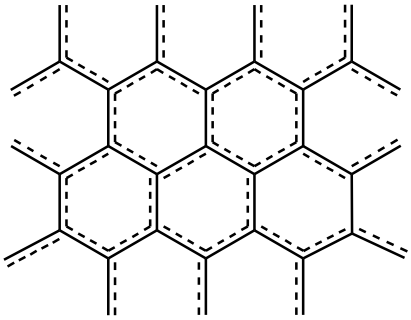

C-sp^2 + C-sp^2 --> C-C σ bonds in plane hexagnal style geometry. Vertical C-p_z orbitals can form a 2-D half-filled energy band

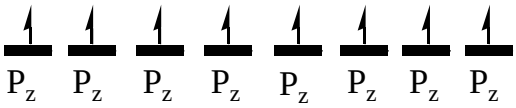

(b) Graphene/Graphite

FIGURE 3.14 Schematic representation of atomic and molecular orbitals in (a) diamond; (b) graphene/graphite.

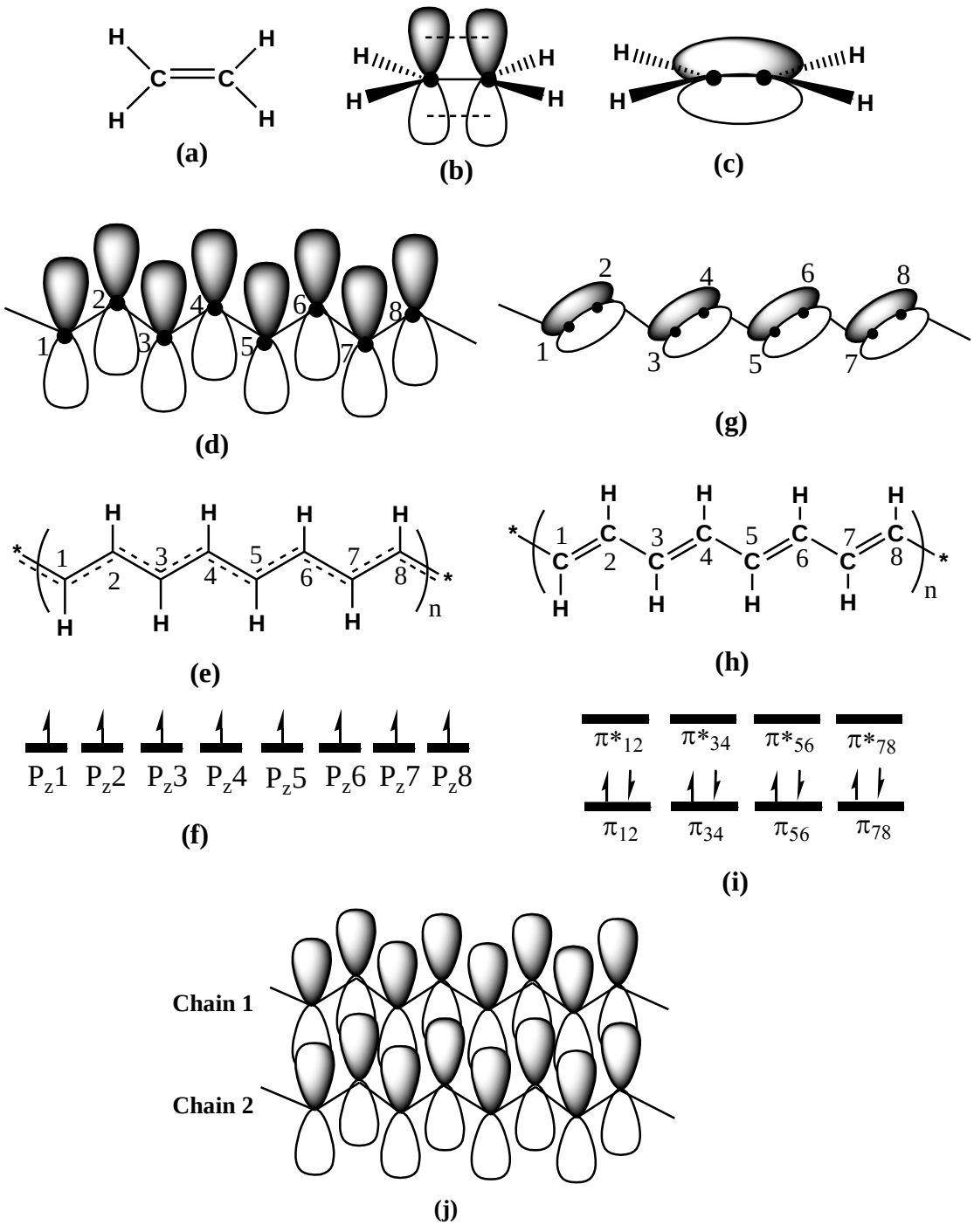

FIGURE 3.15 Schematic representation of C–C double π bonds, represented in (a) chemical structure of ethene (ethylene); (b) scheme of double bond formation by overlapping/coupling of two vertically aligned p_z orbitals at two adjacent carbon sites; (c) schematic shape of a π bonding orbital; (d) atomic p_z orbital representation of PA backbone; (e) chemical structure representation of PA assuming no 1-D Peierls distortion; (f) scheme of frontier orbitals and valence electron of PA assuming no Peierls distortion; (g) scheme of PA conjugated backbone showing π bonding orbitals; (h) chemical structure representation of PA assuming 1-D Peierls distortion applicable; (i) scheme of frontier orbitals and valence electron of PA assuming Peierls distortion; (j) atomic p_z orbital representation of two self-assembled and closely packed PA conjugated backbones.

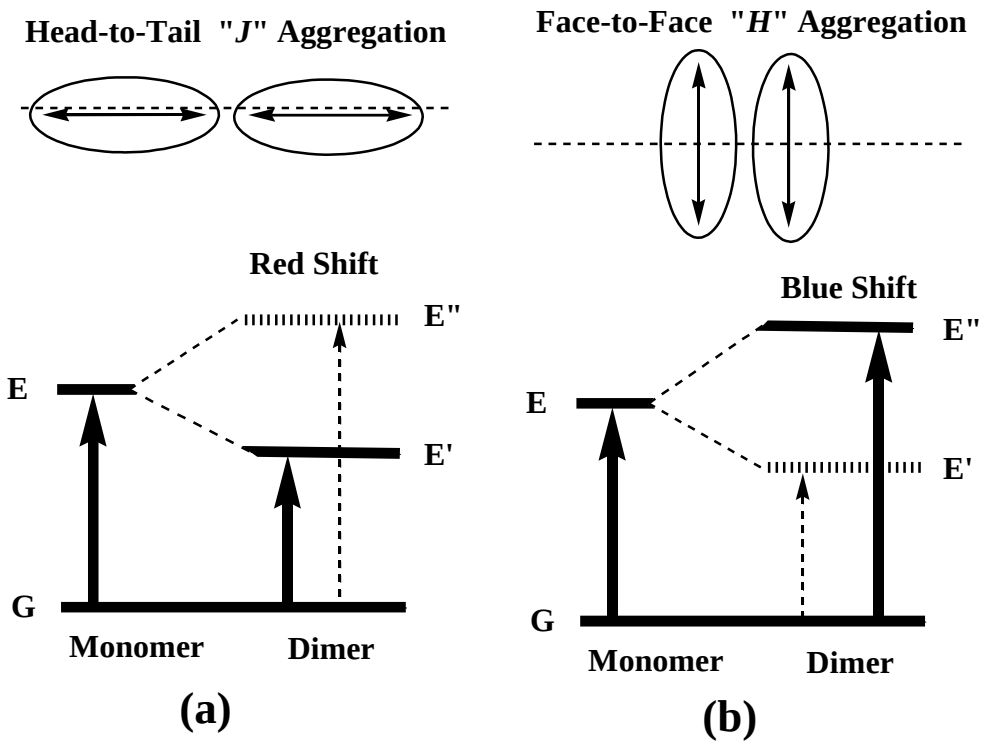

FIGURE 3.16 Molecular aggregates in (a) J-type aggregates; (b) H-type aggregates.

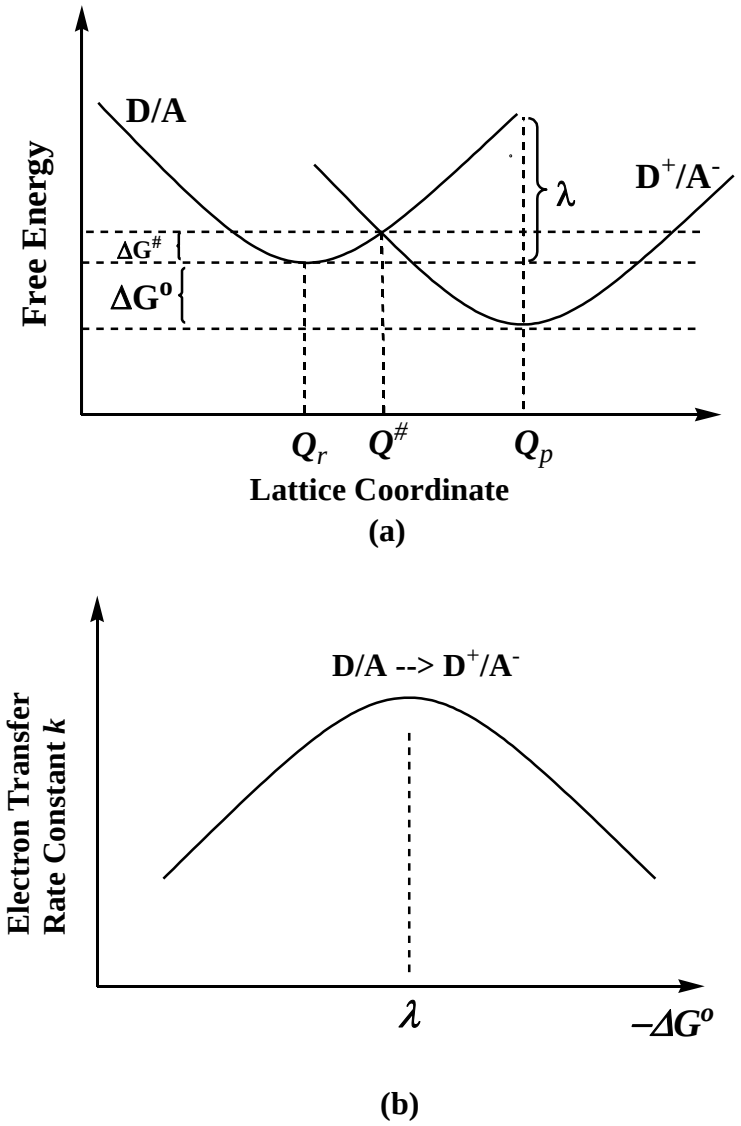

FIGURE 3.17 Electron transfer from a donor to an acceptor represented by (a) free energy surface versus lattice coordinate; (b) electron transfer rate constant versus standard free energy change.

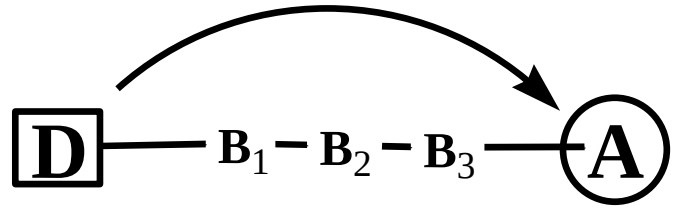

Superexchange: Coherent ET

$$k = k_o e^{-\beta r}$$

(a)

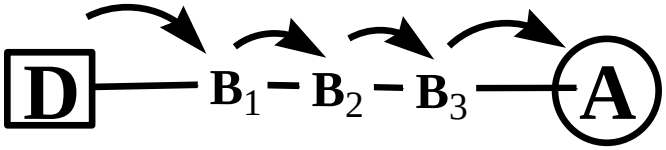

Hopping: Incoherent ET

$$k = k_o / r$$

(b)

FIGURE 3.18 (a) Coherent electron transfer (super-exchange); (b) incoherent electron transfer (hopping).

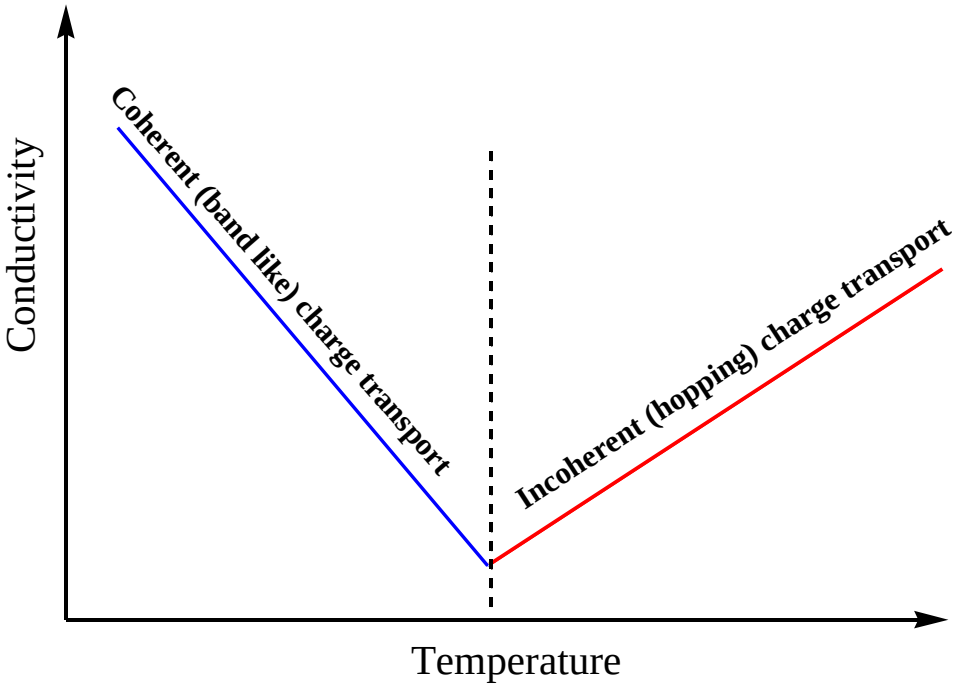

FIGURE 3.19 General scheme of materials electrical conductivity versus temperature for coherent electron transport (mainly band-like electron transport mechanism in most crystal semiconductors) and incoherent electron transport (mainly hopping electron transport mechanism in most amorphous materials).

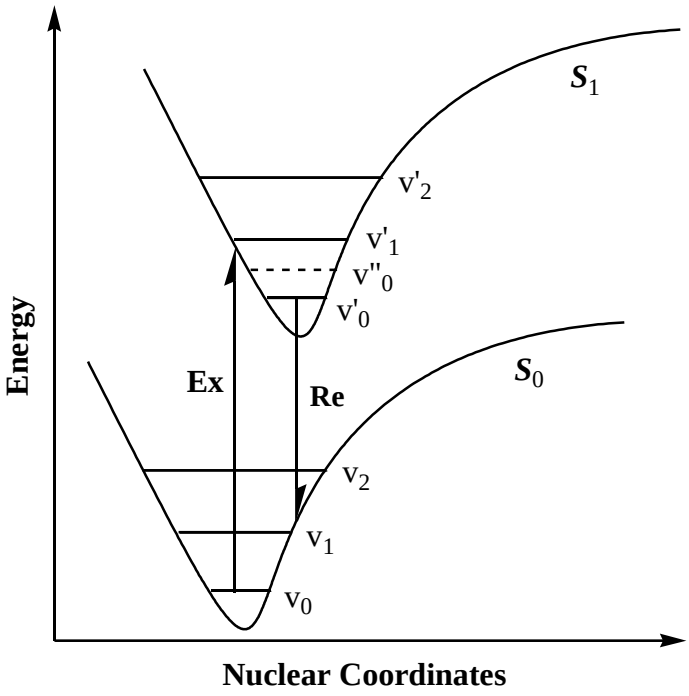

FIGURE 3.20 Scheme of an idealized two-level model showing electronic excitation (Ex), recombination (or relaxation, Re), intra-molecular vibrational modes (v_n and v'_n) and an inter-molecular or aggregate vibrational mode (v''_0).

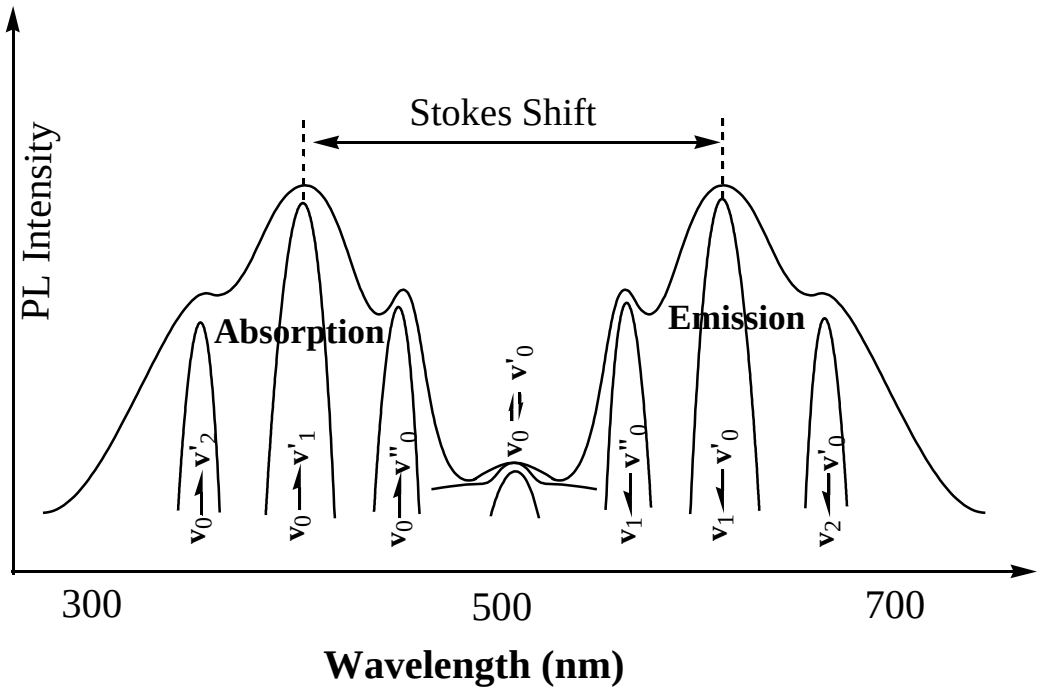

FIGURE 3.21 Scheme of idealized optical absorption and fluorescence emission bands of a two level model, where the sharp component peaks due to intra- or inter-molecular vibrational modes are also indicated. For instance, $v_0 \rightarrow v'_1$ denotes an excitation transition from v_0 level to v'_1 level shown in Figure 3.19.

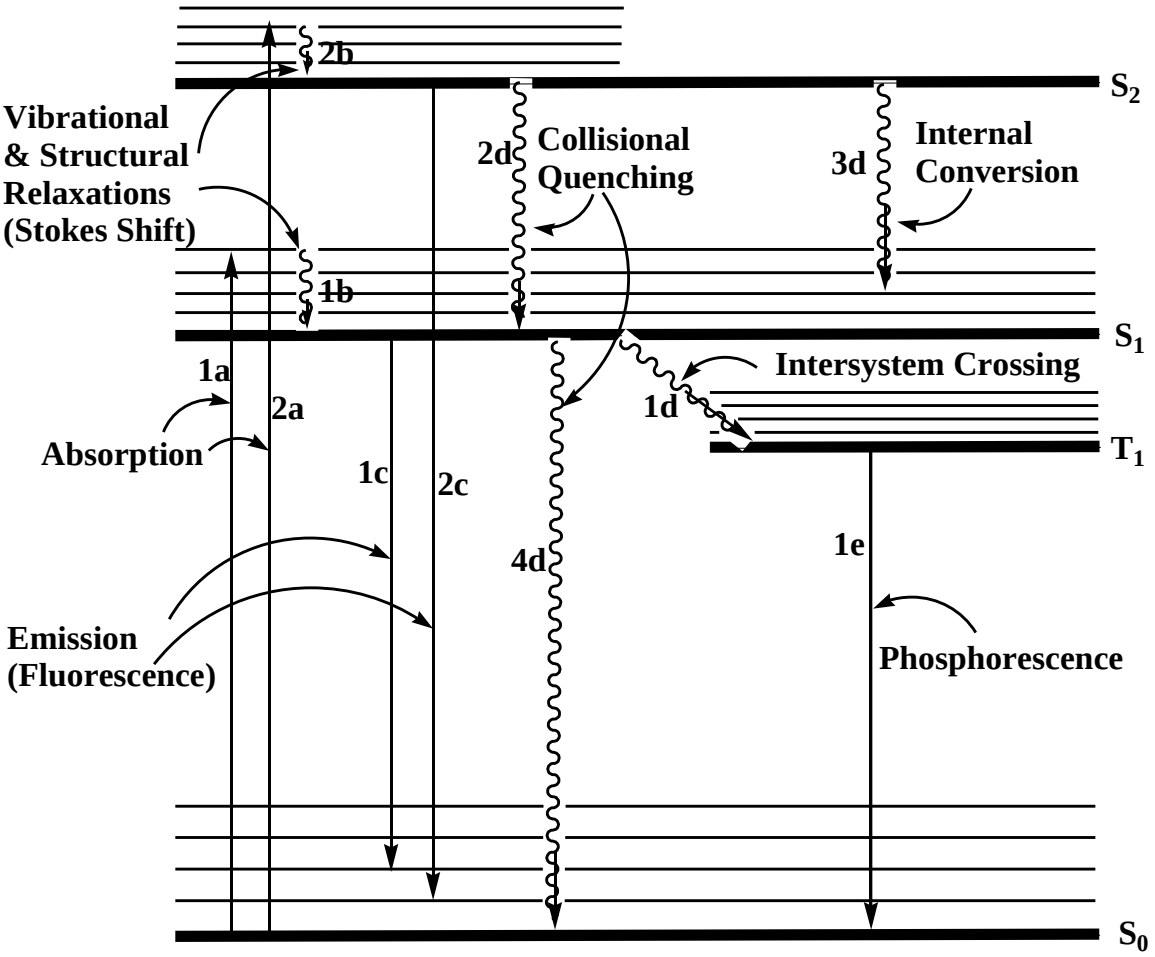

FIGURE 3.22 Jablonski's diagram depicting major transitions of a material in energy regime.

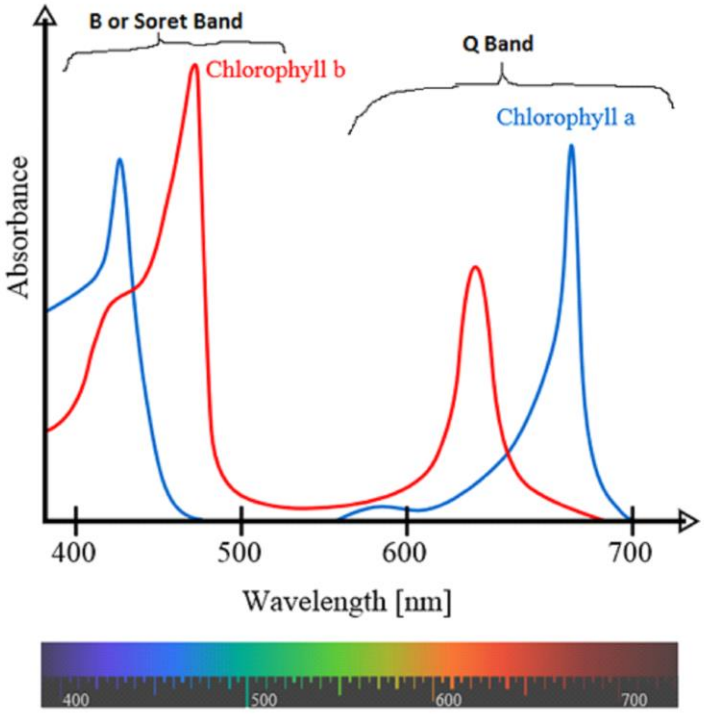

(a)

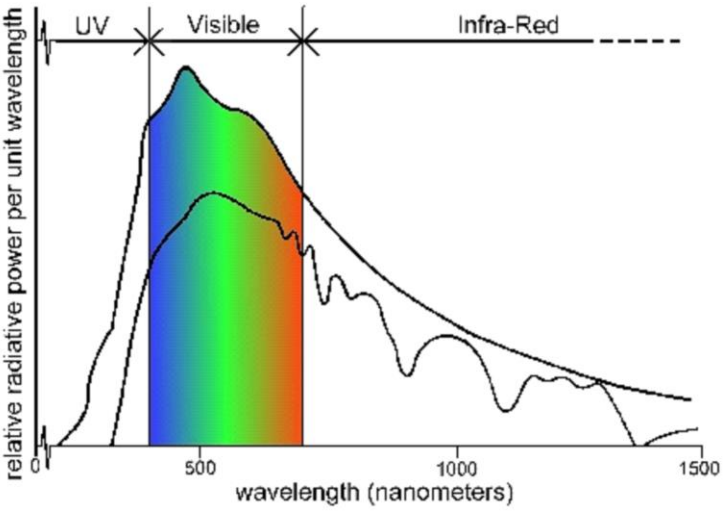

(b)

FIGURE 3.23 (a) UV-Vis absorption spectra of Chlorophyll-a and Chlorophyll-b. (b) Solar radiation spectrum at top of atmosphere (top curve) and sea level (bottom curve).

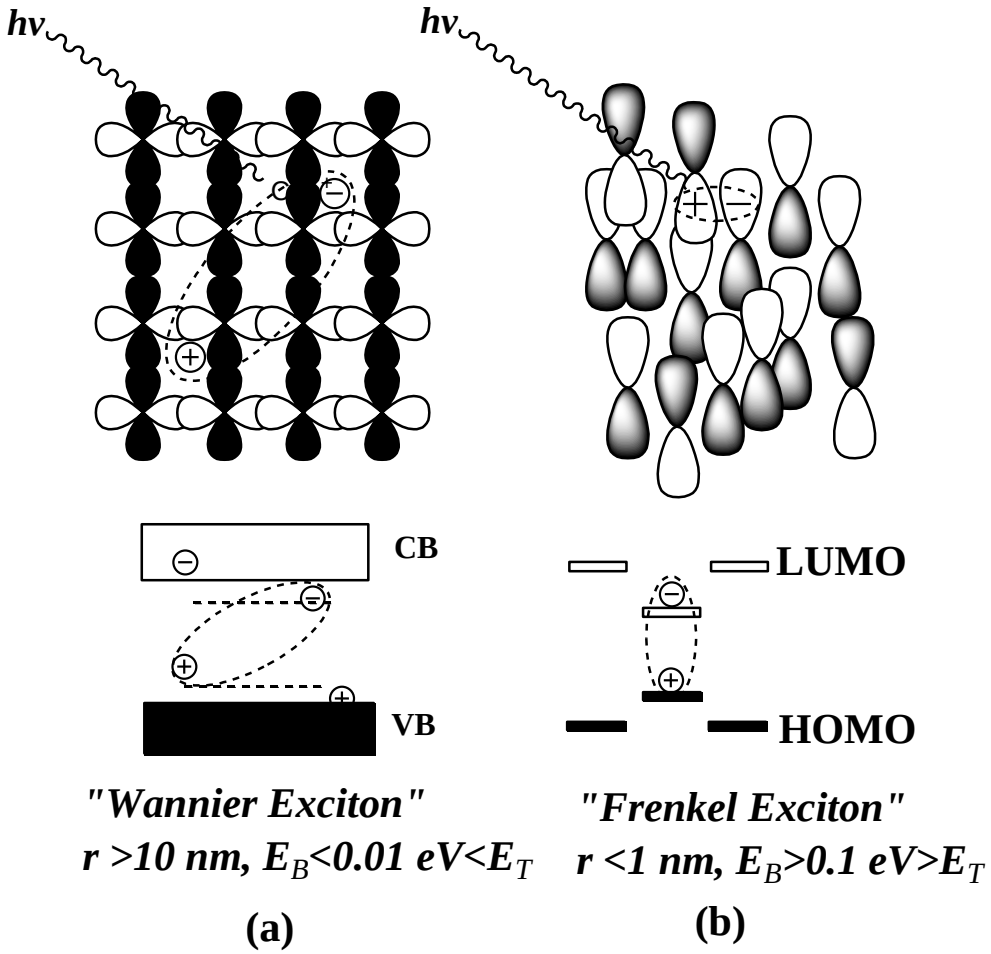

FIGURE 3.24 Schematic representation of (a) Wannier–Mott type excitons; (b) Frenkel-type excitons.

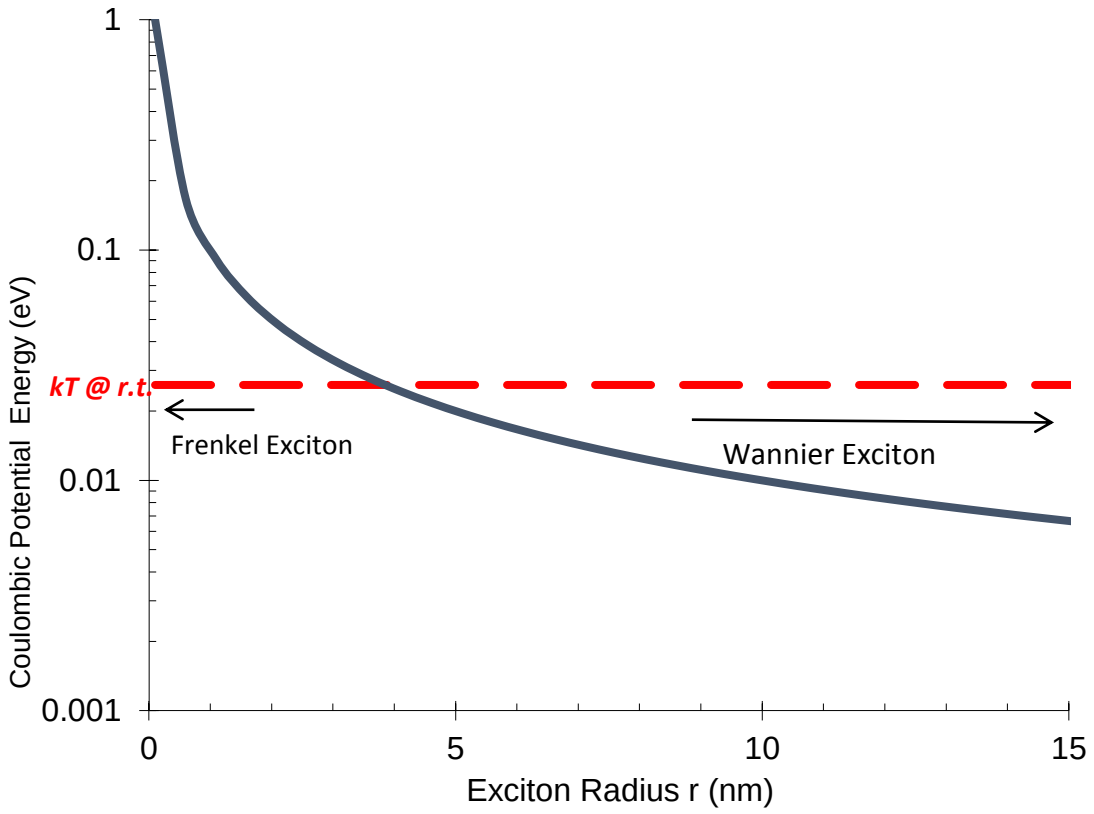

FIGURE 3.25 Scheme of Coulombic potential energy (or exciton binding energy E_B, in approximate values) for typical excitons. .

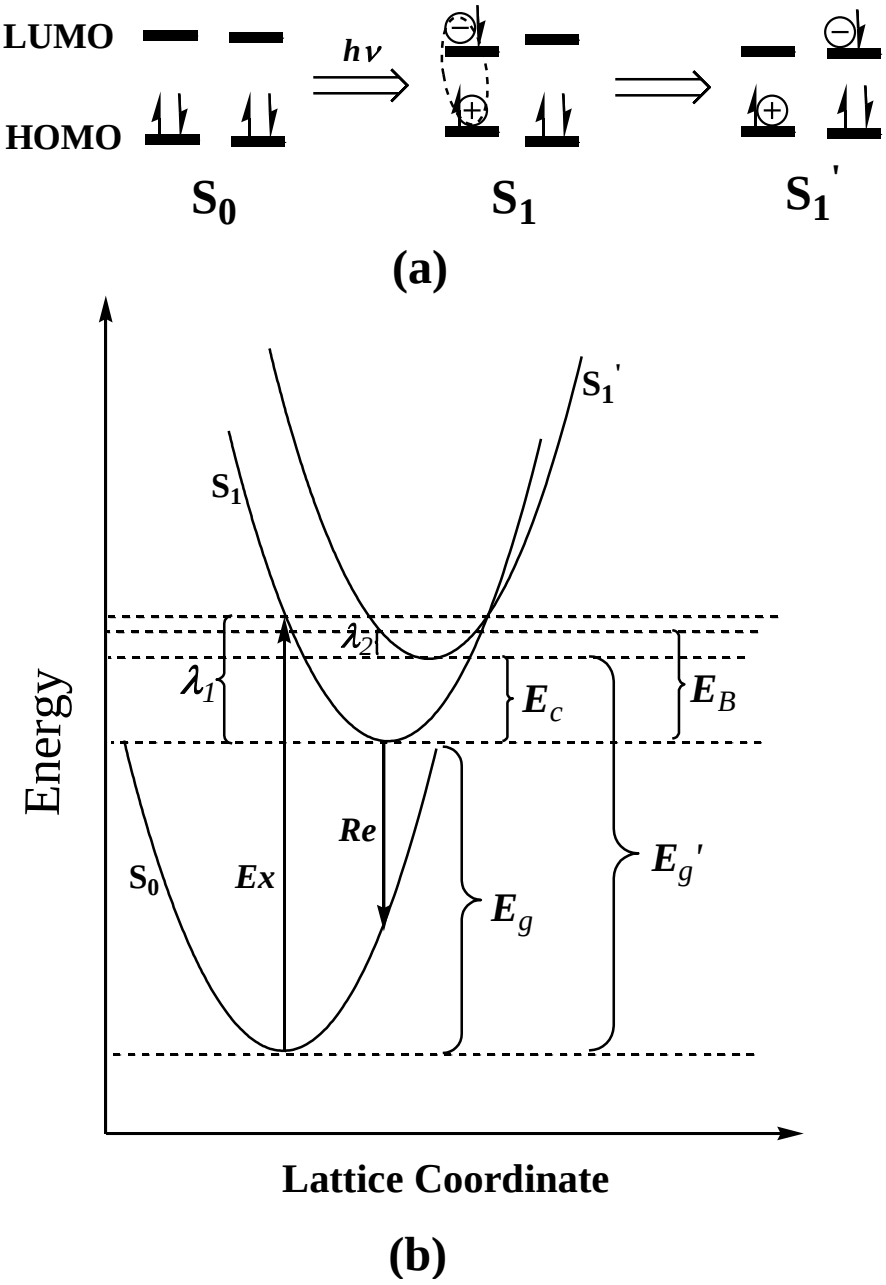

FIGURE 3.26 Scheme of photoelectric carrier generation processes in (a) frontier orbital representation; (b) free energy surface representation.

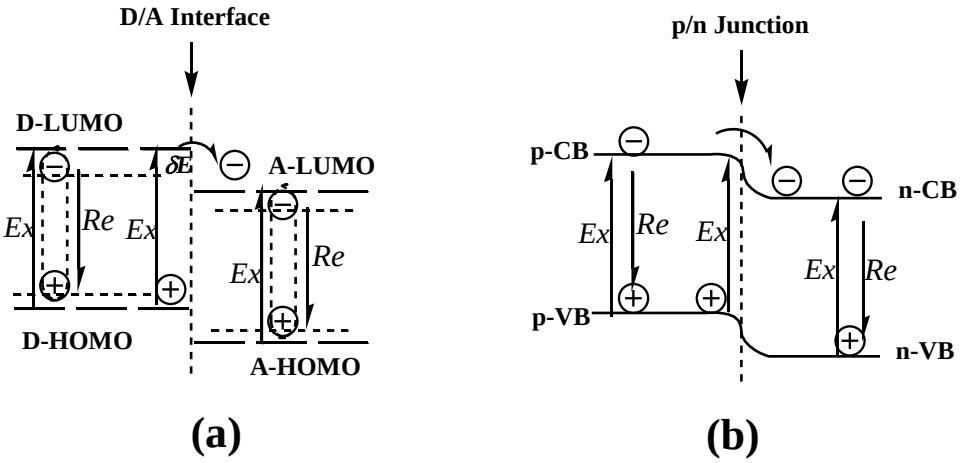

FIGURE 3.27 Scheme of electron (charge) transfers at (a) a D/A interface; (b) a p/n junction. Ex: excitation; Re: recombination (or relaxation).

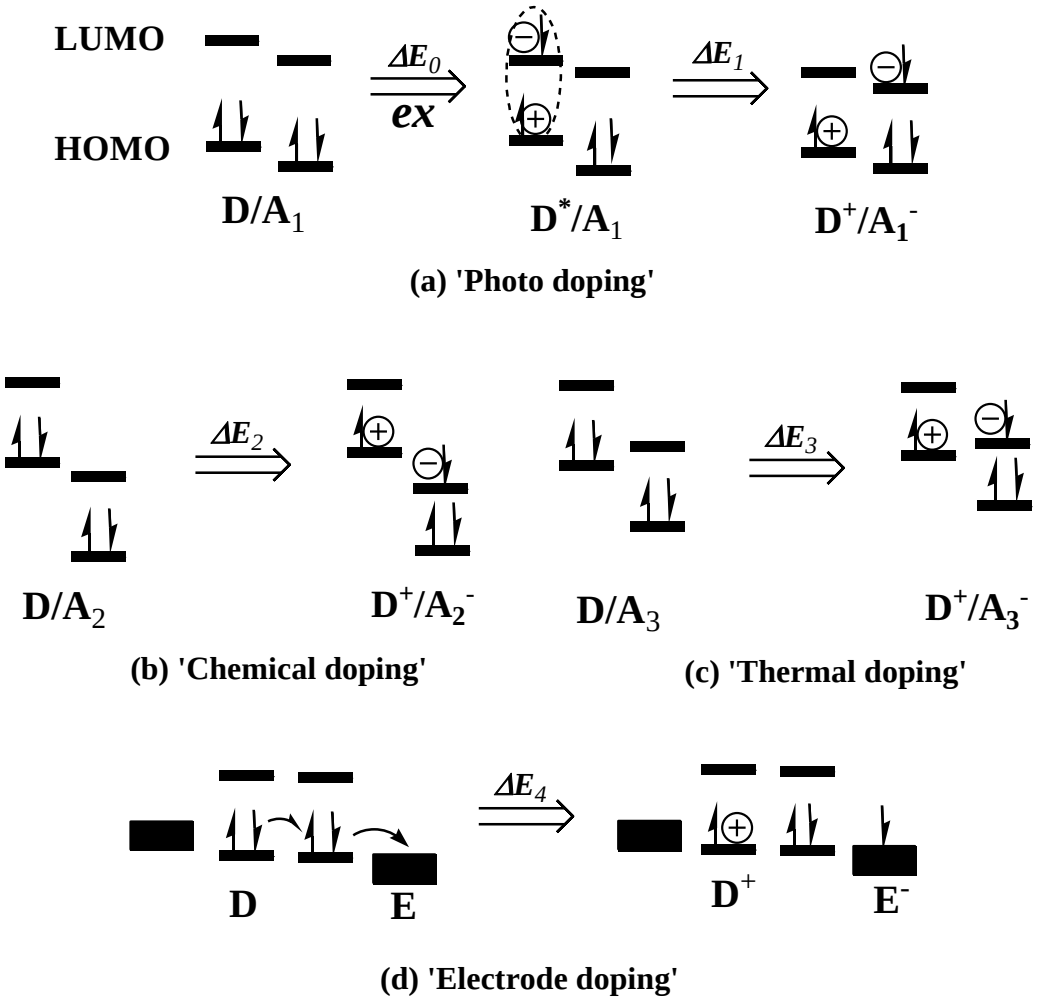

FIGURE 3.28 Scheme of frontier orbitals and electron transfers of (a) photo doping; (b) chemical doping; (c) thermal doping; and (d) electrode doping.

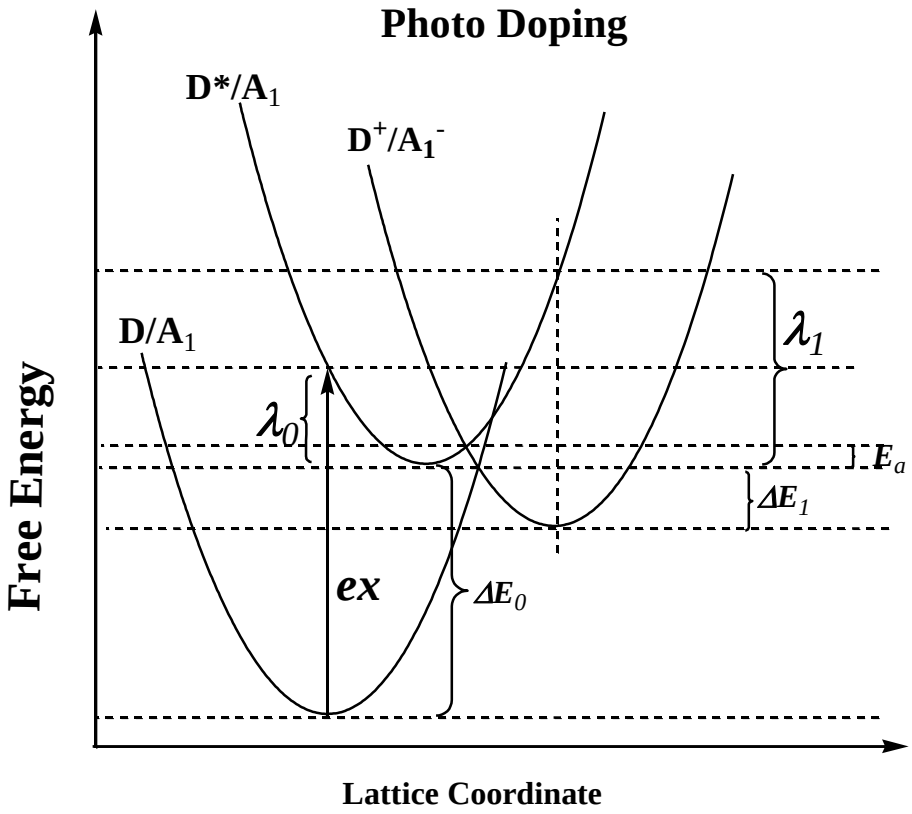

FIGURE 3.29 Scheme of free energy surfaces and electronic transitions of photo doping.

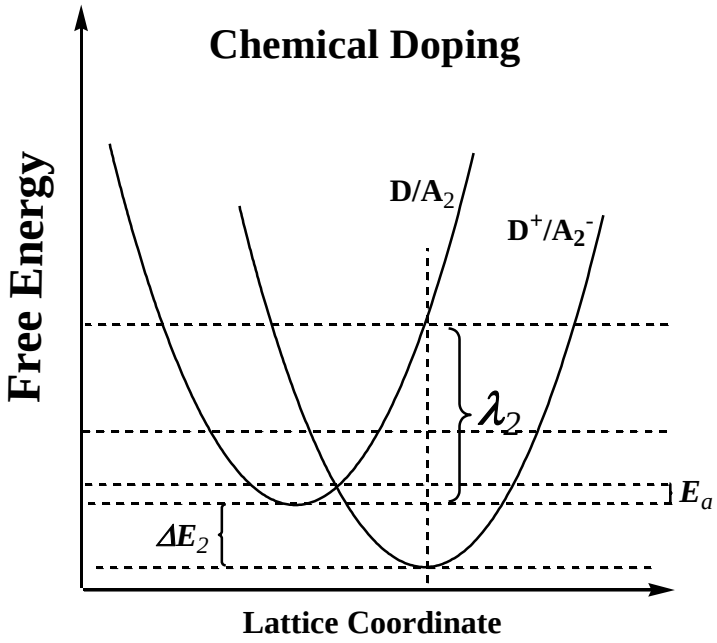

FIGURE 3.30 Scheme of free energy surfaces and electronic transitions of chemical doping.

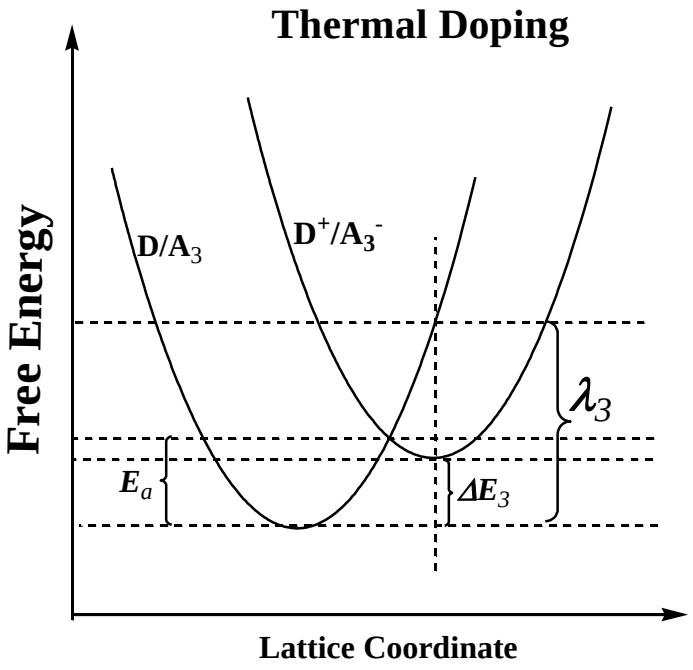

FIGURE 3.31 Scheme of free energy surfaces and electronic transitions of thermal doping.

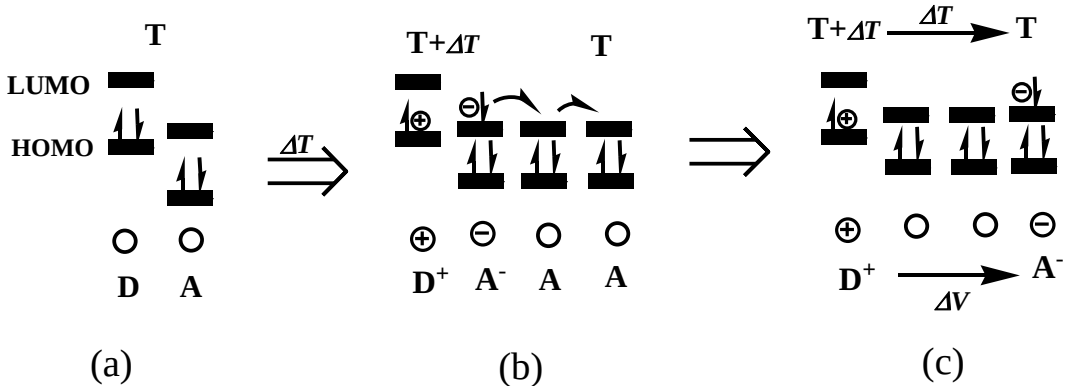

FIGURE 3.32 Scheme of thermoelectric (Seebeck) process based on thermal n-type doping: (a) before heating; (b) after heating and electron transfer or charge separation; (c) after electron transport or migration in a acceptor majority phase.

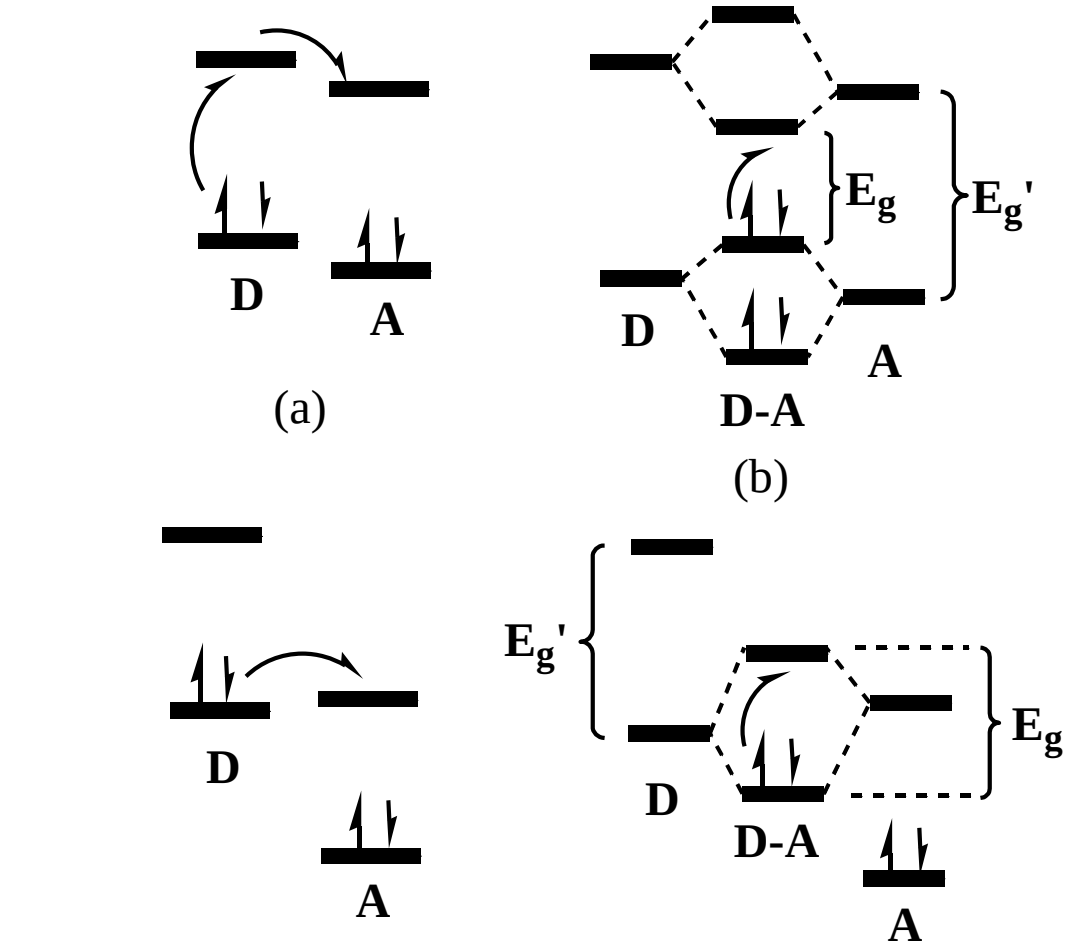

Weak Coupling (WC)
(Small V_{if} or orbital overlap,
$E_a' > 0$, e^- localized)

Strong Coupling (SC)
(Large V_{if} or orbital overlap,
$E_a' = 0$, e^- delocalized)

FIGURE 3.33 Scheme of frontier orbital coupling types between a donor (D) and an acceptor (A) in (a) a weak donor/acceptor pair with weak coupling; (b) a weak donor/acceptor pair with strong coupling; (c) a strong donor/acceptor pair with weak coupling; (d) a strong donor/acceptor pair with strong coupling; (e) Potential profiles of D/A weak coupling; (f) Potential profiles of D-A strong coupling.

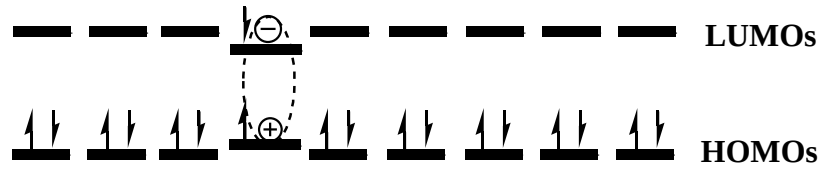

(a) Pure (undoped) 'intrinsic' form

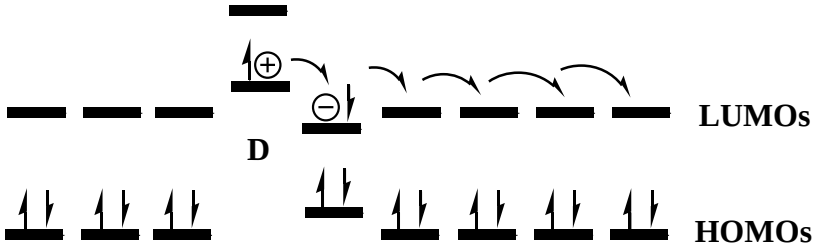

(b) Donor doped 'extrinsic' form (n-type)

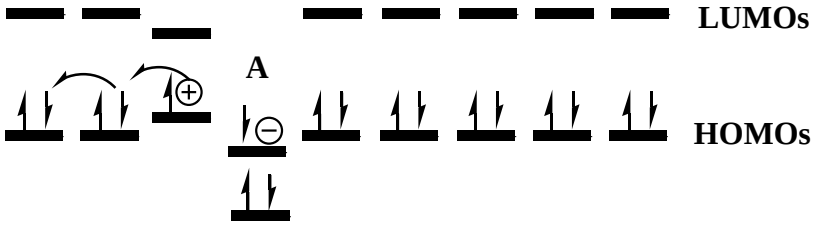

(c) Acceptor doped 'extrinsic' form (p-type)

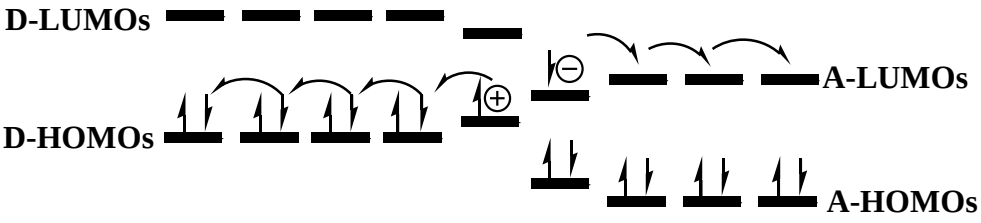

(d) Donor/acceptor 'bicontinous' form

FIGURE 3.34 Frontier orbital and electron transfer schemes of organic/polymeric semiconductors and conductors in (a) pure (intrinsic) form; (b) donor (n-type) doped form; (c) acceptor (p-type) doped form; (d) donor/acceptor (p/n) binary phase separated junction form.

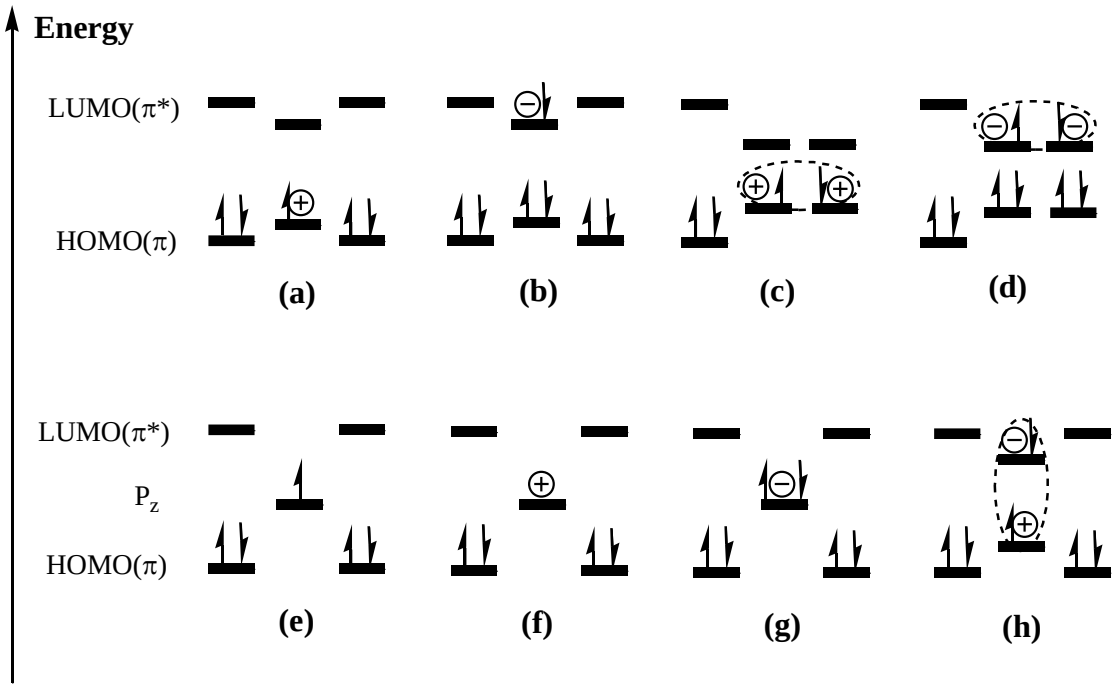

FIGURE 3.35 Orbital levels schemes of carriers: (a) positive (hole) polaron; (b) negative (electron) polaron; (c) positive (hole) bipolaron; (d) negative (electron) bipolaron; (e) neutral soliton; (f) positive (hole) soliton; (g) negative (electron) soliton; (h) neutral exciton–polaron.

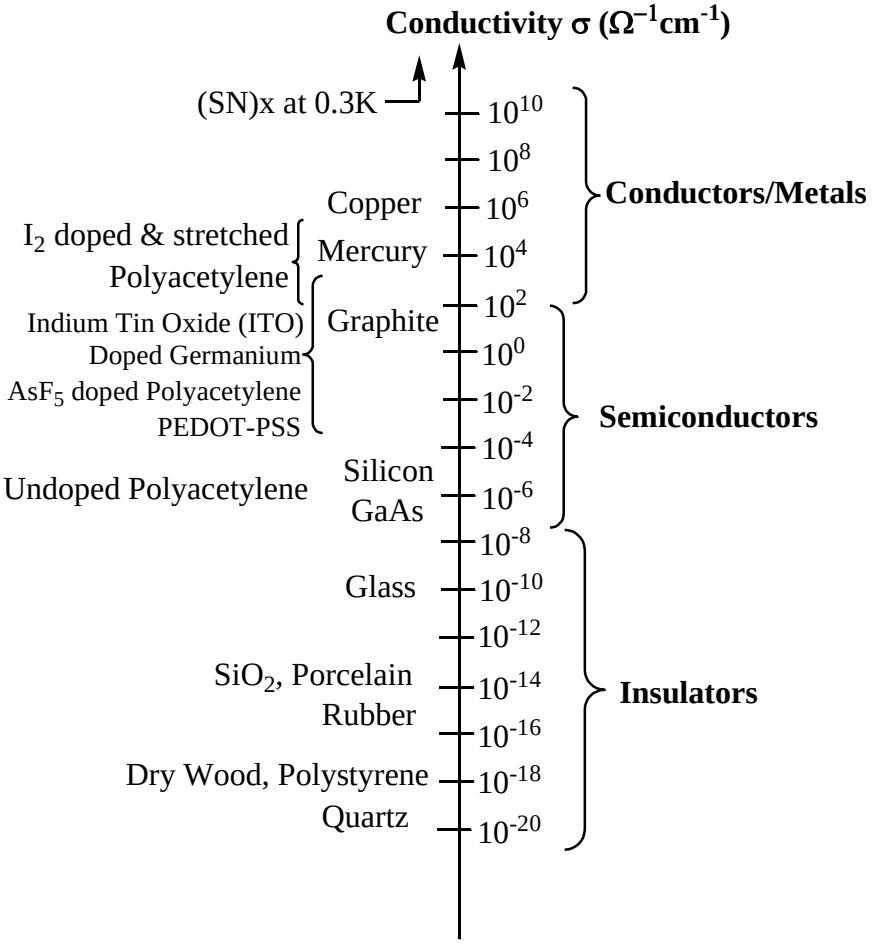

FIGURE 3.36 Room temperature conductivity values (σ) of various materials.

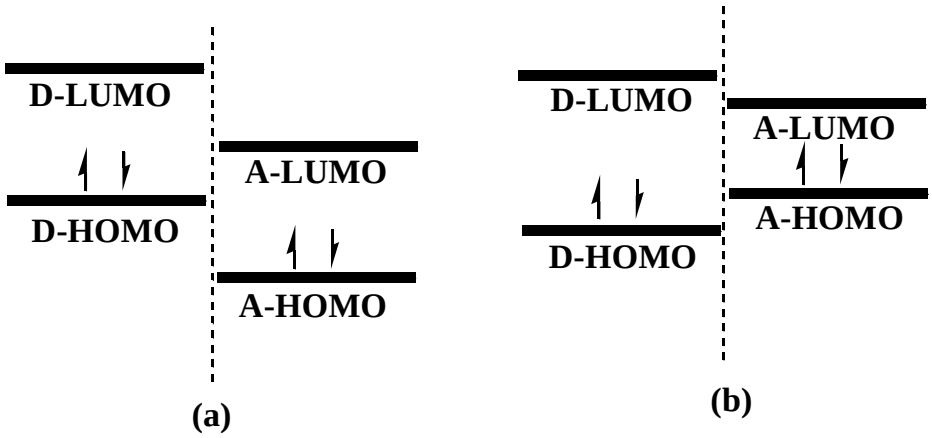

FIGURE 3.37 Frontier orbital energy level representations for a typical (a) electron or charge transfer (CT); (b) energy transfer (ET) between two different materials. D, donor; A, acceptor.

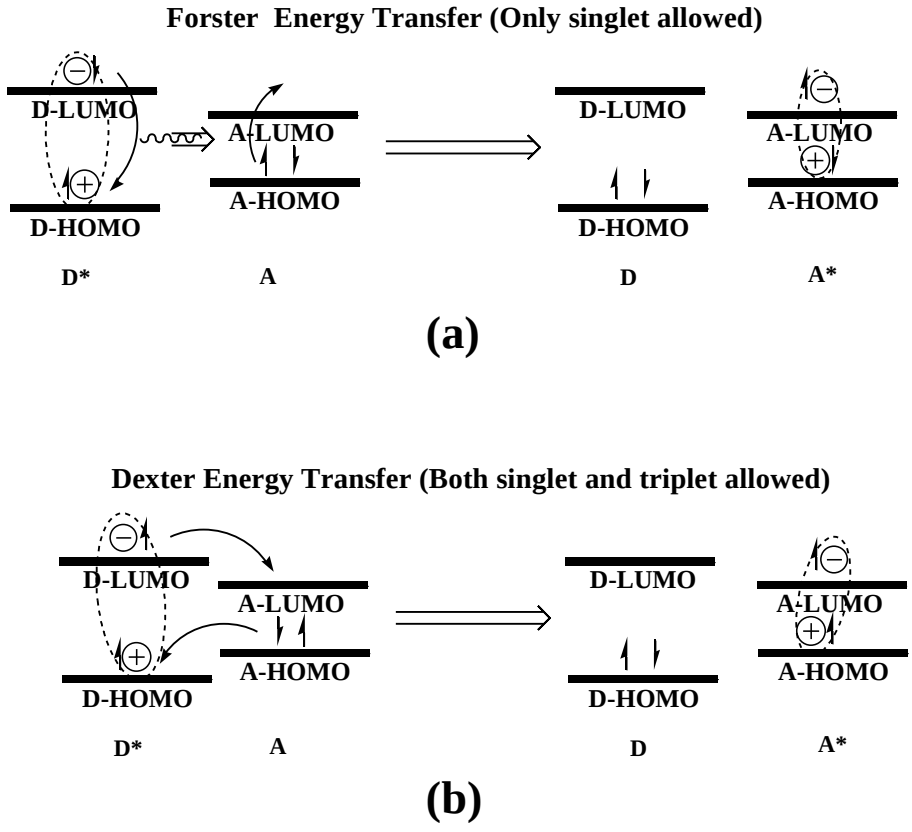

FIGURE 3.38 Scheme of (a) Förster energy transfer; (b) Dexter energy transfer.

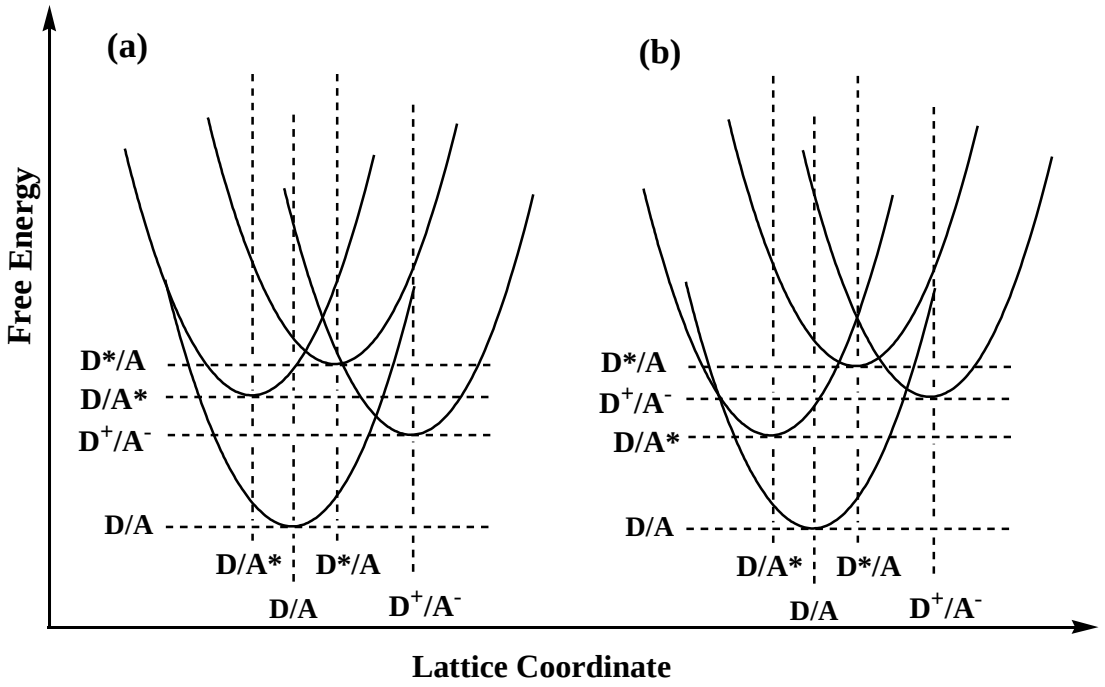

FIGURE 3.39 Free energy surface schemes of a D/A pair in (a) charge transfer (CT); (b) energy transfer (ET) scenarios.

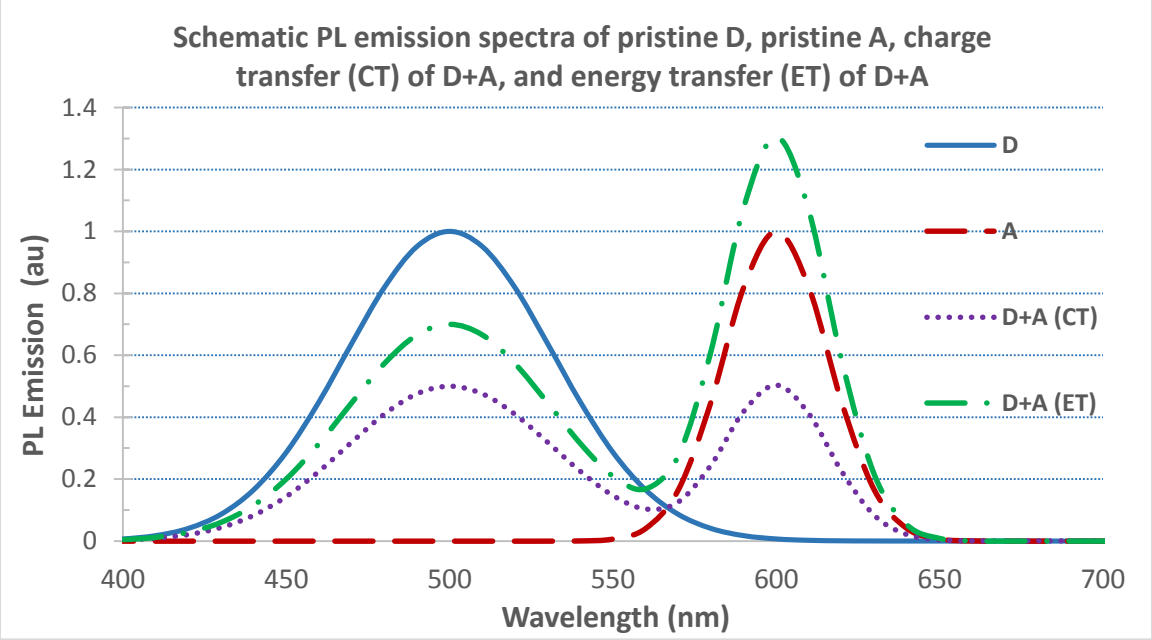

FIGURE 3.40 Schematic photoluminescence (PL) emission spectra of a pristine donor (D), a pristine acceptor (A), blend of the donor and the acceptor (D+A) in case of charge transfer (CT), and blend of the donor and the acceptor (D+A) in case of energy transfer (ET).

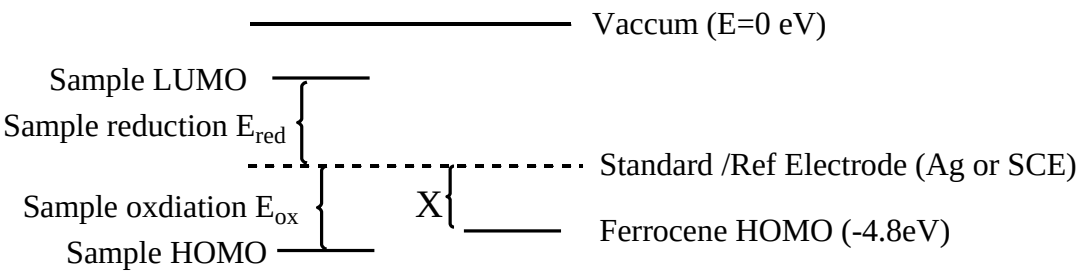

FIGURE 3.41 General energy level scheme of Cyclic Voltammetry (CV), assuming sample HOMO is below E_F of reference electrode, and sample LUMO is above the E_F of reference electrode.

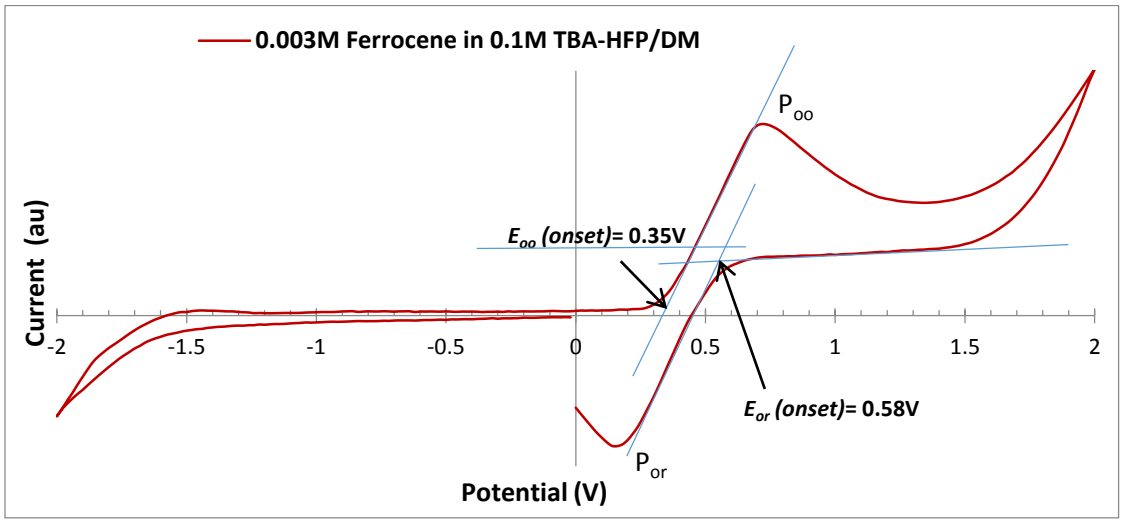

FIGURE 3.42 CV curve of reference material Ferrocene.

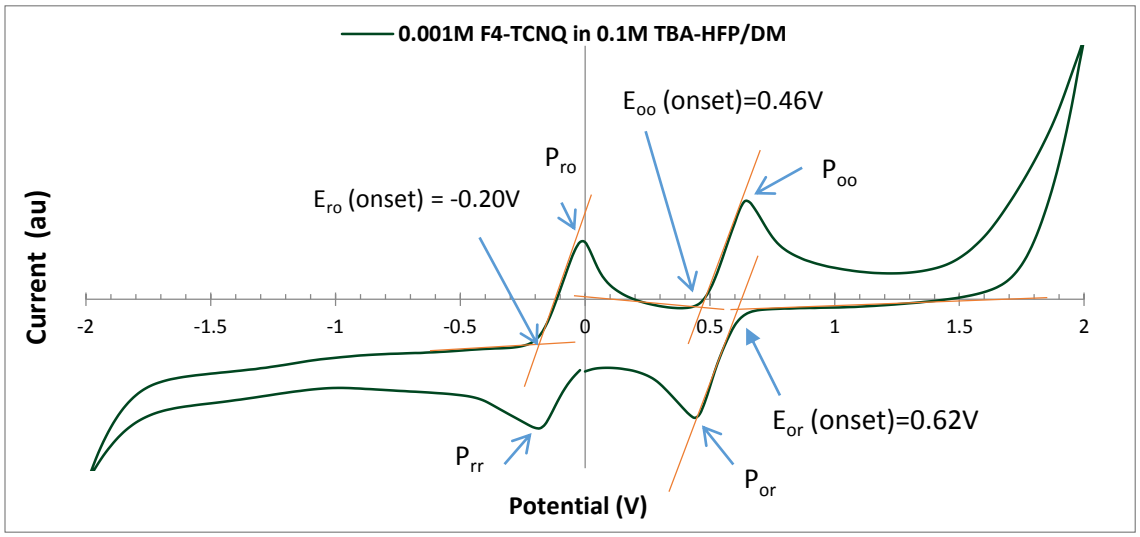

FIGURE 3.43 CV curve of F4-TCNQ.

Tables

TABLE 3.1

Quantum States and Numbers of an Electron in an Atom

Name	Symbol	Orbital Meaning	Range of Values	Value Examples
Principal quantum number	n	Main shell	$1 \leq n$	n = 1, 2, 3, …
Orbital quantum number (azimuthal quantum number)	l	Subshell	$0 \leq l \leq n - 1$	For n = 3: l = 0 (s orbital), 1 (p orbital), 2 (d orbital)
Magnetic quantum number	m_l	Energy shift	$-l \leq m_l \leq l$	For l = 2: $m_l = \pm 2, \pm 1, 0$
Spin quantum number	m_s	Spin	–1/2 or 1/2	Always: –1/2 or 1/2

TABLE 3.2

Key Multiplicity States and Terms

Electron Pattern	Spin Quantum Numbers (m_s)	$S = \Sigma m_s$	Multiplicity $2S + 1$	Term
↑	1/2	1/2	2	Doublet
↓↑	1/2, –1/2	0	1	Singlet
↑↑	1/2, 1/2	1	3	Triplet